DISEASE MECHANISMS OF SPECTRIN SUPERFAMILY PROTEINS

by

ALEXANDRA E ATANG

A dissertation submitted in partial fulfillment of the
requirements for the degree of

DOCTOR OF PHILOSOPHY IN BIOMEDICAL SCIENCES: HEALTH AND ENVIRONMENTAL CHEMISTRY

2024

Oakland University
Rochester, Michigan

Doctoral Advisory Committee:

Adam W. Avery, Ph.D., Chair
Colin G. Wu, Ph.D.
Elizabeth Delorme-Axford, Ph.D.

To my family

ACKNOWLEDGMENTS

This work would not have been possible without the support of my mentor, Adam Avery. Your support and guidance have helped me achieve beyond what I thought possible. Thank you for pushing me and giving me room to grow. This journey has taught me to remain persistent despite challenges.

Sarah Denha, thank you for being my partner through this entire journey. We learned together and have become proud scientists. I will always respect your contributions and dedication to our work. Your resilience is inspiring, and I am better for having worked with you.

For my husband, Alexander Atang, and my children; Nora, Isla and Emil. Thank you for encouraging me to push forward and reminding me that even small steps are progress. I am grateful for the family we have created while working toward this degree. My hope is that my children will grow up healthy and happy and continue to make the world brighter for others, as they have already for me.

Alexandra E Atang

ABSTRACT

DISEASE MECHANISMS OF SPECTRIN SUPERFAMILY PROTEINS

by

ALEXANDRA E ATANG

Adviser: Adam W. Avery, Ph.D.

Spectrin superfamily proteins are a group of evolutionarily linked proteins that share in actin crosslinking functions. Characterized by an N-terminal actin binding domain (ABD), comprised of tandem calponin homology (CH) domains, a variable number of spectrin repeat domains, and in some cases an EF hand motif, these cytoskeletal proteins are an integral feature of the submembranous cellular structure. Mutations within the ACTN2 and SPTBN2 genes that encode α-actinin-2 and β-III-spectrin, respectively are known to cause disease. Predominately expressed in cardiomyocytes of the heart, α-actinin-2 mutations localizing to the ABD are linked to cardiomyopathy, leading to heart failure and sudden cardiac death. ABD localized β-III-spectrin mutations cause the rare neurodegenerative disease, spinocerebellar ataxia type 5 (SCA5). Previous studies of a L253P mutation within the β-III-spectrin ABD revealed an increased actin-binding affinity. Positioning of the L253P mutation to the interface of CH1 and CH2 was demonstrated to promote a conformational opening, leading to high affinity actin interactions. These studies investigate the molecular consequences of nine additional β-III-spectrin ABD-localized, SCA5 missense mutations (V58M, K61E, T62I, K65E, F160C, D255G, T271I, Y272H, and H278R) and three α-actinin-2 ABD-localized,

cardiomyopathy missense mutations (A119T, M228T, and T247M). Importantly, all β-III-spectrin and α-actinin-2 mutations localizing the CH1-CH2 interface increased actin-binding affinity, while the actin-binding surface localized α-actinin-2 mutation, A119T, decreased actin-binding affinity. Using biochemical and biophysical approaches, we demonstrate that the mutant β-III-spectrin and α-actinin-2 ABD proteins can attain a well-folded state. However, thermal denaturation studies show that all ABD mutations are destabilizing, suggesting structural disruptions to the ABDs. Additional *in vivo* studies of the β-III-spectrin mutations indicate an accumulation of protein within neurons, likely a result of increased actin binding-affinity. Altogether, the data indicate aberrant actin-binding affinity is a shared molecular consequence of ABD localized mutations of spectrin superfamily proteins.

TABLE OF CONTENTS

TABLE OF CONTENTS—Continued

TABLE OF CONTENTS—Continued

LIST OF TABLES

LIST OF FIGURES

CHAPTER ONE

INTRODUCTION

1.0 Submembranous Cytoskeletal Proteins

1.0.1 Submembranous Actin Network

Actin is a major component in eukaryotic cells, carrying out functions related to cell structure, motility, cytokinesis and intracellular transport [1–6]. Actin is a highly abundant cytoskeletal protein that creates a vast network of fibers just below the plasma membrane and throughout the cytoplasm [7]. Actin exists as filamentous polymers that are crosslinked and is anchored to the cytoplasmic side of the cell membrane by interacting proteins. The addition of actin monomers to form polymer chains is a rapid adenosine triphosphate-powered process under constant remodeling. Interactions between actin monomer subunits and actin-binding proteins are relatively short lived, allowing for a rapid molecular response to cellular demands [1].

1.0.2 Structural and Functional Elements of Spectrin Superfamily Proteins

The spectrin superfamily is an evolutionarily linked group of proteins that associate with actin filaments to aid in organization of the submembranous actin network. These proteins are well established cytoskeletal components with a great deal of homology [8]. Commonly observed structural elements within the spectrin superfamily include an N-terminal actin binding domain (ABD), comprised of tandem calponin homology (CH) domains, the hallmark rod shaped spectrin repeat domains (SRD) and EF hand motif. These commonly found structural elements are modular in nature and aid in performing the functions required for the spectrin superfamily proteins. This family of

proteins tends to be highly α-helical in secondary structure and form long chains in their tertiary structures [9]. Members of this family are α-actinin, spectrin, dystrophin and utrophin.

1.0.2.1 The Actin-Binding Domain

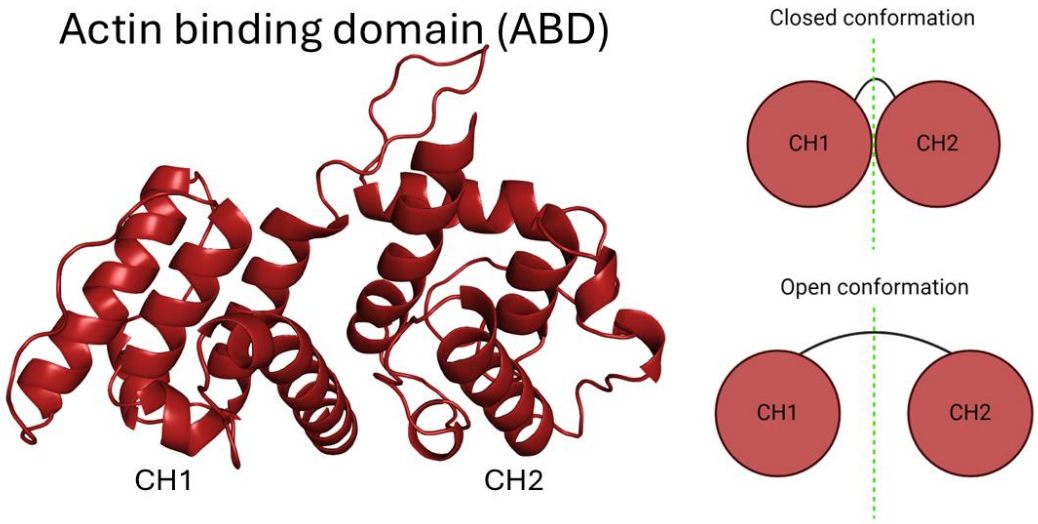

Figure 1.1: Actin Binding Domain (ABD). A. Alpha Fold prediction of β-III-spectrin ABD in closed conformation. B. Cartoon showing the ABD in the closed conformation (top) and the open conformation (bottom). The axis of the interface is noted by a dashed vertical green line. Created with BioRender.com.

The ABD is comprised of tandem CH domains: CH1 And CH2 (Figure 1.1). CH1 and CH2 are closely associated lobes of α-helices connected by a flexible unstructured linker region (Figure 1.1). The interface between CH1 and CH2 is lined with hydrophobic amino acid residues. Crystal structures of α-actinin, dystrophin and utrophin show contact at the hydrophobic CH1/CH2 interface, indicating a closed conformation in its native state [10–14]. Actin monomer subunits and N-terminal ABDs of the spectrin superfamily have a one-to-one stoichiometry [15]. Binding of the ABD is limited by

affinity of the ABD to actin [16,17]. Early cryo-EM data showed the α-actinin ABD bound to actin and though it was determined that an opening of the CH interface was required for this interaction, the resolution was too low to determine which residues or even which CH domain directly bound actin [18]. A higher resolution, 6.9 Angstrom cryo-EM structure produced in 2017 of the β-III-spectrin ABD bound to F-actin showed direct binding of CH1 to actin (Figure 1.2) [19]. This negates previous suggestions of actin binding activity found in the first helix of CH2 [13,20]. Rather CH2 has a regulatory role in mediating the actin-CH1 interaction [19]. Due to the highly conserved nature of the ABDs in the spectrin superfamily, these conclusions inform on the mechanistic binding of other closely related actin-binding proteins, such as α-actinin, dystrophin and utrophin [18,19,21]. In fact, subsequent studies of spectrin related proteins have confirmed the direct interaction of CH1 with F-actin [22,23].

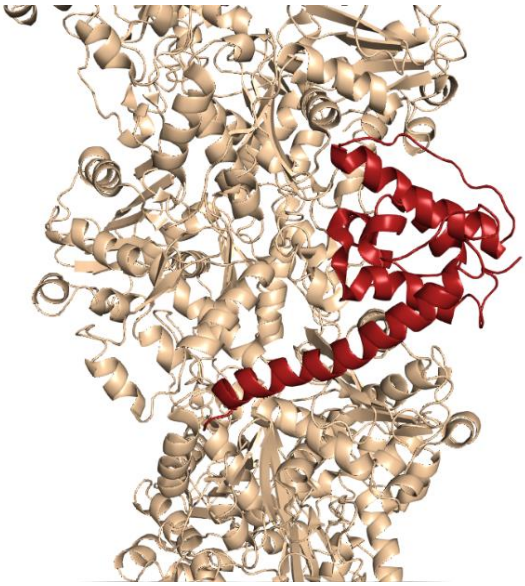

Figure 1.2: Cryo-EM structure of F-actin (tan) bound to calponin homology (CH) subdomain 1 of β-III-spectrin (red). PDB: 6ANU

1.0.2.2 The Spectrin Repeat Domains

The defining domain of the spectrin family of proteins is the SRD. Though not entirely sequence conserved between proteins, the form of the triple helix rod structure is conserved (Figure 1.3) [24]. SRDs are highly variable in number repeats present. For example, α-actinin has four SRDs, while β-spectrin proteins have between seventeen and thirty SRDs [8]. The SRDs are flexible α-helical rods that when linked, dictate both the length and flexibility of the protein. Fewer repeats lead to decreased flexibility and less axial compression [25–29].

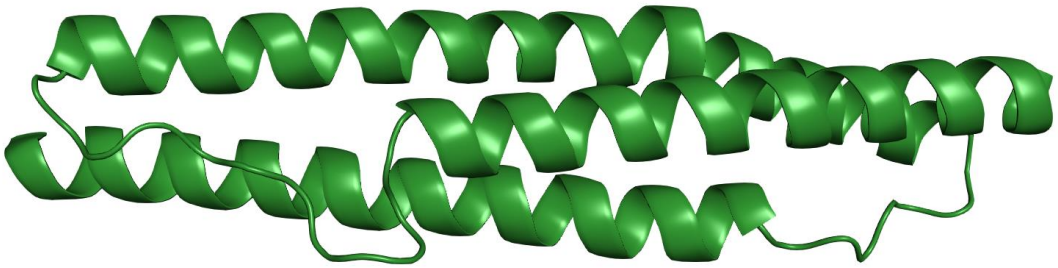

Figure 1.3: Alpha Fold prediction of spectrin-repeat domain (SRD).

1.0.2.3 The EF Hand Motif

EF hand motifs are not present in every member of the spectrin superfamily but are present at the C-terminal of α-actinin and α-spectrin. The motif is structurally related to calmodulin, a calcium binding protein [30]. Some EF-hand motifs have lost the ability to bind calcium and are thus non-functional [31,32]. Alpha-actinin-1 and α-actinin-4 are calcium sensitive, each of the two EF-motifs binding one calcium atom, while α-actinin-2 and α-actinin-3 are calcium insensitive [31]. Alpha-spectrin has retained its calcium-binding ability [33].

1.1 Alpha-Actinins and Spectrins

1.1.1 Evolutionary History

Many actin-crosslinking cytoskeletal proteins are conserved across species and helped uncover the evolutionary link between the ancestral α-actinin protein and modern spectrins. Studies in *Drosophila melanogaster* identified conserved N-terminal regions of the spectrin superfamily proteins; β-spectrin, α-actinin and dystrophin [34]. Genetic sequence and structural similarities between Drosophila α-spectrin and vertebrate α-spectrin further established an evolutionary link [35]. In humans, the α-actinin and erythroid β-spectrin genes are found in proximity on chromosome 14, indicating a close biological relationship [36,37].

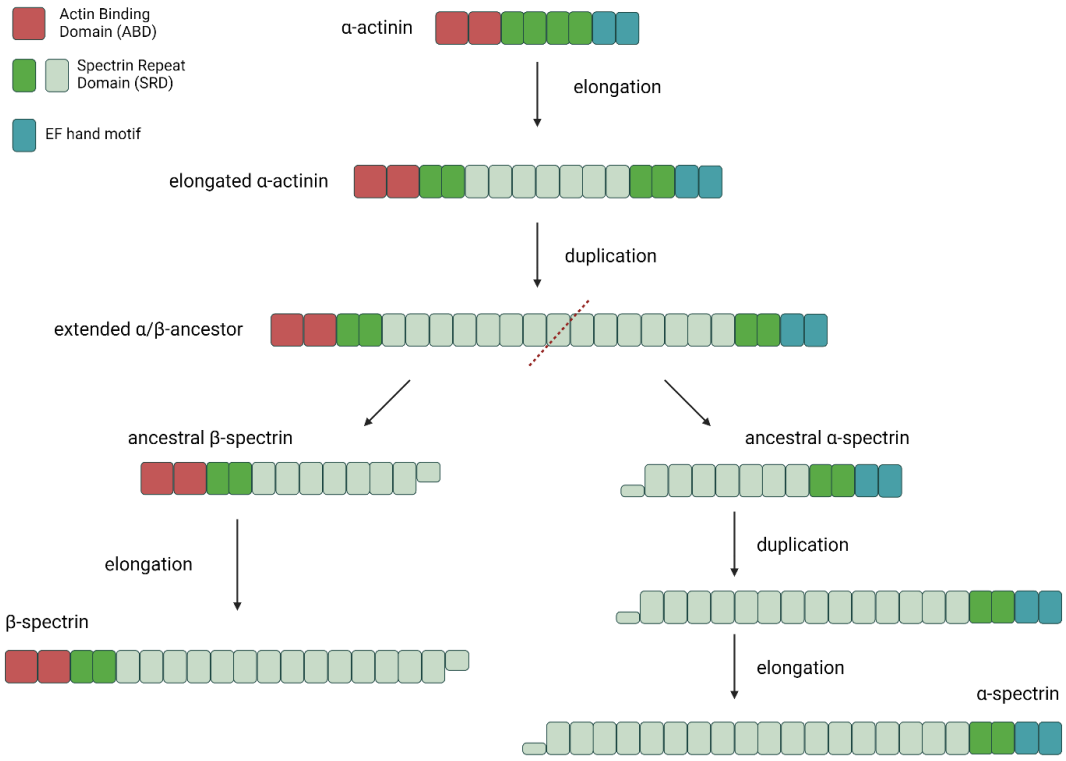

Figure 1.4: Block diagram of the evolutionary events related to ancestral α-actinin and modern spectrins. Adapted from Broderick and Winder, 2005 and Pascual 1997. Created in BioRender.com.

Phylogenetic analysis elucidated the elongation, duplication and cleavage of the ancestral α-actinin protein to give rise to the modern β- and α-spectrin proteins (Figure 1.4) [38]. The first elongation event inserted a block of seven SRDs between SRD2 and SRD3 to form an elongated α-actinin molecule. A duplication of the seven SRD block was then reinserted into the elongated α-actinin to form the extended α- and β-spectrin ancestor. At this point, the evolution of α and β-spectrin diverge. Ancestral β-spectrin retained the N-terminal ABD, α-actinin SRD1 and SRD2, and one of the seven SRD blocks. Independent elongation events within the SRD region eventually formed a monomer of stable length to form the modern β-spectrin protein. Ancestral α-spectrin retained the second SRD block, α-actinin SRD3 and SRD4, and EF-hands. An additional duplication event of the seven SRD block and independent elongation events within the SRD chain gave rise to the modern α-spectrin protein [9,38,39]. Once SRD length stabilized for the precursor proteins of α-actinin and both spectrins, the lineages evolved separately to form the human isoforms [40].

1.1.2 Structure and Function of Alpha-Actinins and Spectrins

1.1.2.1 Structure of Modern Human Alpha-Actinin and Spectrins

The conserved domains of the spectrin superfamily of cytoskeletal proteins confer similar functions in actin-crosslinking. Alpha-actinin is comprised of an N terminal actin binding domain (ABD), four spectrin repeat domains (SRD) and a C terminal EF hand motif. Alpha-actinin exists as an antiparallel dimer with the EF hand domain associating with the linker region between the ABD and SRDs (Figure 1.5) [21]. Similarly, β-spectrin has an N-terminal ABD, 17 SRDs and a C-terminal pleckstrin homology (PH) domain. Alpha-spectrin has 20 N-terminal SRDs, and a C-terminal EF 2 hand motif.

Beta-spectrin binds α-spectrin to form an anti-parallel (Figure 1.5). Two heterodimers then associate to form a heterotetramer through the binding SRD17 of β-spectrin in one heterodimer to SRD1 of α-spectrin in the second heterodimer [9]. The presence of an ABD at each end of the α-actinin dimer and spectrin heterotetramer enables crosslinking of actin filaments. The spectrin and α-actinin functional units differ greatly in length. The number of SRDs in each monomer, and dimer versus heterodimer configuration is responsible for this difference [40].

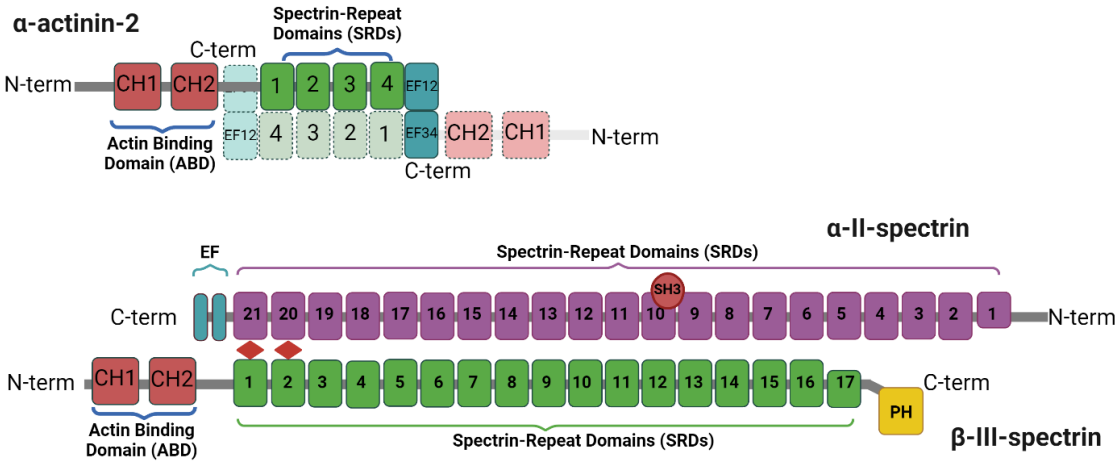

Figure 1.5: Block diagram of α-actinin-2 dimer (top) and α-II/β-III-spectrin dimer (bottom). Created with BioRender.com.

1.1.2.2 Spectrin Function and Forms

Spectrin was first identified and isolated from erythrocyte cytoskeletons washed of hemoglobin [9,41,42]. The membrane associated spectrin-actin lattice network allows the cell to withstand mechanical stresses present in the circulatory system [8]. As a major component of the cytoskeleton, spectrin is thought to provide an elastic quality that confers mechanical resilience and organization of membrane proteins [43,44]. Similarly,

neuronal spectrin is thought to provide mechanical resilience throughout neuronal processes and allow for signaling events [45–48]. Spectrins can be divided into α- and β-spectrins. In humans, there are two isoforms of α-spectrin: α-I and II-spectrin, encoded by the genes *SPTA1* and *SPTAN1*, respectively. Beta-spectrin isoforms are: β-I, II, III, IV and V-spectrin, encoded by *SPTB, SPTBN1, SPTBN2, SPTBN4* and *SPTBN5* respectively. Alpha-spectrins are comprised of 20 N-terminal SRDs, and an EF-hand motif. B-spectrins contain an N-terminal ABD, 17 SRDs and a C-terminal PH domain. Though α- and β-spectrin are ubiquitous components of the cell cytoskeleton expressed in many cell types, α-I and β-I-spectrin are traditionally thought of as erythrocytic. α-II, β-II, III, and IV-spectrin are enriched in neuronal cells. β-V is considered non-erythrocytic and is expressed in many tissues at low levels [49].

1.1.2.3 Alpha-Actinin Function and Forms

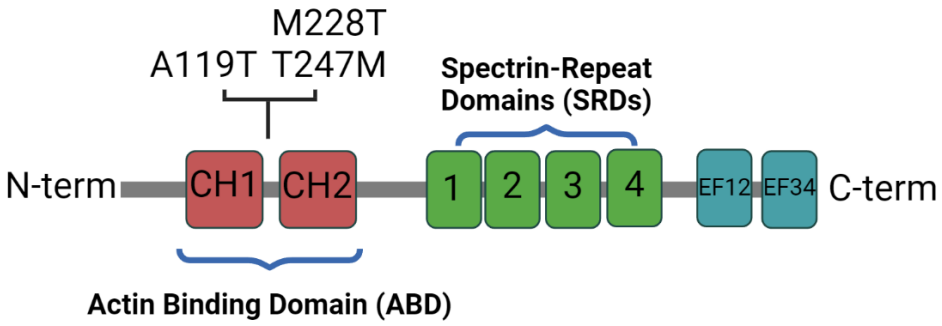

Figure 1.6: Block diagram of α-actinin-2. Created with BioRender.com.

Alpha-actinin is the ancestral member of the spectrin superfamily of proteins and is expressed in most eukaryotes [31,38,50,51]. As with the rest of the spectrin superfamily of proteins, α-actinin crosslinks actin filaments in the cytoskeleton [52]. In

humans, there are four isoforms of α-actinin, the non-muscle isoforms; α-actinin-1 and α-actinin-4, and the muscle isoforms; α-actinin-2 and α-actinin-4 [53]. All four isoforms are comprised of an N-terminal ABD, four SRDs and 4 EF hand motifs (Figure 1.6). The functional unit of α-actinin is an anti-parallel dimer with the ABDs free to bind one actin filament subunit [21]. The relatively short distance between the ABDs is determined by the number of SRDs. The SRDs allow the α-actinin dimer to flex and rotate but retain their rigidity [21,54,55]. Additionally, the SRDs serve as a platform for interacting proteins [24]. Within the muscle isoforms, the vestigial EF hand motifs have lost the calcium binding function [31]. The non-muscle isoforms have retained the calcium binding function [32]. Alpha-actinin isoforms have a large amount of homology but are not interchangeable [53,56]

1.2 Disease Associated Proteins of the Spectrin Superfamily

The spectrin superfamily hosts many human disease associated proteins including: β-II, III and IV-spectrin, α-actinin-1,-2, and -4; and dystrophin [8,57–64]. The ancestral protein, α-actinin gave rise to two proteins of interest, α-actinin-2 and β-III-spectrin. Both proteins are associated with human disease pathogenesis in cardiomyopathies and spinocerebellar ataxia type 5 (SCA5). Interestingly, both diseases indicate aberrant actin-binding affinity in their molecular pathologies.

1.2.1 Role of Neuronal β-III-Spectrin

The cerebellum is a region of the brain situated at the base of the skull and top of the spinal cord. It is responsible for coordination of smooth movements, including walking, hand-eye coordination, and clear speech. As a heterotetramer of α-II and β-III-spectrin, neuronal spectrin complexes are thought to organize the membrane periodic

structure of the highly distinctive cerebellar Purkinje cells (Figure 1.7). Beta-III-spectrin is highly enriched in the soma and dendrites of cerebellar Purkinje cells [65,66]. Purkinje cells are extensively branched neurons with many postsynaptic structures, called spines. These neurons require a well-organized spectrin-actin network at the plasma membrane for cell morphology, function and dendritic spine development [43,66]. In cultured neurons, loss of β-III-spectrin alters the morphology, increases excitatory postsynaptic excitation, and decreases the number of dendritic spines [67]. Additionally, the number of synapses decreases with loss of β-III-spectrin, as well as a mislocalization of the synaptic cellular components: metabotropic glutamate receptor 1α (mGluR1α) and delta-2 glutamate receptor (GluRδ2) [68–70].

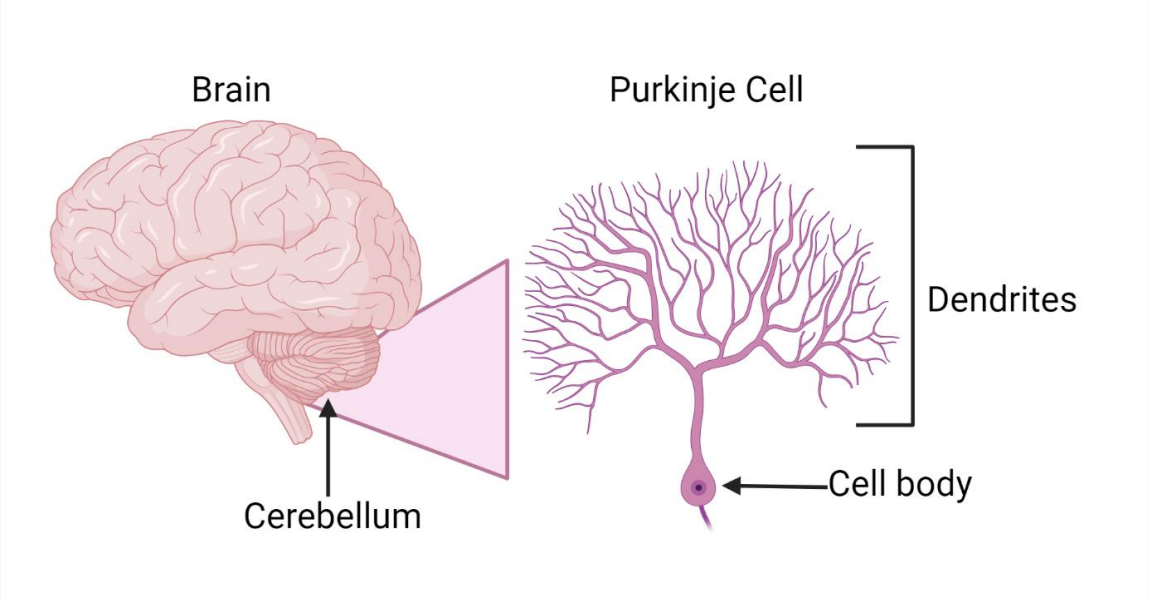

Figure 1.7: Cartoon images of the cerebellum (left) and the structure of a Purkinje cell (right). Created with BioRender.com.

Beta-III-spectrin knockout mouse models show the physiological effects of mislocalized synaptic cellular components. A destabilization of the surface excitatory amino acid transporter 4 (EAAT4) in Purkinje cells has been observed in mice lacking expression of β-III-spectrin [71–73]. Additionally, a loss of β-III-spectrin decreases levels of; another transporter, glutamate-aspartate transporter, (GLAST), a known spectrin complex protein binding partner, ankyrin-R, and sodium currents in Purkinje cells [72,73]. These mislocalized cellular components suggest a decrease in excitatory neurotransmitter activity and overall decrease in Purkinje cell output, leading to neurodegeneration. In fact, the mice deficient in β-III-spectrin exhibit seizures, underperformance in cognitive tasks, and morphological defects in prefrontal cortex neurons [68,73,74].

1.2.2 Spinocerebellar Ataxia Type 5

SCA5 stems from autosomal dominant mutations within the gene *SPTBN2*, which encodes β-III-spectrin [69]. The age of onset can range from infantile to late adulthood. Adult, or late onset of symptoms include atrophy of the cerebellar cortex, progressive limb and gait ataxia, slurred speech and abnormal eye movements [75–77]. Early onset of symptoms is also associated with cerebellar atrophy and loss of coordinated movements, as well as delayed motor development and intellectual disability [78–81]. Other β-III-spectrin related neurological disorders are Spectrin-Associated Autosomal Recessive Cerebellar Ataxia Type 1 (SPARCA1) and Spinocerebellar ataxia, autosomal recessive 14 (SCAR14) [69,74,82,83]. Interestingly, the severe early onset symptoms caused by some dominant SCA5 mutations are similar to the symptoms present in the recessive neurodevelopmental disorders SPARCA1/SCAR14 [78,81,84]. Subcellular localization

and cellular morphology inform on the physiology of disruptions to the normal expression of β-III-spectrin. Heterotetramers of β-III-spectrin and α-II-spectrin crosslink actin filaments beneath the plasma membrane in the cytoskeleton of cerebellar Purkinje cells [85,86]. SCA5 pathogenesis primarily affects the population of cerebellar Purkinje cells, where β-III-spectrin is particularly enriched in the soma and dendrites [65,66]. In mouse and cultured neuron studies, β-III-spectrin was shown to be critical for normal development of dendritic arbors, spine morphology, and synaptic signaling [66–68,73,85]. While the knockout mouse model shows the role of β-III-spectrin in localizing cellular components, it fails to replicate the cerebellar and cortical physiological phenotype typical of patients diagnosed with SCA5 [68,74,87]. Rather than a model exhibiting a loss of function allele, a model showing the physiological effects of a gain of function allele may be more informative [83].

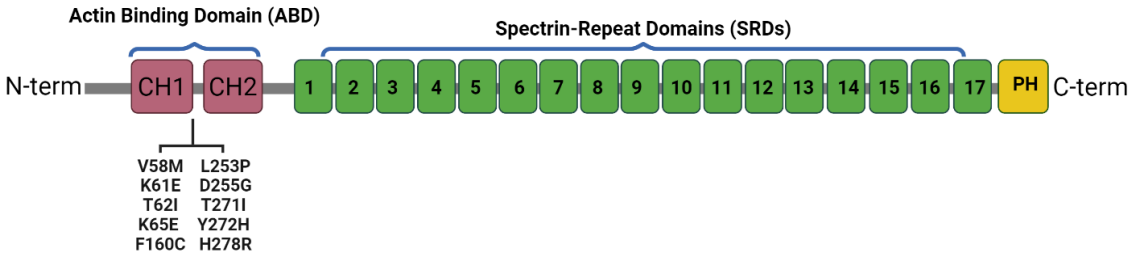

Figure 1.8: Block diagram of β-III-spectrin. Created with BioRender.com.

Disease associated mutations are found throughout the *SPTBN2* coding sequence. The β-III-spectrin monomer contains an N-terminal ABD, 17 SRs, and a C-terminal PH domain (Figure 1.8). The initial three SCA5 mutations mapped to *SPTBN2* included the ABD localized leucine to proline substitution at amino acid residue 253 (L253P). This

late onset mutation was identified in multiple family members and characterized extensively [69]. More recently, availability of genomic data has identified mutations along the length of the protein, including clusters of missense mutations to the ABD. These mutations are associated with both early and late onset of symptoms, exhibiting a range of severity [58,75,78–80,84,88–90].

The ABD is comprised of tandem CH subdomains, CH1 and CH2. The native CH2-localized L253 residue is situated deep in a hydrophobic pocket at the CH1-CH2 interface. Biochemical studies show a 1000-fold increase in actin-binding affinity of the mutant L253P protein compared to the wildtype protein [57]. Additional biophysical studies, including cryo-EM, show that the L253P mutation leads to an opening of the CH1-CH2 interface. Thereby removing obstruction caused by CH2 and allowing CH1 to bind actin readily [19].

In vivo studies of cultured mouse Purkinje neurons and in vivo *Drosophila melanogaster* gave insight to the effects of the L253P mutation. Cultured Purkinje cells expressing β-III-spectrin harboring the L253P mutation exhibit a reduction of dendritic β-III-spectrin and overall dendritic arbor defects [85]. In Drosophila, fly β-spectrin, the homolog to human β-III-spectrin is well conserved. The native fly residue L246 is equivalent to human L253. Expression of mutant L246P fly β-spectrin transgene in class IV dendritic arborization (da) sensory neurons caused reduced dendritic arborization. The mutant L246P β-spectrin was also found to accumulate in the soma and proximal dendrites. This is unlike the wild-type protein which was distributed more broadly in the dendritic arbor [91]. Further, rescue experiments performed in Drosophila with an endogenous, lethal β-spectrin loss-of-function allele ($\beta spec^{em21}$), showed that a transgene

containing wild-type fly β-spectrin could rescue lethality. In contrast, a transgene encoding the L246P β-spectrin did not rescue and was additionally neurotoxic even in a wild-type background (no $\beta spec^{em21}$ allele) [91,92].

Though the pathogenic mechanism is still being investigated, several studies support altered actin binding leading to disease. The cryo-EM study visualizing the binding of CH1 to actin also shows a previously unresolved N-terminal helix preceding CH1 to also bind actin [19]. When the N-terminal helix is truncated, the high-affinity actin binding induced by the L253P mutation is reduced below the wild-type threshold, though not abolished. Interestingly, rescue experiments of Drosophila overexpressing the truncated fly β-spectrin harboring the L246P mutation reduced neurotoxicity [92]. These studies support the importance of the spectrin-actin interaction in ABD-localized SCA5 disease pathogenesis.

Currently, there are no treatments or cures for SCA5. Understanding the molecular mechanism of SCA5 mutations is key in developing targeted small-molecule therapeutics. Recent progress has been made in identifying small molecule compounds that reduced binding of the SCA5 L253P mutant β-III-spectrin to actin [93].

1.2.3 Role of α-actinin-2

Cardiac muscle contracts due to synchronized movements of sarcomeres. Sarcomeres are the functional unit of muscle tissue and require a high level of organization to maintain healthy function. Major components of the sarcomere are thin filaments, formed from actin; thick filaments, formed from myosin; and elastic filaments, formed from titin (Figure 1.9) [94–96]. Actin thin filaments are anchored at the Z-disc, myosin thick filaments are anchored at the M-line and titin elastic filaments connect thick

filaments to the Z-disc, in a region called the I band [94–97]. The Z-disc is the boundary between sarcomeres. Alpha-actinin-2 localizes to the Z-disc in sarcomeres and functions to crosslink thin actin filaments [98]. Expressed in both skeletal and cardiac muscle fibers [31], α-actinin-2 is required for normal sarcomere organization [56]. Alpha-actinin-2 localizes to the Z-disc, and as a homodimer, cross-links actin filaments of neighboring sarcomeres [20,99]. This highly dynamic crosslinking by α-actinin-2 to actin is required for Z-disc assembly [14,21,100]. Previous studies have shown that disease associated mutations can be incorporated to the Z-disc, but are not able to freely move out, potentially hindering the rapid remodeling required for muscle tissues [14]. This suggests aberrant actin binding activity may play a role in disease pathogenesis.

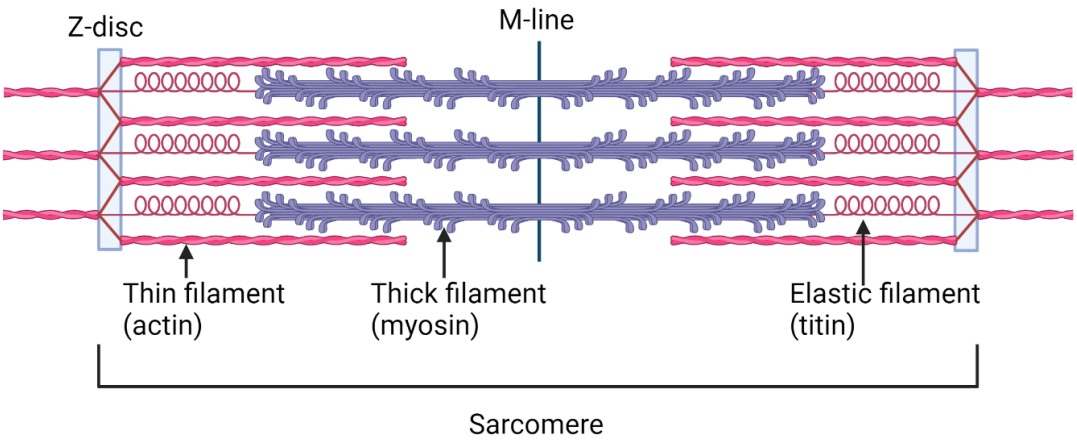

Figure 1.9: Cartoon of a labeled sarcomere. Created with BioRender.com

1.2.4 Alpha-Actinin-2 Related Cardiomyopathy

Alpha-actinin-2 is encoded by *ACTN2* and many amino acid substitution variants are associated with several cardiomyopathy and cardiac manifestations [101–106]. In the heart, the ventricular myocardium can show thinning, thickening, or stiffening, as seen in

dilated cardiomyopathy (DCM), hypertrophic cardiomyopathy (HCM) or restrictive cardiomyopathy (RCM), respectively [107]. These cardiomyopathies can lead to heart failure and sudden cardiac death [103,108]. Heart failure due to cardiomyopathy affects approximately 7 million people in the United States annually and is expected to rise [109].

DCM [105], HCM [101] and RCM [106] cases genetically linked to *ACTN2* typically display autosomal dominant inheritance [107]. However, many recently reported variants [110] lack substantial information regarding family history and require further functional studies to determine impacts to the α-actinin-2 protein. Numerous cardiomyopathy associated variants in α-actinin-2 cluster to the ABD, localizing to the actin-binding surfaces of the CH1/CH2 interface (Figure 1.8) [14,103,110]. Binding of the ABD has been shown to be a direct result of opening at the CH interface, allowing CH1 to bind F-actin directly, while CH2 has a regulatory effect. As with β-III-spectrin, it appears the N-terminal helix proceeding CH1, binds F-actin as well [18,19].

1.3 Research Summary

The body of work presented here aims to gain a deeper understanding of two disease related proteins: β-III-spectrin and α-actinin-2. Both proteins have shared homology and actin-crosslinking functions. Aberrant actin-binding affinity is indicated in disease pathogenesis for both β-III-spectrin linked SCA5 and α-actinin-2 linked cardiomyopathies. Chapter 2 describes the biochemical characterization of nine SCA5 associated ABD localized missense mutations in β-III-spectrin. These mutations were recently identified in patients ranging from 4 months to 48 years of age. The biochemical

and biophysical analyses identified a decrease in thermal stability as well as an increase in actin-binding affinity. Chapter 3 describes the biochemical characterization of three cardiomyopathy associated ABD localized missense mutations in α-actinin-2. The biochemical and biophysical analyses identified a decrease in thermal stability and loss of cooperative unfolding. Two variant proteins display an increase in actin-binding affinity and one protein showed a decrease in actin-binding affinity, indicating aberrant actin-binding affinity in disease pathogenesis. Chapter 4 explores the effect of five SCA5 associated mutations on dendritic arbor morphology using in vivo Drosophila studies.

CHAPTER TWO

INCREASED ACTIN BINDING IS A SHARED MOLECULAR CONSEQUENCE OF NUMEROUS SCA5 MUTATIONS IN β-III-SPECTRIN

2.1 Abstract

Spinocerebellar ataxia type 5 (SCA5) is a neurodegenerative disease caused by mutations in the *SPTBN2* gene encoding the cytoskeletal protein β-III-spectrin. Previously, we demonstrated that a L253P missense mutation, localizing to the β-III-spectrin actin-binding domain (ABD), causes increased actin-binding affinity. Here we investigate the molecular consequences of nine additional ABD-localized, SCA5 missense mutations: V58M, K61E, T62I, K65E, F160C, D255G, T271I, Y272H, and H278R. We show that all of the mutations, similar to L253P, are positioned at or near the interface of the two calponin homology subdomains (CH1 and CH2) comprising the ABD. Using biochemical and biophysical approaches, we demonstrate that the mutant ABD proteins can attain a well-folded state. However, thermal denaturation studies show that all nine mutations are destabilizing, suggesting a structural disruption at the CH1-CH2 interface. Importantly, all nine mutations cause increased actin binding. The mutant actin-binding affinities vary greatly, and none of the nine mutations increase actin-binding affinity as much as L253P. ABD mutations causing high-affinity actin binding, with the notable exception of L253P, appear to be associated with early age of symptom onset. Altogether, the data indicate increased actin-binding affinity is a shared molecular consequence of numerous SCA5 mutations, which has important therapeutic implications [111].

2.1 Introduction

Spinocerebellar ataxia type 5 (SCA5) is a neurodegenerative disease stemming from autosomal dominant mutations in the *SPTBN2* gene encoding the cytoskeletal protein β-III-spectrin. Beta-III-spectrin is highly expressed in cerebellar Purkinje cells [65], the cell population targeted in SCA5 pathogenesis [69]. Within Purkinje cells, β-III-spectrin localizes to the soma and dendrites [65,66]. Mouse and cultured neuron models showed that β-III-spectrin function is required for normal dendritic arborization, spine morphology, and synaptic signaling [66–68,73,85]. Structurally, β-III-spectrin contains an N-terminal actin-binding domain (ABD), followed by seventeen spectrin-repeat domains, and a C-terminal pleckstrin homology domain. Analogous to other β-spectrins, the functional unit of β-III-spectrin is considered a heterotetramer composed of two β-III-spectrin subunits and two α-II-spectrin subunits. Super-resolution imaging of cortically localized β-III-spectrin supports a role for the β-III/α-II-spectrin heterotetramer in crosslinking actin filaments beneath the plasma membrane [85,86]. This spectrin-actin network, together with the spectrin adaptor protein, ankyrin-R, is likely important for maintaining proper subcellular localization of post-synaptic membrane proteins [66,72,112]. Many SCA5 mutations are known to localize to the ABD of β-III-spectrin [78], supporting the importance of actin binding and the formation of a spectrin-actin network to β-III-spectrin function.

Initial mapping of three SCA5 mutations to the *SPTBN2* gene was performed in 2006 [69]. These mutations, which included an ABD-localized L253P missense mutation, are associated with atrophy of the cerebellar cortex, and adult onset of symptoms that included progressive limb and gait ataxia, slurred speech and abnormal eye movements

[76,77,113]. More recently, additional heterozygous, dominant *SPTBN2* missense mutations were reported that are associated with early onset (infantile to adolescent) of symptoms. In addition to cerebellar atrophy and ataxia, these early onset cases are characterized by delayed motor development and sometimes intellectual disability [78–81]. These more severe symptoms resemble those of the neurodevelopmental disorder SPARCA1[74]/SCAR14[82], caused by homozygous recessive *SPTBN2* mutations. The SPARCA1/SCAR14 mutations are truncating mutations that are typically loss-of-function associated. Significantly, clinically normal parents heterozygous for the SPARCA1/SCAR14 loss-of-function alleles point away from haploinsufficiency as a disease mechanism for the heterozygous SCA5 mutations. For SCA5 mutations, the underlying dominant negative molecular mechanisms responsible for variability in age of onset and symptom severity are not known. Indeed, most SCA5 mutations have not been experimentally investigated at the molecular or cellular level.

We previously characterized the ABD-localized L253P missense mutation. The native L253 residue is positioned at the interface of the two calponin-homology subdomains (CH1 and CH2) comprising the ABD. Biochemically we showed that the L253P mutation causes a ~1000-fold increase in actin-binding affinity [57]. Through biophysical approaches, including cryo-EM, we showed that high-affinity actin binding caused by the CH2-localized L253P mutation, is due to an opening of the CH1-CH2 interface [19]. This alleviates CH2 occlusion of CH1, allowing CH1 to bind actin. We further showed that L253P induced high-affinity actin binding also requires an N-terminal helix, preceding CH1, that directly binds actin [92]. In neurons, L253P reduces dendritic localization of β-III-spectrin, and induces dendritic arbor defects in cultured

Purkinje cells [85] and Drosophila sensory neurons [91]. Truncation of the N-terminal helix preceding CH1 abolishes L253P-induced high-affinity actin binding and rescues L253P-induced dendritic arbor defects and neurotoxicity in Drosophila [92], supporting aberrant actin binding as a pathogenic mechanism. How other ABD-localized SCA5 mutations impact the structure and function of the ABD has yet to be explored.

In the present work, we characterize the molecular consequences of nine additional, heterozygous, missense mutations localizing to the β-III-spectrin ABD. Unlike L253P, many of these mutations are associated with early onset symptoms.

2.2 Materials and Methods

2.2.1 Protein Expression and Purification

Table 2.1: Sequence of DNA primers used in this study. The following primers were used to introduce SCA5 mutations into the β-III-spectrin ABD coding sequence and are listed 5' to 3':

Mutation	Forward Primer	Reverse Primer
V58M	CTGGCAGATGAACGAGAAGCTATGCAGAAGAAAACCTTCACCAAG	CTTGGTGAAGGTTTTCTTCTGCATAGCTTCTCGTTCATCTGCCAG
K61E	GAACGAGAAGCTGTGCAGAAGGAAACCTTCACCAAGTGGGTAAAC	GTTTACCCACTTGGTGAAGGTTTCCTTCTGCACAGCTTCTCGTTC
T62I	GAGAAGCTGTGCAGAAGAAAATCTTCACCAAGTGGGTAAACTC	GAGTTTACCCACTTGGTGAAGATTTTCTTCTGCACAGCTTCTC
K65E	GTGCAGAAGAAAACCTTCACCGAGTGGGTAAACTCGCACCTGGCC	GGCCAGGTGCGAGTTTACCCACTCGGTGAAGGTTTTCTTCTGCAC
F160C	GTCTGGACCATCATCCTTCGATGCCAGATCCAAGACATCAGTGTG	CACACTGATGTCTTGGATCTGGCATCGAAGGATGATGGTCCAGAC
D255G	GGACTTACCAAGCTGCTGGGTCCCGAAGACGTGAATGTGGACC	GGTCCACATTCACGTCTTCGGGACCCAGCAGCTTGGTAAGTCC
T271I	GCCAGATGAGAAGTCAATCATTATCTATGTGGCTACTTACTACC	GGTAGTAAGTAGCCACATAGATAATGATTGACTTCTCATCTGGC

Table 2.1- Continued

Mutation	Forward Primer	Reverse Primer
Y272H	GATGAGAAGTCAATCAT TACCCATGTGGCTACTTA CTACCATTAC	GTAATGGTAGTAAGTAGC CACATGGGTAATGATTGA CTTCTCATC
H278R	CTATGTGGCTACTTACTA CCGTTACTTCTCCAAGAT GAAG	CTTCATCTTGGAGAAGTA ACGGTAGTAAGTAGCCAC ATAG

Mutations for V58M, K61E, T62I, K65E, F160C, D255G, T271I, Y272H, and H278R were introduced into the β-III-spectrin ABD using the previously generated pE-SUMO-ABD WT construct [19], through site-directed PCR mutagenesis (PfuUltra High-Fidelity DNA Polymerase, Agilent) using the primers listed in Table 2.1. The resulting mutant DNAs were sequence verified. The previously generated pE-SUMO-ABD-L253P construct was utilized for subsequent experiments [92]. pE-SUMO-ABD constructs were transformed into Rosetta 2 (DE3) *E. coli* (Novagen). 250 mL to 1 L bacteria cultures were grown in LB broth with ampicillin (100 µg/mL) and chloramphenicol (34 µg/mL). ABD protein expression was induced with 0.5 mM IPTG, for 6 h, at 300 RPM and room temperature. Bacteria cultures were pelleted at 2987 RCF for 30 min at 4 °C, and pellets stored at -20 °C until further use. Bacterial pellets were resuspended in lysis buffer (50 mM Tris pH 7.5, 300 mM NaCl, 25% sucrose, and protease inhibitors (Complete Protease Inhibitor tablet, EDTA-free, Roche)), and lysed by incubation with lysozyme (Sigma) for 1 h at 4 °C, followed by a freeze-thaw cycle in an isopropanol-dry ice bath. To the lysate, $MgCl_2$ (10 mM final concentration) and DNase1 (Roche) (8 U/mL final concentration) were added and incubated with slow stirring for 1 h at 4 °C. Lysates were clarified at 18,000 RPM at 4 °C for 30 min, in a Sorvall SS-34 rotor. Supernatants were syringe filtered through 0.45 µm disk filters and loaded into Poly-Prep (Biorad)

chromatography columns containing Ni-NTA agarose (Qiagen) equilibrated in binding buffer containing 50 mM Tris pH 7.5, 300 mM NaCl and 20 mM imidazole. The columns were washed with binding buffer and then ABD proteins eluted with 50 mM Tris pH 7.5, 300 mM NaCl and 150 mM imidazole. For each mutant, elution fractions containing ABD protein was pooled and loaded into a Slide-a-Lyzer, 10 K MWCO, dialysis cassette (ThermoScientific) and dialysis performed overnight in 25 mM Tris pH 7.5, 150 mM NaCl, 5 mM β-mercaptoethanol, at 4 °C. 6X-His-SUMO tag was cleaved from ABD proteins using 1:10 mass ratio of Ulp1 SUMO protease:ABD in a 2 h incubation at 4 °C. Cleaved 6X-His SUMO tags and His-tagged SUMO protease were removed from the ABD proteins using 0.5 – 1 mL Ni-NTA agarose in a Poly-Prep chromatography column. Eluted fractions containing ABD proteins were pooled for each mutant and loaded into a Slide-a-Lyzer, 10 K MWCO, dialysis cassette for dialysis in 10 mM Tris pH 7.5, 150 mM NaCl, 2 mM $MgCl_2$, 1 mM DTT, at 4 °C for 15 h. Recovered ABD proteins were measured for concentration using Bradford assay and snap frozen in liquid nitrogen and stored at -80 °C for future use.

2.2.2 Circular Dichroism Measurements

Purified ABD proteins were thawed and clarified at 43,000 RPM at 4 °C for 30 min, in a Beckman TLA 100.3 rotor. Bradford assay (Biorad) was used to determine the ABD protein concentrations. ABD proteins were diluted to 150 – 200 ng/µL in buffer containing 10 mM Tris pH 7.5, 150 mM NaCl, 2 mM $MgCl_2$, 1 mM DTT. CD spectra were obtained in a Jasco J-815 Spectropolarimeter with a Peltier temperature controller. A baseline correction using diluent buffer was acquired immediately before analysis. Analyses were carried out between 200 and 260 nm at 25 °C. Wave length scans were an

average of five accumulations using a 1.0 mm cuvette. Thermal denaturation studies for each ABD protein were obtained in triplicate in a Jasco J-810 or J-815 Spectropolarimeter with Peltier temperature controller. Unfolding was measured at 222 nm with increasing temperature from 20 – 85 °C with a pitch of 1 °C per minute. To determine the melting temperature, non-linear regression analysis was performed using Prism 8 (GraphPad Software, Inc.) using an equation for two state transition, as previously described [114], and provided here:

$$Y = (\alpha_N + \beta_N \mathrm{T})/\{1 + e^{4T_m(T-T_m)/T\Delta T}\} + (\alpha_D + \beta_D \mathrm{T})/\{1 + e^{4T_m(T_m-T)/T\Delta T}\} \quad (2.1)$$

Where Y is the measured signal at 222 nm, α_N and β_N are intercept and slope of native state, T is the measured temperature, ΔT is the unfolding transition width, T_m is the fit melting temperature, and α_D and β_D are the intercept and slope of the denatured state. Constraints are as follows $\alpha_N > -0.2$, β_N and $\beta_D > 0$ and $\alpha_D < 1.1$.

2.2.3 F-actin Co-sedimentation Assays

F-actin was prepared and purified from rabbit skeletal muscle (Pel-Freez Biologics) as previously described [92]. Purified ABD proteins were thawed and clarified at 43,000 RPM at 4 °C for 30 min, in a Beckman TLA 100.3 rotor. Bradford assay (Biorad) was used to determine the F-actin and ABD protein concentrations. As performed previously [92], binding reactions were prepared with 2 µM ABD protein and increasing concentrations of F-actin (3 – 120 µM) in F-buffer (10 mM Tris pH 7.5, 150 mM NaCl, 0.5 mM ATP, 2 mM $MgCl_2$, and 1 mM DTT). After 30 min incubation at room temperature, binding reactions were centrifuged at 50,000 RPM for 30 min at 25 °C in a TLA-100 rotor (Beckman). Promptly after centrifugation, supernatants were sampled and mixed with Laemmle sample buffer (Biorad). Collected supernatant samples

were separated by SDS-PAGE and bands were visualized using Coomassie Brilliant Blue R-250 (Biorad) solution. After sufficient destaining to remove background, gels were imaged using the 680 nm channel of an Azure Sapphire imager. ABD protein band fluorescence intensities were quantified from image files using Image Studio Lite version 5.2 software. A standard curve was generated using various amounts of ABD proteins on a Coomassie stained gel to relate ABD fluorescence intensity to known ABD concentrations. The standard curves were used to convert raw fluorescence ABD signals to concentration for the binding assays. Using Prism 8 (GraphPad Software, Inc.), dissociation constants (Kd) were determined through a nonlinear regression fit for a one-site specific binding equation (2.2),

$$Y = X/(Kd + X) \quad (2.2)$$

where Y is the bound ABD fraction and X is the free F-actin concentration [15], with Bmax constrained to 1, as described previously [19].

2.2.4 Structural Modeling

The β-III-spectrin ABD structural homology model was generated through the i-Tasser server [115]. The top template structure was the plectin ABD (PDB ID: 1MB8). The crystal structure of β-II-spectrin calponin homology domain 2 (PDB ID: 1BKR) was used for alignment with the generated β-III-spectrin ABD homology model. Analyses of the structures, including identification of predicted contacts for different mutated residues, and alignment, was performed with PyMOL v2.5.4.

2.2.5 Statistical Analysis

Statistical significance was determined in Prism 8 (GraphPad Software, Inc.) for all melting temperatures and dissociation constants (above 1 μM), by One-way ANOVA

followed by Dunnett multiple comparisons post hoc test. P-values less than 0.05 were deemed significant.

2.3 Results

2.3.1 Clinical Summary of ABD-Localized Mutations

Here we report the molecular characterization of nine ataxia-associated, ABD-localized, missense mutations in β-III-spectrin. These mutations include: V58M, K61E, T62I, K65E, F160C, D255G, T271I, Y272H, and H278R. All mutations were heterozygous in patients, consistent with a dominant mechanism of action. T62I, K65E, F160C, D255G, and T271I were identified in patients with infantile onset (<12 mo) symptoms [78–80,84]. The compound heterozygous mutation Y272H/W2065* was identified in an infantile-onset patient [80]. Notably, parents carrying a single mutated allele (Y272H/+ or W2065*/+) were clinically normal (age of parents not reported). Thus, Y272H appears to genetically interact with W2065* to cause disease. This suggests that Y272H by itself is either insufficiently disruptive to cause symptoms, or the mutation causes mild, late onset symptoms not yet presenting in the Y272H/+ parent. For this study, only the normal clinical phenotype of the heterozygous (Y272H/+) parent will be considered. H278R was associated with adolescent symptom onset (11 years)[58]. K61E was early onset at an unconfirmed age, but evaluated at 9 years [84]. V58M was associated with adult onset (31 years) [84]. In addition to T271I and T62I characterized in this study, T271N [90] and T62N [88] mutations, not characterized here, are also associated with early age of onset. Additionally, another recently reported ABD-localized mutation, I162M [89], is associated with late onset of symptoms, but is not

characterized in this study. A detailed summary of clinical features is provided in Table 2.2.

Table 2.2: Clinical presentations of ataxia-associated mutations in the actin-binding domain of β-III-spectrin. Mutations not characterized in this study are shaded in grey.

***SPTBN2* gene mutation**	**Inheritance**	**Clinical Onset, Sex**	**Age at last evaluation**	**Clinical Features**	**Brain MRI findings**
c. 172 G > A (p. V58M) [84] heterozygous	familial	37 y, M n=1	61 y	Progressive cerebellar ataxia; Memory problems	Cerebellar Atrophy (Mild, stable)
c. 181 A > G (p. K61E) [84] heterozygous	de novo	Unknown, F n=1	9 y	Cerebellar ataxia; Hyperreflexia; Hypotonia; Dysarthria; Nystagmus	Cerebellar Atrophy
c.185 C >T (p. T62I) [80] heterozygous	not known	8 mo, F n=1	18 y	Cerebellar ataxia; Cognitive delay; Psychomotor delay; Microcephaly; Nystagmus; Hypotonia; Mild bradykinesia	Cerebellar Atrophy
c. 185 C > A (p. T62N) [88] heterozygous	de novo	5 mo, M n=1	1 y 4 mo	Cerebellar ataxia; Hypotonia; Brisk reflexes; Motor and cognitive developmental delay; Nystagmus; Strabismus	Severe Cerebellar Atrophy
c. 193 A > G (p. K65E) [78] heterozygous	de novo	4 mo, M n=1	11 y	Ataxia; Hypotonia; Ataxic gait; Dysarthria (understandable); Strabismus; Horizontal nystagmus; Dysmetria; Intention tremor (mild)	Progressive Cerebellar Atrophy
c.479 C > T (p. F160C) [80] heterozygous	de novo	5 mo, M n=1	5 y	Cerebellar ataxia; Psychomotor delay; Strabismus; Hypotonia; Cognitive delay; Unable to walk; Nonverbal	Progressive Cerebellar Atrophy
c. 486 C > G (p. I162M) [89] heterozygous	familial	48 y, F n=1	53 y	Cerebellar ataxia; Dysarthria; Ataxic gait	Moderate Cerebellar Atrophy

Table 2.2- Continued

***SPTBN2* gene mutation**	**Inheritance**	**Clinical Onset, Sex**	**Age at last evaluation**	**Clinical Features**	**Brain MRI findings**
c. 758 T > C (p. L253P) [113] heterozygous	familial	15-50 y, mean = 32.8 y, n=15	20 - 62 y	Stance, gait, and limb ataxia (14/15); Dysarthria (13/15); Intention tremor (5/15); Rest tremor (2/15); Nystagmus (13/15)	Cerebellar Atrophy
c. 764 A > G (p. D255G) [78] heterozygous	de novo	1 y, F n=1	8 y	Ataxia; Strabismus; Hypotonia; Bradykinesia; Ataxic gait; Dysarthria (difficult to understand); Intention tremor (moderate); ADHD	Progressive Cerebellar Atrophy
c.812 C > T (p. T271I) [79] heterozygous	de novo	6 mo, M n=1	8 y	Cerebellar ataxia; Motor developmental delay; Brisk reflexes; Ataxic gait and limb movements; Dystonia; Intention tremor	Progressive Cerebellar Atrophy
c. 812 C > A (p. T271N) [90] heterozygous	de novo	Unknown n=1	4 y 7 mo	Ataxia; Psychomotor retardation	Cerebellar Hypoplasia
c.888 T > C; + (p. Y272H/+) [80] heterozygous	familial	Unknown n=1	Adulthood	No symptoms	NA
c.833 A > G (p. H278R) [58]	de novo	11 y, F n=1	19 y	Cerebellar ataxia; Ataxic gait; Nystagmus	Cerebellar Atrophy

2.3.2 ABD-Localized Mutations Cluster to the CH1-CH2 Interface

To explore the position of the mutations in the β-III-spectrin ABD, a structural homology model was generated using iTasser [115], in which the plectin ABD (PDB ID: 1MB8) was the top template. The β-III-spectrin ABD is comprised of two subdomains, calponin homology domains 1 and 2 (CH1 and CH2), (Figure 2.1). Strikingly, all of the mutations are positioned at or near the interface of CH1 and CH2, like L253P. The native V58, K61, T62 and K65 amino acids localize to CH1 helix A, and are predicted to

directly contact CH2 residues. Notably, T62 and K65 directly contact CH2 residue L253, interactions we previously highlighted in our characterization of the L253P mutation [57]. The native F160 residue localizes to CH1 helix F. The F160 sidechain is not directly oriented towards CH2. However, F160 is predicted to contact CH1 residue, W66, which in turn contacts CH2 residues L253 and T271.

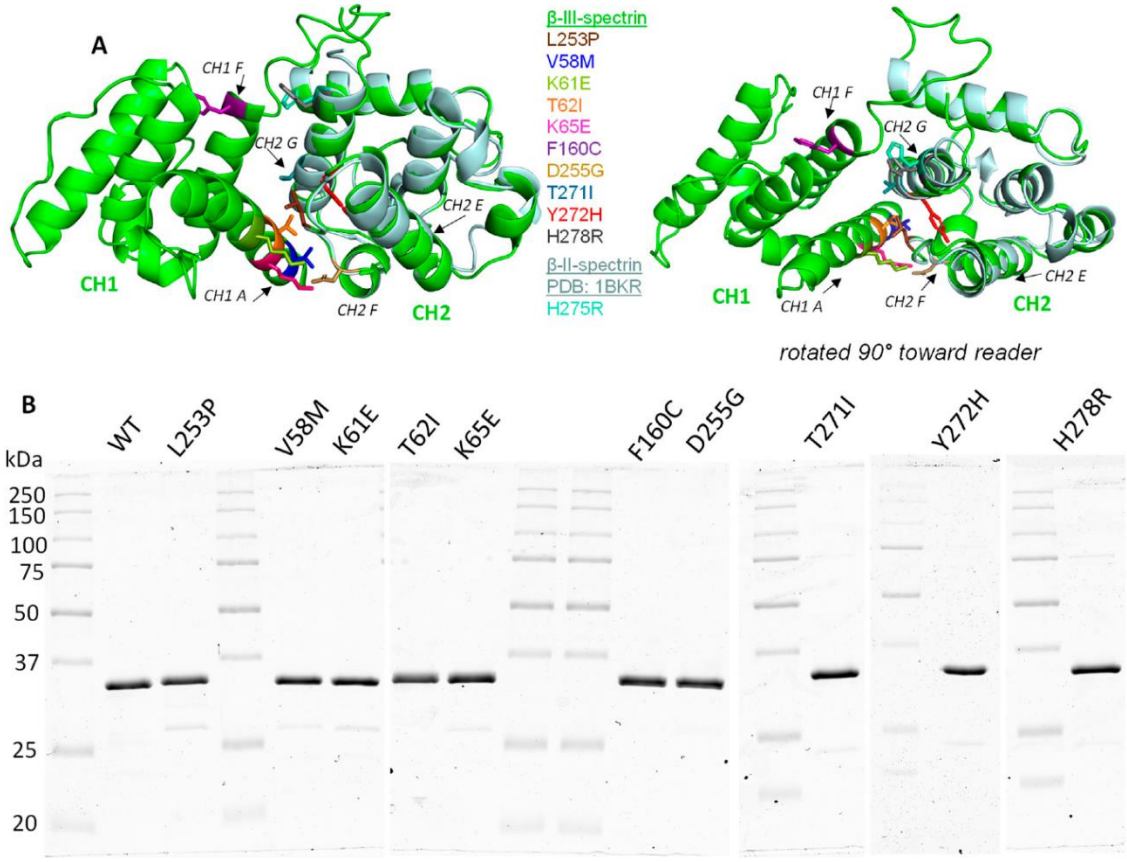

Figure 2.1: Position of SCA5 missense mutations in the actin-binding domain, and purification of mutant ABDs. A. Homology model of β-III-spectrin actin-binding domain (ABD; green), containing CH1 and CH2 subdomains (left) and a second view rotated 90° toward reader (right). Amino acids are color-coded for sites of mutations. The crystal structure of the isolated β-II-spectrin CH2 domain (blue-silver) is aligned with β-III-spectrin CH2. All mutated residues localize to the interface of the CH1 and CH2 subdomains. B. Coomassie blue stained gel images showing purified wild-type (WT) and mutant ABD proteins. All ABD proteins run at the predicted size of 32 kDa.

Mutations localizing to CH2 include D255G, T271I, Y272H, H278R and L253P. The native D255 localizes to a loop connecting CH2 helices E and F, and is predicted to form salt bridges with CH1 residues, K61 and K65. T271, Y272 and H278 localize to CH2 helix G. T271 is predicted to directly contact CH1 residues W66 and I157, in addition to contacting CH2 residue L253. Y272 forms extensive hydrophobic contacts with L253, suggesting that Y272 plays an important role in coordinating the position of L253. In the homology model, H278, while oriented towards CH1, is not predicted to contact CH1 residues. To further evaluate the position of H278, we analyzed the equivalent amino acid (H275) in a crystal structure of the isolated CH2 subdomain of β-II-spectrin [17]. Alignment of the β-II-spectrin CH2 domain with the β-III-spectrin ABD homology model shows that β-II-spectrin H275 is oriented towards CH1 and predicted to contact CH1 Q161. Thus, this suggests that β-III-spectrin H278 also contacts CH1 Q161. In sum, the mutated residues cluster to the CH1-CH2 interface. Many of the mutated residues contact each other, forming an interaction network likely important for bridging CH1 and CH2. The common position of these mutations at the CH1-CH2 interface suggests that the mutations have similar structural and functional impacts on the ABD.

2.3.3 SCA5 Mutant ABDs can Attain a Well-Folded State, but are Destabilized

To test how the SCA5 mutations impact the structure and function of the ABD, we expressed the wild-type and mutant ABD proteins in *E. coli* and performed protein purification. All ABD proteins were purified to homogeneity or contain only minor contaminating bands, (Figure 2.1). To determine if the SCA5 mutations impact the folded state of the ABD, circular dichroism (CD) spectroscopy was performed. Similar to our prior characterization [57], the wild-type ABD shows an α-helical absorption profile

with characteristic minima at 208 and 222 nm, (Figure 2.2). Similarly, all ABD mutants showed pronounced α-helical profiles.

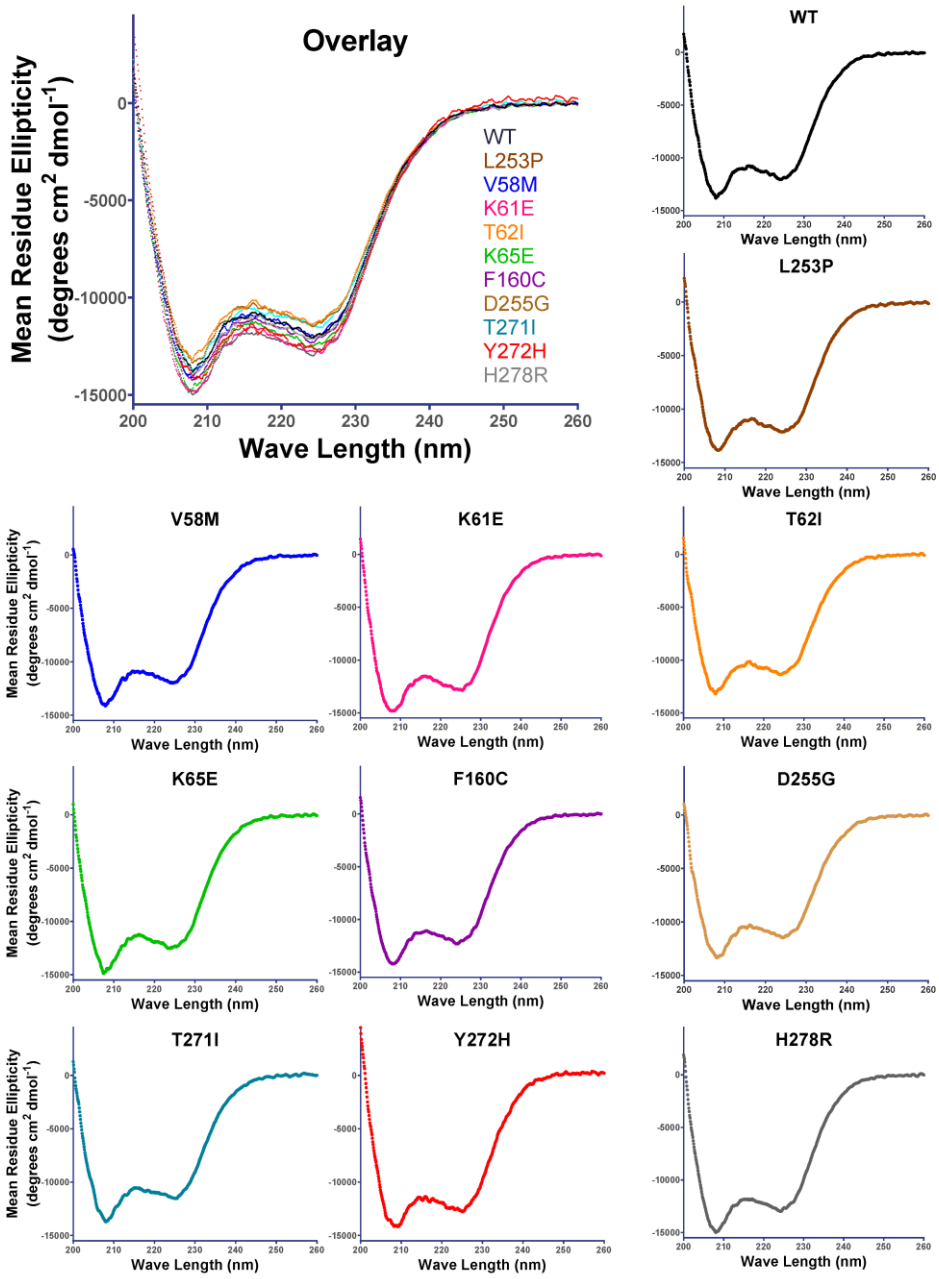

Figure 2.2: Circular dichroism absorption spectra show α-helical profiles for wild-type and mutant ABDs. CD spectra between 200 nm and 260 nm for individual wild-type, L253P, V58M, K61E, T62I, K65E, F160C, D255G, T271I, Y272H, and H278R ABD proteins. Minima at 208 and 222 nm are characteristic of α-helical fold. Spectra are average of n = 5 accumulations.

From this we conclude that all the mutant ABDs can attain a well-folded state without significant disruption to secondary structure. To determine how the mutations impact the stability of the ABD, CD thermal denaturation studies were performed. The wild-type

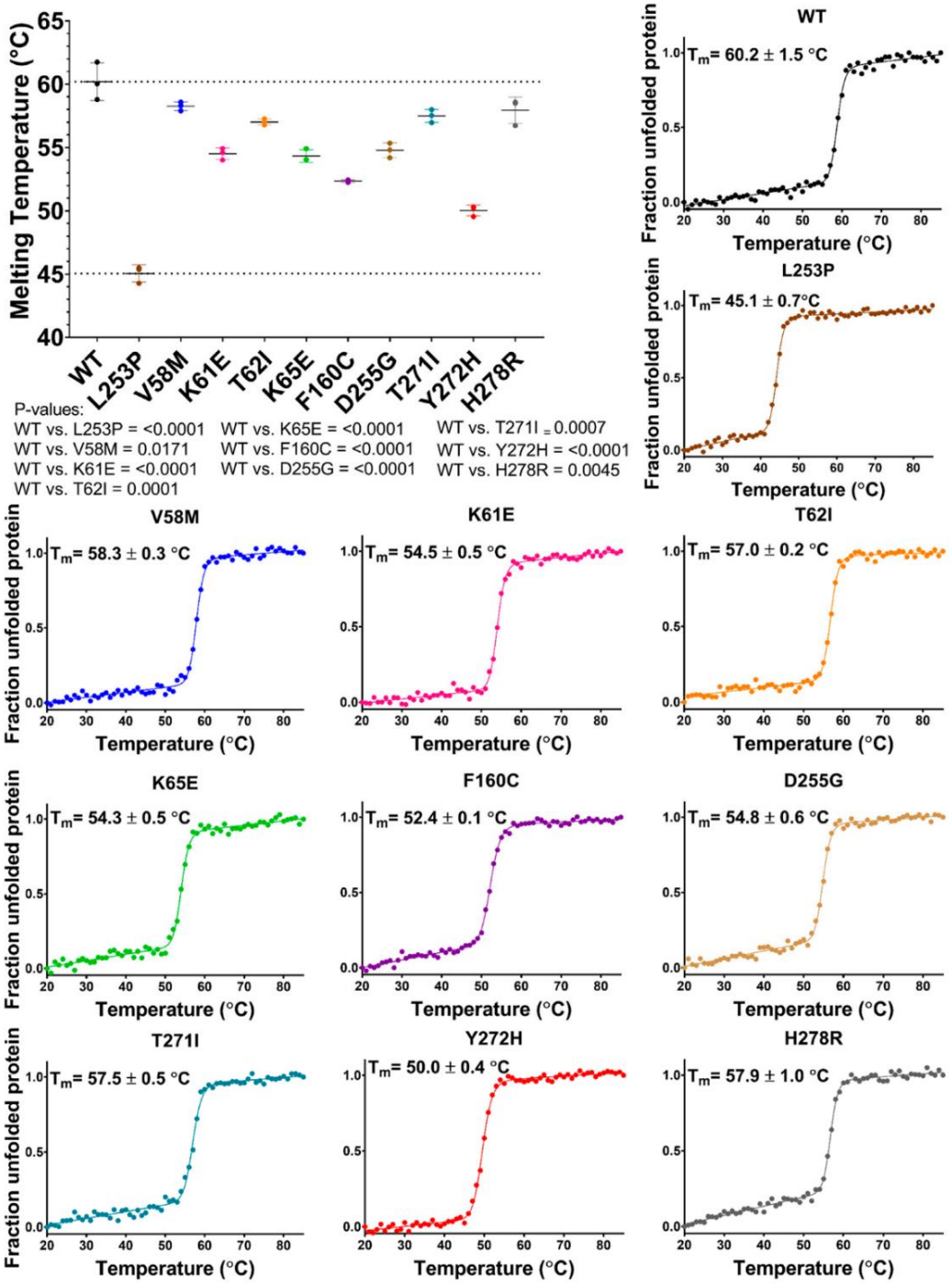

Figure 2.3: Thermal denaturation curves showing that all ABD proteins unfold cooperatively, but mutants are destabilized. Melting curves of purified ABD proteins, generated by monitoring circular dichroism absorption at 222 nm while heating sample. The cooperative, two-state, transitions indicate well-folded proteins. All mutant ABD proteins have Tm's significantly lower than wild-type. Statistical significance was determined by One-way ANOVA followed by multiple comparisons post hoc test. P-values are reported below the upper left panel. Tm = average +/- standard deviation, with n = 3.

ABD unfolded in a cooperative manner, characterized by a two-state transition and a melting temperature (Tm) of 60.2 ± 1.5°C (Figure 2.3), consistent with our prior report [57]. All mutant ABD proteins also displayed cooperative unfolding, further supporting a well-folded state for the mutant proteins. However, the mutants unfolded at statistically significant lower temperatures relative to wild-type, with Tm values ranging from 50.0 ± 0.4 to 58.3 ± 0.3°C. An exception was L253P, which unfolded with a much lower Tm, 45.1 ± 0.7°C, consistent with our prior characterization [57]. We previously showed that L253P protein destabilization is associated with an opening of the CH1-CH2 interface [19]. Thus, the current denaturation studies, together with the common position of the mutations at the CH1-CH2 interface, strongly suggest that all the mutations have a shared effect to structurally destabilize the CH1-CH2 interface.

2.3.4 All of the SCA5 Mutations Increase Actin-Binding Affinity

Previously, we showed that the L253P mutation causes a ~1000-fold increase in actin-binding affinity, with an estimated Kd of 75 nM [57]. To determine how the additional SCA5 mutations impact actin binding, *in vitro* co-sedimentations assays were performed using the purified ABD proteins. In these binding assays, a fixed amount of ABD (2 μM) is mixed with increasing concentrations of F-actin (3-120 μM), and the

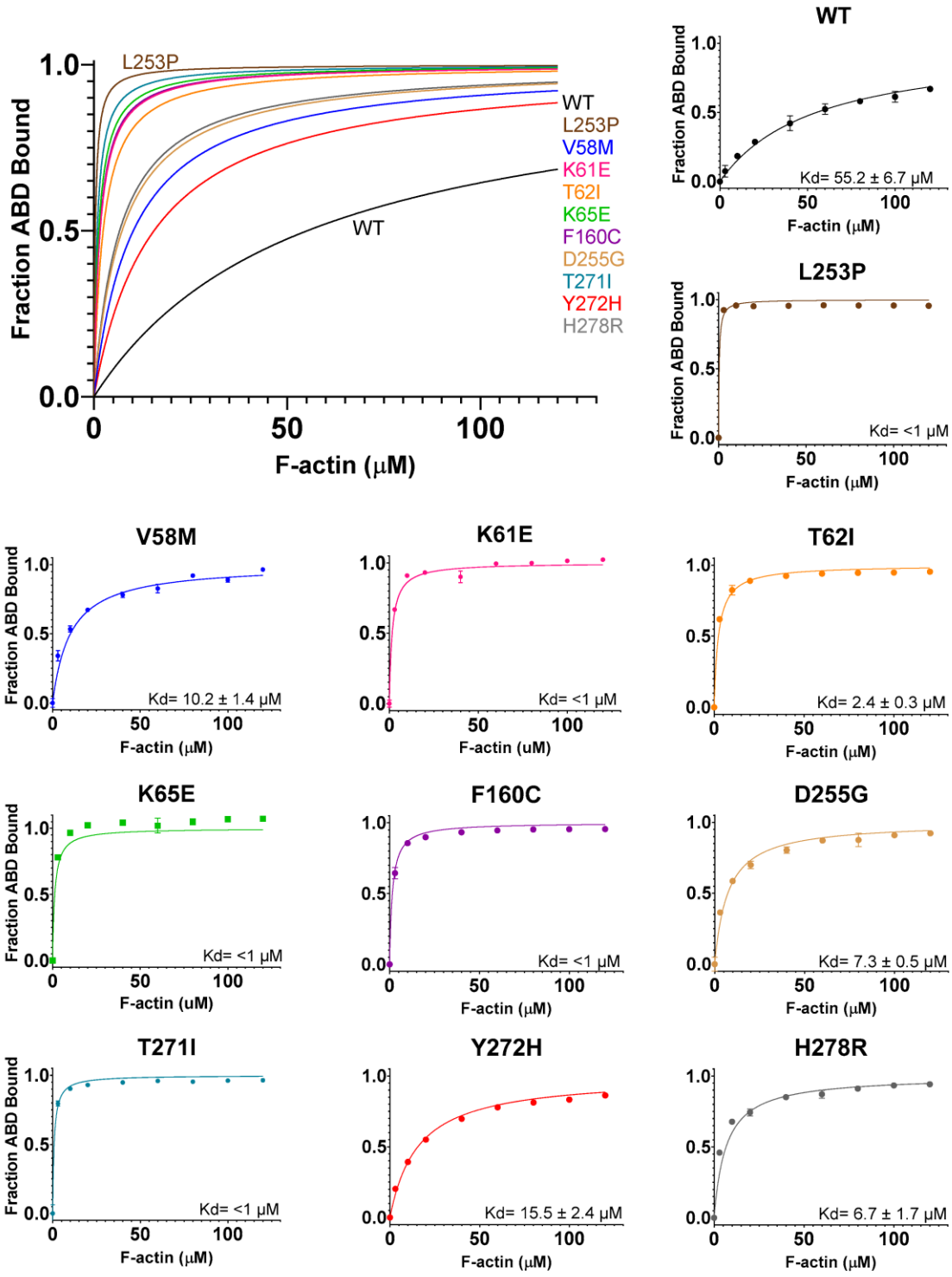
L253P
WT
V58M
K61E
T62I
K65E
F160C
D255G
T271I
Y272H
H278R
Fraction ABD Bound
F-actin (μM)
WT
Kd= 55.2 ± 6.7 μM
L253P
Kd= <1 μM
V58M
Kd= 10.2 ± 1.4 μM
K61E
Kd= <1 μM
T62I
Kd= 2.4 ± 0.3 μM
K65E
Kd= <1 μM
F160C
Kd= <1 μM
D255G
Kd= 7.3 ± 0.5 μM
T271I
Kd= <1 μM
Y272H
Kd= 15.5 ± 2.4 μM
H278R
Kd= 6.7 ± 1.7 μM

Figure 2.4: Actin co-sedimentation assays showing that all mutations increase actin-binding affinity. Co-sedimentation of ABD proteins and actin reveal greater actin affinities for all mutant ABD proteins compared to wild-type. Representative binding data and curve fit is shown for each mutant ABD protein. Kd = average +/- standard deviation, with n = 6 or more binding assays.

The wild-type ABD bound F-actin with a Kd of 55.2 ± 6.7 μM, (Figure 2.4). Significantly, all of the mutant ABDs bound actin with higher affinity than wild-type. Consistent with an estimated 75 nM Kd, the L253P ABD was entirely bound to F-actin at all F-actin concentrations tested (3 μM to 120 μM). Except at the lowest actin concentrations (3-10 μM), the K61E, K65E, F160C and T271I mutant ABDs were also fully bound to actin. This indicates that K61E, K65E, F160C and T271I mutations also cause high-affinity actin binding (submicromolar Kd). In contrast, V58M, T62I, D255G, Y272H and H278R mutations caused more modest increases in actin affinity. The Kd values for V58M, T62I, D255G, Y272H and H278R were statistically significant relative to wild-type, and equaled 10.2 ± 1.4 μM, 2.4 ± 0.3 μM, 7.3 ± 0.5 μM, 15.5 ± 2.4 μM and 6.7 ± 1.7 μM, respectively. In sum, all of the mutations cause increased actin-binding affinity, consistent with the shared position of these mutations at the CH1-CH2 interface. Notably, the actin-binding affinities vary greatly among the different mutations, with L253P causing the highest affinity and Y272H causing the smallest increase in affinity.

2.4 Discussion

Here we build upon our prior studies of the L253P mutation by characterizing nine additional, ABD-localized missense mutations. Strikingly, our structural analyses revealed that all of the newly characterized mutations, like L253P, localize to the CH1-CH2 interface. Many of the native residues are predicted to contact each other, forming

an interaction network likely important for bridging CH1 and CH2. Our circular dichroism analyses showed that the mutations are destabilizing, likely reflecting a structural uncoupling of CH1 and CH2, as we showed previously for L253P [19]. Our prior studies of the L253P mutation [19], along with studies of spectrin-related ABD proteins [18,22,23], established that opening of the CH1-CH2 interface is required for binding of CH1 to actin. Consistent with the position of the newly characterized mutations at the CH1-CH2 interface, and the destabilizing impact of these mutations, we show that all of the mutations cause increased actin binding. Thus, SCA5 mutations localizing to the ABD appear to act through a common molecular mechanism. It will be important to further validate a shared disease mechanism using in vivo approaches, for example, with mouse models, cultured Purkinje neurons, or patient-based materials.

Our prior studies of the L253P mutation in Drosophila suggest that high-affinity actin binding mislocalizes the spectrin cytoskeleton in neurons, causing the mutant β-spectrin and associated proteins to accumulate in the soma and be depleted in the dendritic arbor [91]. Consequently, distal dendrites degenerate and dendritic arbor outgrowth is reduced. Recently, a similar mislocalization of L253P β-III-spectrin was reported in transfected mouse Purkinje neurons [85]. Here the L253P mutant caused misorientation of dendrites, resulting in reduced planarity of the Purkinje cell dendritic arbor. If increased actin binding drives pathogenesis for all ABD-localized SCA5 mutations, then we expect that the nine newly characterized mutations will result in spectrin mislocalization and arborization defects in these neuronal systems, similar to L253P. However, for the newly characterized mutations, the observed neuronal defects

may be less severe due to the lesser effect of these mutations to increase actin-binding affinity, relative to L253P.

A potentially important finding from the present study is that the actin-binding affinities of the mutants vary greatly. Perhaps this variability in actin-binding affinity contributes to the variability in age of onset (and symptom severity). In Table 2.3, our experimentally determined Kd values are listed for each of the mutations, along with clinical data on age of symptom onset. As evident in Table 3, most of the nine newly characterized mutations are associated with early onset of symptoms (infant to adolescent). These early onset mutations are associated with single digit micromolar to submicromolar Kd values. In contrast, with a Kd value of 10 μM, V58M is associated with adult onset of symptoms (37y). Further Y272H, with a Kd of 16 μM, causes the smallest increase in actin binding among the mutations. A Y272H/+ parent, of unknown age, was reported to be clinically normal [80]. This supports that a modest increase in actin binding can be tolerated (no clinical phenotype), and that symptoms are more likely to present as actin-binding affinity increases. In sum, a correlation appears to be emerging in which high-affinity actin binding (submicromolar to single digit micromolar Kd) is associated with early age of symptom onset, and that smaller increases in actin-binding affinities (10 micromolar or higher Kd) are associated with later onset or no disease symptoms. However, a strong correlation is still difficult to establish, as most of the mutations are de novo, and n values equal 1. Thus, it is important to collect clinical data on age of onset from additional patients carrying the same mutations, and to further characterize distinct ABD-localized, ataxia-associated mutations, as they are reported. For example, the recently reported T62N and T271N mutations are early onset, and

would be expected to have submicromolar to single digit micromolar Kd values. In contrast, a CH1-CH2 interface mutation, I162M, causes late onset symptoms, and would be expected to have a higher Kd value. Importantly, the L253P mutation, which causes the highest actin-binding affinity, but is associated with late onset of symptoms (mean = 32.8y), is a major outlier to our proposed association between actin-binding affinity and age of onset, as discussed below.

Table 2.3: Actin-binding affinity and age of symptom onset for different ABD mutations

Mutation	Kd (μM)	Age of onset
L253P	< 1	15-50 y, mean=32.8 y, n=15
T271I	< 1	6 mo, n=1
K65E	< 1	4 mo, n=1
F160C	< 1	5 mo, n=1
K61E	< 1	Not reported; clinical evaluation at 9 y, n=1
T62I	2.4 ± 0.3	8 mo, n=1
H278R	6.7 ± 1.7	11 y, n=1
D255G	7.3 ± 0.5	12 mo, n=1
V58M	10.2 ± 1.4	37 y, n=1
Y272H/+	15.3 ± 2.0	Y272H/+ parent is clinically normal, n=1
Wild-type	55.2 ± 6.7	NA

Our data show that L253P is unique among the mutations in that it causes 1) the highest actin-binding affinity, and 2) the greatest protein destabilization. It thus seems likely that the decreased clinical severity of L253P is attributed to one or both of these features. Our current and prior [57] thermal denaturation studies show in vitro that L253P ABD begins to unfold near physiological temperature. It is thus possible that L253P β-III-spectrin is prone to denaturation and enhanced protein turnover in cells at physiological temperature. Increased protein turnover of the L253P mutant would reduce its abundance in neurons, corresponding to a reduction in neurotoxicity and a later age of

symptom onset. However, in transiently transfected HEK293T cells, wild-type and L253P β-III-spectrin ABD or full-length proteins showed similar protein levels by western blot analyses [91]. Clarkson et al additionally showed that L253P β-III-spectrin did not induce pathways associated with unfolded protein response [87]. Moreover, we showed that L253P, and a L253A mutation, which causes high-affinity actin binding, but is less destabilizing than L253P, cause similar mislocalization (absence from plasma membrane extensions and internal accumulation on actin-rich vesicles) of β-III-spectrin in HEK293T cells [91]. This supports that the behavior of the L253P mutant β-III-spectrin in cells is driven by elevated actin binding, not protein denaturation/unfolding. Alternatively, it is possible that high-affinity actin binding localizes the L253P mutant to a distinct population of actin filaments not bound by the ABD mutants with relatively lower actin-binding affinity. Future studies assessing the impact of L253P versus the other ABD mutations on mutant β-III-spectrin steady-state protein levels and subcellular localization in cultured Purkinje neurons, mouse models, or patient-based materials, may clarify why L253P has reduced toxicity/late onset symptoms.

Our finding here that increased actin-binding affinity is a shared molecular consequence of numerous SCA5 mutations has important therapeutic implications. Specifically, it suggests that a small molecule drug that can alleviate high-affinity actin binding may be broadly useful as a SCA5 therapeutic. Recently we reported the identification of several small molecules capable of reducing binding of the L253P mutant to actin in vitro [93]. This established that the spectrin-actin interaction can be targeted by small molecules. Potentially these compounds will be effective in reducing actin binding caused by the multiple different SCA5 mutations characterized here. Our

analysis of Kd versus age of symptom onset suggests that reducing actin-binding affinity to a Kd value of ~16 μM (Y272H) or higher may be needed to fully eliminate toxicity caused by the ABD mutations.

CHAPTER THREE

CARDIOMYOPATHY-ASSOCIATED VARIANTS ALTER THE STRUCTURE AND FUNCTION OF THE α-ACTININ-2 ACTIN-BINDING DOMAIN

3.0 Abstract

Hypertrophic cardiomyopathy (HCM), dilated cardiomyopathy (DCM), and restrictive cardiomyopathy (RCM) are characterized by thickening, thinning, or stiffening, respectively, of the ventricular myocardium, resulting in diastolic or systolic dysfunction that can lead to heart failure and sudden cardiac death. Recently, variants in the *ACTN2* gene, encoding the protein α-actinin-2, have been reported in HCM, DCM, and RCM patients. However, functional data supporting the pathogenicity of these variants is limited, and potential mechanisms by which these variants cause disease are largely unexplored. Currently, NIH ClinVar lists 34 *ACTN2* missense variants, identified in cardiomyopathy patients, which we predict are likely to disrupt actin binding, based on their localization to specific substructures in the α-actinin-2 actin binding domain (ABD). We investigated the molecular consequences of three ABD localized, HCM-associated variants: A119T, M228T and T247M. Using circular dichroism, we demonstrate that the mutant ABD proteins can attain a well-folded state. However, thermal denaturation studies show that all three mutations are destabilizing, suggesting a structural disruption. Importantly, A119T decreased actin binding, and M228T and T247M cause increased actin binding. We suggest that altered actin binding underlies pathogenesis for cardiomyopathy mutations localizing to the ABD of α-actinin-2 [116].

3.1 Introduction

In the United States, the prevalence of heart failure due to cardiomyopathy was estimated at 6.7 million cases in 2020, an increase of 12% over 2 years [109]. Two of the most common cardiomyopathies are Dilated Cardiomyopathy (DCM) and Hypertrophic Cardiomyopathy (HCM), combined estimated to occur in greater than 0.2% of the general population [117,118]. Restrictive Cardiomyopathy (RCM), a less common form, is estimated to account for 5% of total cardiomyopathy cases [119]. These disorders are characterized by thickening (HCM), thinning (DCM), or stiffening (RCM) of the ventricular myocardium [107]. These alterations to the ventricle wall cause diastolic or systolic dysfunction, and can lead to heart failure and sudden cardiac death [108]. A better understanding of cardiomyopathy etiology and pathogenesis is thus important for reducing the burden of cardiac disease for a significant portion of the population.

The familial forms of DCM, HCM, and RCM typically display autosomal dominant inheritance [107]. Interestingly, dominant mutations in the *ACTN2* gene encoding the Z-disk protein α-actinin-2 have been reported in DCM [105], HCM [101] and RCM [106] patients. How different variants in the *ACTN2* gene give rise to different cardiomyopathies is unclear. Currently, the NIH ClinVar database [110] lists 324 cardiomyopathy-associated *ACTN2* variants that result in amino acid changes in the encoded α-actinin-2 protein. The pathogenicity of two *ACTN2* missense variants, A119T and M228T, is supported by co-segregation of the variants with heart disease across multiple generations within families [101,102]. However, for most reported *ACTN2* variants, the pedigree is either too small, or no family history is available to conclude that

a genetic variant is disease causing. In these cases, additional functional studies are needed to determine if a variant is detrimental to α-actinin-2 function.

Alpha-actinin-2 is expressed in skeletal and cardiac muscle fibers [31], and is required for normal sarcomere organization in the heart [56]. Within the Z-disk, α-actinin-2 functions to cross-link antiparallel actin filaments from neighboring sarcomeres. Alpha-actinin-2 contains an N-terminal actin-binding domain (ABD; amino acids 1-259) consisting of two calponin homology subdomains (CH1 and CH2). Assembly of the Z-disk requires α-actinin-2 binding to actin. Interestingly, α-actinin-2 localization to the Z-disk is highly dynamic [14,21,100]. This suggests that dynamic binding of α-actinin-2 to F-actin is required in healthy tissue to enable rapid Z-disk remodeling.

Alpha-actinin is the ancestral member of the spectrin superfamily of cytoskeletal proteins that includes the human disease-associated proteins: β-III-spectrin; α-actinin-1 and -4; filamin A, B, and C; and dystrophin [8,57–62,120–122]. We previously characterized a β-III-spectrin L253P missense mutation that is localized to the ABD and causes the neurological disorder spinocerebellar ataxia type 5 (SCA5). In vitro co-sedimentation assays revealed that L253P causes a striking 1000-fold increase in actin affinity [57]. Further, our cryo-EM structure of F-actin complexed with the L253P ABD demonstrated that actin binding requires a conformational “opening” at the interface of the two CH domains that comprise the ABD. This enables CH1 to bind actin aided by the previously uncharacterized, unstructured N-terminal region that becomes α-helical upon binding [19]. Strikingly, this N-terminal helix preceding the conserved CH1 domain is required for association with actin, as truncation eliminates binding. Alpha-actinin-2 likely binds actin by a similar mechanism. Indeed, our review of cryo-EM data for the α-

actinin-4-actin complex [18] suggested that the N-terminus of α-actinin-2 also binds actin [19].

However, mechanistic studies of cardiomyopathy-associated variants in the α-actinin-2 ABD are scarce. Haywood et al, reported that the HCM-associated variant A119T caused protein destabilization *in vitro,* aggregation of the mutant α-actinin-2 in cardiomyocytes, and reduced Z-disk incorporation [14]. A119T was reported to cause a 2-fold decrease in actin-binding affinity [14], although the reported decrease in affinity was not statistically significant. A study of an HCM-associated variant, T247M, established in iPSC-derived cardiomyocytes, showed that the variant is disruptive at the cellular level, inducing HCM phenotypes, including Z-disk myofibrillar disarray and disrupted contractility [100]. Moreover, T247M, like A119T, caused α-actinin-2 aggregation and reduced incorporation into Z-disks [123]. How the T247M variant impacts actin binding is not known. A recent study has shown that homozygous expression of HCM associated M228T variant in mice is embryonic lethal [97]. Further, low α-actinin-2 mutant protein levels suggested that the mutant promotes destabilization contributing to increased proteolysis [97]. Because of the dynamic nature of α-actinin-2 at the Z-disk, and the requirement of actin binding for α-actinin-2 incorporation into the Z-disk, it is likely that ABD variants that disrupt actin binding will adversely impact cardiomyocyte function.

In this study, we report our analyses of the structural position of numerous cardiomyopathy-associated *ACTN2* missense variants to assess the potential of the variants to disrupt α-actinin-2 actin binding. We further report our characterization of the

structural and functional consequences of select missense variants localized to different substructures in the α-actinin-2 ABD.

3.2 Materials and Methods

3.2.1 Structural Analysis

Analyses were performed using a crystal structure of the wild-type α-actinin-2 ABD (PDB:5A36) [14]. Actin binding region identified by homology comparison with three different ABDs including of β-III-spectrin, filamin A and utrophin ABD-actin complexes [19,23,124]. Analyses of the structure, including identification of predicted contacts for different mutated residues, was performed with PyMOL v2.5.4

3.2.2 Protein Expression and Purification

The coding sequence for α-actinin-2-ABD was obtained from Addgene (RefSeq: NM_001103.3, Plasmid ID 52669) and PCR amplified using the forward primer AAACACCTGCAAAAAGGTATGAACCAGATAGAGCCCGGC and reverse primer AAATCTAGATTACTCCGCGCCCGCAAAAGCGTG. The PCR product was digested with restriction enzymes AarI and XbaI and ligated into BsaI digested, pE-SUMOpro (LifeSensors). Mutations were introduced into the generated pE-SUMO-α-actinin-2 ABD through site-directed PCR mutagenesis (PfuUltra High-Fidelity DNA Polymerase, Agilent). The following primers were used to introduce cardiomyopathy mutations into the α-actinin-2 ABD sequence.

Table 3.1: Sequence of DNA primers used in this study. Primers are listed 5' to 3'

Mutation	Forward Primer	Reverse Primer
A119T	GTGAAACTGGTGTCCATC GGCACTGAAGAAATTGTT GATGGCAAT	ATTGCCATCAACAATTTCTTC AGTGCCGATGGACACCAGTTT CAC

Table 3.1-Continued

Mutation	Forward Primer	Reverse Primer
M228T	AGCACCTGGATATTCCTA AAACGTTGGATGCTGAAG ACATCGTG	CACGATGTCTTCAGCATCCAA CGTTTTAGGAATATCCAGGTG CT
T247M	CCCGATGAAAGAGCCATC ATGATGTACGTCTCTTGC TTCTACCAC	GTGGTAGAAGCAAGAGACGT ACATCATGATGGCTCTTTCAT CGGG

Sequence verified mutant and wild-type DNAs were transformed into Rosetta 2 (DE3) *E. coli* (NOVAgen.1 L bacteria cultures in LB broth containing ampicillin (100 µg/mL) and chloramphenicol (34 µg/mL) were grown at 37 °C. Upon OD_{550} of 0.50, ABD protein expression was induced with 0.5 mM IPTG for 6 hours at 300 RPM shaking at room temperature. Bacteria cultures were pelleted at 2987 RCF for 30 min at 4 °C, and pellets stored at -20°C until further use. Bacterial pellets were prepared for lysis through resuspension in lysis buffer (50 mM Tris pH 7.5, 300 mM NaCl, 25% sucrose, and protease inhibitors (Complete Protease Inhibitor tablet, EDTA-free, Roche)), and incubated with lysozyme (Sigma) for 1 h at 4 °C, followed by a freeze-thaw cycle in an isopropanol-dry ice bath. To the lysate, $MgCl_2$ (10 mM final concentration) and DNase1 (Roche) (8 U/mL final concentration) were added and stirred slowly for 1 h at 4 °C. Lysates were clarified at 18,000 RPM at 4 °C for 30 min, in a Sorvall SS-34 rotor. Supernatants were decanted and syringe filtered through 0.45 µm disk filters. Poly-Prep (Biorad) chromatography columns containing Ni-NTA agarose (Qiagen) were equilibrated in binding buffer (50 mM Tris pH 7.5, 300 mM NaCl and 20 mM imidazole) and filtrate was loaded. Binding buffer was used to wash the columns and ABD proteins were eluted with elution buffer (50 mM Tris pH 7.5, 300 mM NaCl and 150 mM imidazole). Elution fractions for each ABD protein were pooled and loaded into a Slide-

a-Lyzer, 10 K MWCO, dialysis cassette (ThermoScientific) and dialysis carried out overnight in SUMO buffer (25 mM Tris pH 7.5, 150 mM NaCl, 5 mM β-mercaptoethanol), at 4 °C. Cleavage of the 6X-His-SUMO tag from the ABD protein was performed using 1:10 mass ratio of Ulp1 SUMO protease:ABD in a 1 h incubation at 4 °C. Poly-Prep chromatography columns containing 1 mL Ni-NTA agarose equilibrated in SUMO buffer were used to remove cleaved 6X-His SUMO tags and His-tagged SUMO protease from the ABD proteins. Eluted fractions containing ABD proteins were pooled for each ABD and loaded into a Slide-a-Lyzer, 10 K MWCO, dialysis cassette for dialysis in storage buffer (10 mM Tris pH 7.5, 150 mM NaCl, 2 mM MgCl2, and 1 mM DTT), at 4 °C overnight. Purified ABD proteins were recovered and measured for concentration using Bradford assay (Biorad). ABD proteins were snap frozen in liquid nitrogen and stored at -80 °C for future use.

3.2.3 Circular Dichroism Measurements

Previously purified ABD proteins were thawed and clarified at 43,000 RPM at 4 °C for 30 min, in a Beckman TLA 100.3 rotor. Bradford assay was used to determine the ABD protein concentrations. ABD proteins were diluted to 150 – 200 ng/µL in storage buffer. CD spectra and thermal denaturation studies were performed with a Jasco J-815 Spectropolarimeter with a Peltier temperature controller. Baseline correction scans were obtained using the storage buffer immediately prior to analysis. Analyses ranged between 200 and 260 nm at 25 °C. Immediately following wavelength scans, unfolding was measured at 222 nm with steadily ramping temperatures from 20 – 85 °C. Using Prism 9 (GraphPad), a nonlinear regression analysis was performed to determine melting

temperature for two-state and three state transitions [114]. The two-state unfolding is fit by equation 3.1,

$$Y = (\alpha_N + \beta_N \mathrm{T})/\{1 + e^{4T_m(T-T_m)/T\Delta T}\} + (\alpha_D + \beta_D \mathrm{T})/\{1 + e^{4T_m(T_m-T)/T\Delta T}\} \quad (3.1)$$

where α_N, β_N, α_D, and β_D are the intercepts and slopes of the respective native and denatured states, Y is the signal at 222 nm at temperature T, ΔT is the unfolding transition width and T_m is the melting temperature. The three-state unfolding is fit by the expanded equation 3.2,

$$Y = (\alpha_N + \beta_N \mathrm{T})/\{1 + e^{4T_{m1}(T-T_{m1})/T\Delta T}\} + (\alpha_1 + \beta_1 \mathrm{T})/\{1 + e^{4T_{m1}(T_{m1}-T)/T\Delta T}\} + (\alpha_1 + \beta_1 \mathrm{T})/\{1 + e^{4T_{m2}(T-T_{m2})/T\Delta T}\} + (\alpha_D + \beta_D \mathrm{T})/\{1 + e^{4T_{m2}(T_{m2}-T)/T\Delta T}\} \quad (3.2)$$

where, α_1 and β_1 are the intercept and slope of the intermediate state, T_{m1} and T_{m2} are the respective melting temperatures of the first state between folded and the intermediate and the second state between the intermediate and unfolded state. The four-state unfolding is fit by the expanded equation 3.3,

$$Y = (\alpha_N + \beta_N \mathrm{T})/\{1 + e^{4T_{m1}(T-T_{m1})/T\Delta T}\} + (\alpha_1 + \beta_1 \mathrm{T})/\{1 + e^{4T_{m1}(T_{m1}-T)/T\Delta T}\} + (\alpha_1 + \beta_1 \mathrm{T})/\{1 + e^{4T_{m2}(T-T_{m2})/T\Delta T}\} + (\alpha_2 + \beta_2 \mathrm{T})/\{1 + e^{4T_{m2}(T_{m2}-T)/T\Delta T}\} + (\alpha_2 + \beta_2 \mathrm{T})/\{1 + e^{4T_{m3}(T-T_{m3})/T\Delta T}\} + (\alpha_D + \beta_D \mathrm{T})/\{1 + e^{4T_{m3}(T_{m3}-T)/T\Delta T}\} \quad (3.3)$$

where, α_2 and β_2 are intercept and slope of the second intermediate state, T_{m2} and T_{m3} are the melting temperatures of the second state between the first and second intermediate and the second intermediate and the unfolded state.

3.2.4 F-actin Co-sedimentation Assays

Purified F-actin was prepared from rabbit skeletal muscle (Pel-Freez Biologics) as previously described [92]. Purified ABD proteins were thawed and clarified as described above. F-actin and ABD protein concentrations were determined though Bradford assay.

As performed previously [92], binding reactions were prepared with 2 µM ABD protein and F-actin concentrations ranging from 3 – 120 µM in F-buffer (10 mM Tris pH 7.5, 150 mM NaCl, 0.5 mM ATP, 2 mM MgCl2, and 1 mM DTT). Immediately following 30 min incubation in ambient room temperature, binding reactions were centrifuged at 50,000 RPM for 30 min at 25 °C in a TLA-100 rotor (Beckman). Following centrifugation, supernatants were immediately sampled and mixed with 4X Laemmle sample buffer (Biorad). Samples of supernatant were separated by SDS-PAGE and resulting bands were visualized using Coomassie Brilliant Blue R-250 (Biorad) solution, followed by background removal with destain solution. An Azure Sapphire imager on the 680 nm channel was used to document the gels. The generated image files allowed quantification of ABD protein band fluorescence intensities using Image Studio Lite version 5.2 software. A standard curve was generated using incremental amounts of ABD proteins (0-2 µM) on a similarly treated gel, relating supernatant ABD fluorescence intensity to known ABD concentrations. As previously described [57], dissociation constants (Kd) were calculated using Prism 9 (Graphpad) through a nonlinear regression fit utilizing a one-site specific binding equation, constraining Bmax to 1.

3.3 Results

3.3.1 Cardiomyopathy Missense Variants Localize to Actin-Binding Surfaces or the CH1-CH2 Interface in the α-Actinin-2 ABD

We analyzed 71 cardiomyopathy-associated *ACTN2* variants in NIH ClinVar to evaluate the potential of the variants to disrupt actin binding, based on their localization to specific substructures in the ABD. We mapped predicted actin-binding surfaces in the crystal structure of the wild-type α-actinin-2 ABD (PDB: 5A36) [14] based on homology

to the actin-binding surfaces identified in cryo-EM models of β-III-spectrin, filamin A and utrophin ABD-actin complexes [19,22,23] (Figure 3.1).

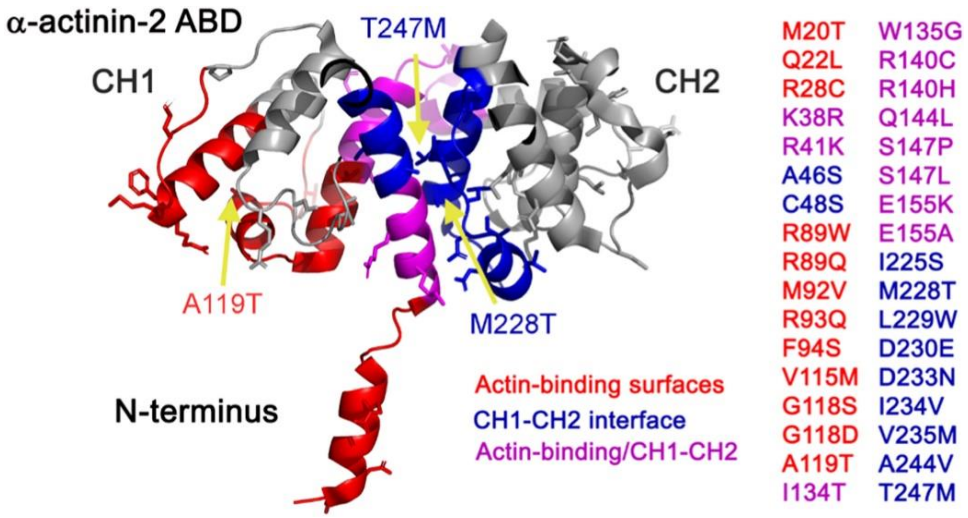

Figure 3.1: Mapping of ACTN2 variants in the ABD. The α-actinin-2 ABD crystal structure (PDB: 5A36) with actin-binding surfaces (red), contact regions between CH1 and CH2 subdomains (blue), and regions involved in both interactions (magenta). Listed are 34 cardiomyopathy missense variants localizing to these surfaces (sidechains of native residues shown). Yellow arrows indicate positions of A119T, M228T and T247M.

In addition, residues mediating interaction of CH1 to the regulatory CH2 subdomain were identified using Pymol. Of the 71 ClinVar variants in the ABD, 34 localize to actin-binding surfaces in CH1 or the N-terminus, or to the CH1-CH2 interface. We predict that variants localizing to actin-binding surfaces will decrease actin binding. In contrast, variants localizing to the CH1-CH2 interface are likely to increase actin binding by alleviating CH2 occlusion of CH1 binding to actin.

3.3.2 Human α-Actinin-2 Cardiomyopathy Missense Variants Attain Folded States but Lose Cooperative Protein Unfolding.

To assess the impact of the variants on ABD structure, circular dichroism (CD) spectroscopy was performed. The CD absorption spectra for the wild-type ABD shows

minima at 208 and 222 nm, an absorption profile characteristic of an alpha-helical protein, (Figure 3.2). Similarly, the three variants showed nearly identical absorption profiles. This indicates the variant ABDs are well-folded like wild-type.

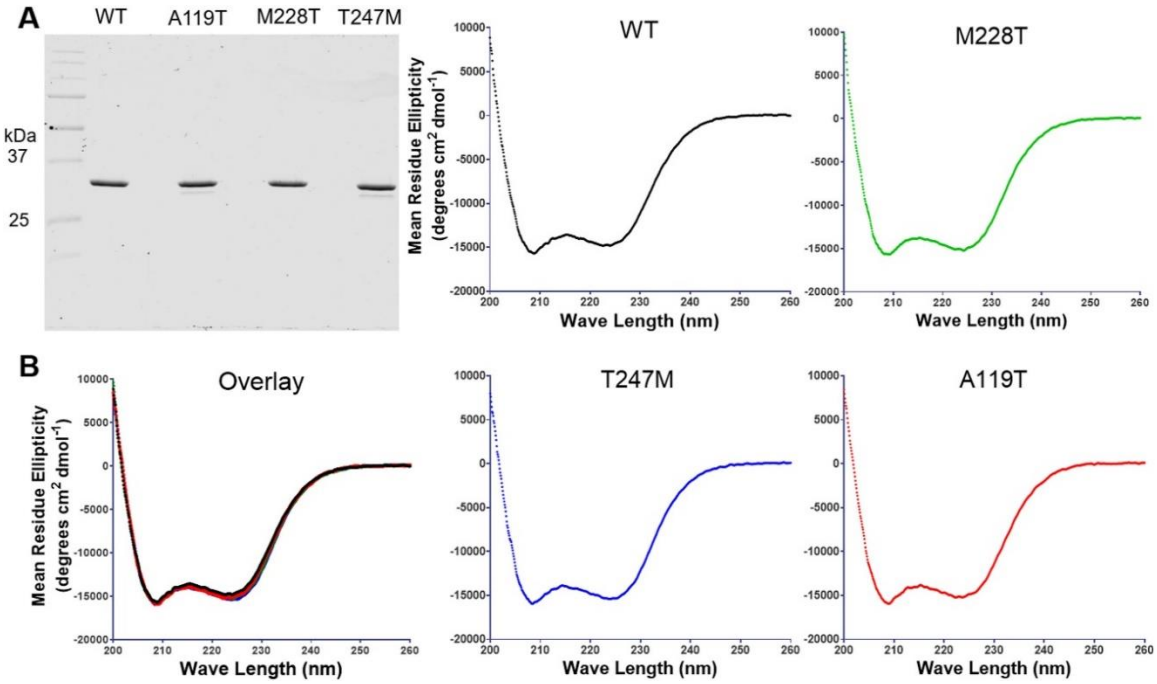

Figure 3.2: α-actinin-2 mutants attain secondary structures similar to wild-type. A. Coomassie blue stained gel image showing purified wild-type (WT) and mutant ABD proteins. All ABD proteins ran at the predicted size of 30 kDa. B. Circular dichroism absorption spectra show α-helical profiles for wild-type and mutant ABDs. CD spectra between 200 nm and 260 nm for individual WT, A119T, M228T, and T247M proteins. Minima at 208 and 222 nm are characteristic of α-helical fold.

CD was further used to monitor the unfolding of the ABD proteins as a function of temperature. The wild-type protein displayed cooperative unfolding, with a single step, two-state transition, and a melting temperature (T_m) of 63.5˚C, (Figure 3.3). This T_m is similar to a previously reported T_m (62.3˚C) for a wild-type α-actinin-2 ABD construct containing amino acids 19-266 [14].

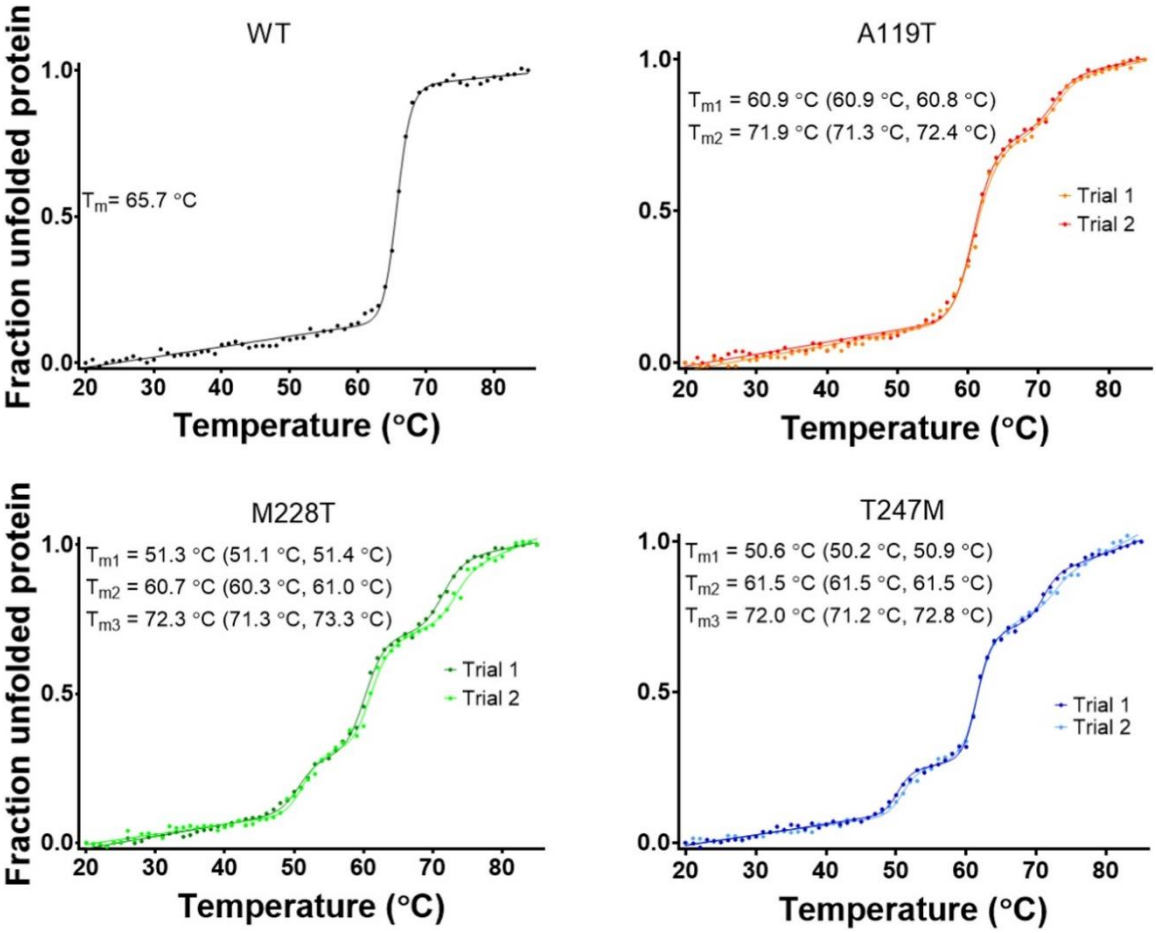

Figure 3.3: Thermal denaturation curves showing that mutant ABD proteins exhibit a loss of cooperative unfolding. Melting curves of purified ABD proteins, obtained by observing circular dichroism absorption at 222 nm while heating sample from 20 °C to 85 °C. The cooperative, two-state, transition is observed for wild-type ABD. A three-state transition is observed for A119T ABD in trial 1 (orange) and trial 2 (red). A four-state transition is observed for M228T ABD; trial 1 (dark green) and trial 2 (light green) and T247M ABD; trial 1 (dark blue) and trial 2 (light blue). For each transition, the Figure 3.3 continued- average Tm from duplicate melts is indicated, followed by the individual replicate Tm values in parentheses.

In contrast, the melt curves for all mutants showed unfolding at lower temperatures and a clear loss in cooperative unfolding. The melt curve for A119T showed two transitions that were fit with two T_m values: T_{m1} = 60.9˚C and 71.9˚C (average T_m's from duplicate melt curves). Duplicate melting curves were nearly identical, supporting the accuracy of

the melt profile. Interestingly, M228T and T247M mutants unfolded with very similar melt curves. These melt curves showed three transitions. For M228T, the three T_m values were 51.3˚C, 60.7˚C and 72.3˚C. For T247M, the T_m values were similar: 50.6˚C, 61.5˚C and 72.0˚C. The loss in cooperativity for M228T and T247M suggests reduced physical coupling between CH subdomains and is consistent with our model that increased actin binding is associated with opening of the CH1/CH2 interface.

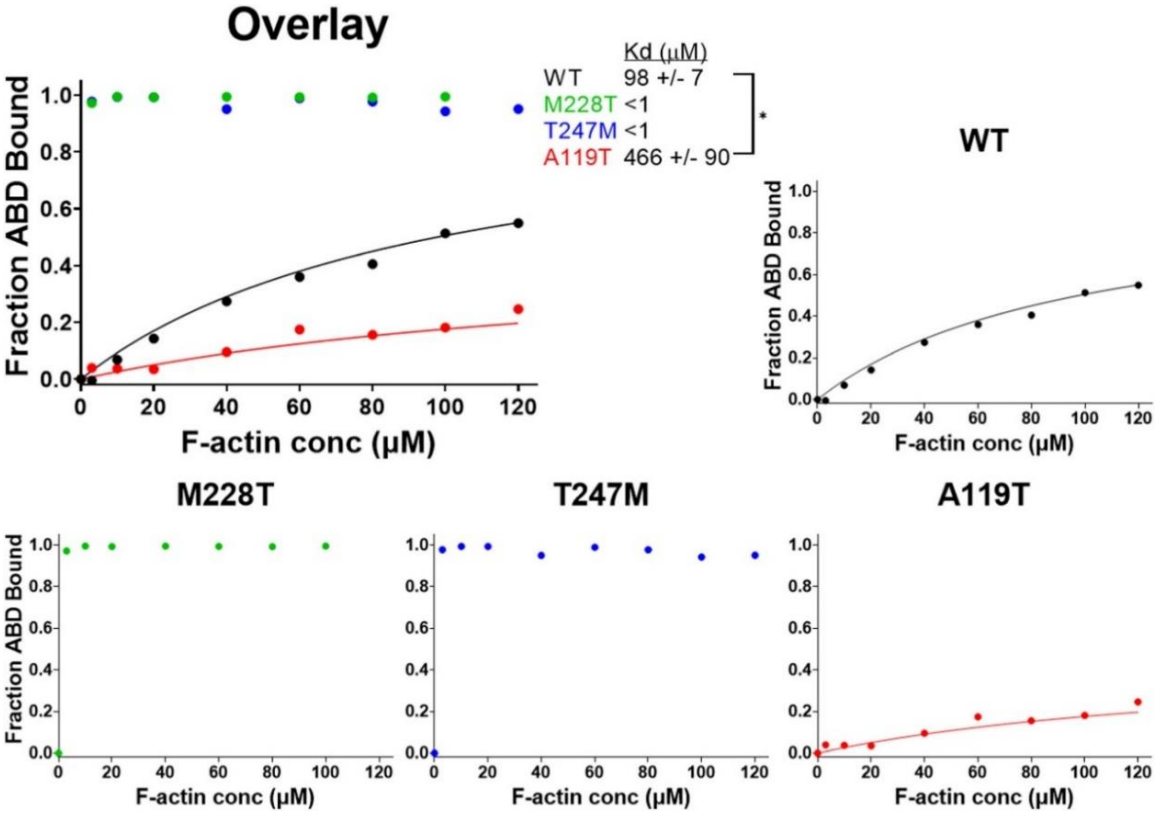

Figure 3.4: Actin co-sedimentation assays showing that ABD mutations cause aberrant actin binding. Co-sedimentation of M228T and T247M ABD proteins show increased actin binding compared to wild-type. Co-sedimentation of A119T ABD protein shows decreased actin binding compared to wild-type. Representative binding data and curve fit is shown for wild-type and A119T ABD proteins. At 2 μM, M228T and T247M ABD proteins are completely bound to actin. Representative binding data is shown for M228T and T247M. Kd value shown as mean ±SD, n = 4-6 binding assays.

3.3.3 Human α-Actinin-2 Cardiomyopathy Missense Variants Disrupt Actin Binding

To test our prediction that CH1-CH2 interface variants in α-actinin-2 will increase actin binding, actin co-sedimentation assays were performed for the variants M228T and T247M. We additionally tested the A119T variant that localizes to an actin binding surface and is thus predicted to decrease actin binding.

The wild-type ABD showed dose responsive binding with increasing F-actin concentration, (Figure 3.4). The average dissociation constant (Kd) of the wild-type ABD was 98 ± 7 μM. Significantly, both M228T and T247M ABDs were entirely bound to actin over the entire range of actin concentrations. This indicates that both M228T and T247M mutant ABDs bind actin with much higher affinity than wild-type, with Kd values that must be submicromolar. In contrast, A119T resulted in reduced binding of the ABD to actin. The Kd value of A119T was 466 ± 90 μM, a statistically significant reduction in the equilibrium binding constant relative to wild-type. Thus, our predictions for the impact of A119T, M228T and T247M on the binding of the ABD to actin were correct.

3.4 Discussion

Many cardiomyopathy-associated missense variants have been reported in the *ACTN2* gene. However, the molecular consequences of these variants in the encoded α-actinin-2 protein are largely unexplored. Here we focused on variants that localize to the actin-binding domain (ABD) of α-actinin-2. Of 71 ABD-localized variants, 34 are positioned at actin-binding surfaces in CH1 or the N-terminus, or the CH1/CH2 interface. Importantly, we showed that two CH1/CH2 interface variants, M228T and T247M, increase actin

binding, in agreement with our prediction for the interface-localized variants. We also investigated a A119T variant that localizes to an actin-binding surface. This variant was previously reported to decrease actin binding [14]. However, the previously reported decrease in affinity was not statistically significant [14]. Here we clarified the effect of the A119T variant. We showed that the A119T variant, indeed, decreases actin binding, raising the Kd ~4-fold, with statistical significance. We expect that many of the other 31 variants mapping to direct actin-binding surfaces or the CH1/CH2 interface, will also disrupt actin binding. However, some of the variants are conservative substitutions that may not disrupt structure/function (for example, K38R or R41K). Experimentally confirming the impact of the variants on actin binding is thus important for establishing pathogenicity.

Our thermal denaturation studies revealed that A119T, M228T and T247M are structurally destabilizing. All three variants caused the ABD to begin to unfold at lower temperature relative to wild-type. Unexpectedly, all three variants also caused a loss of cooperative unfolding, with melt curves revealing multiple steps of unfolding for different substructures within the ABD. M228T and T247M showed three unfolding events, and the three different Tm's were very similar between the two variants. This is consistent with the two variants being localized to the CH1/CH2 interface, and consequently causing similar disruption to ABD structure. In contrast, A119T, buried in CH1, was characterized by two unfolding events, and thus reflects a distinct structural impact on the ABD. Notably, melt curves for all three variants contained an unfolding event with T_m of ~72˚C. This shared T_m suggests the unfolding of a relatively stable ABD substructure common to all three variants. A loss of cooperative unfolding was not

reported previously in thermal denaturation studies for the A119T mutant ABD [14]. Instead, the A119T mutant appeared to unfold with a single transition, with a T_m of 60.8˚C, slightly lower than the 62.3˚C reported for wild-type [14]. This difference may reflect greater sensitivity of our CD measurements with a different spectrapolarimeter. The previously characterized A119T ABD also lacked the N-terminal 18 residues; we previously showed that N-terminal residues preceding CH1 impact the stability of the related ABD of β-III-spectrin [19]. Interestingly, loss of cooperative unfolding was not observed for any of ten different missense variants in the related ABD of β-III-spectrin [111]. Most of the β-III-spectrin variants localized to the CH1/CH2 interface, including L253P and T271I, which are at the equivalent residue positions as α-actinin-2 M228T and T247M, respectively. This suggests a fundamental difference in physical coupling of substructures within the β-III-spectrin and α-actinin-2 ABDs.

Our work suggests that altered actin binding underlies pathogenesis for cardiomyopathy mutations in the ABD of α-actinin-2. Prior work in cardiomyocytes showed that A119T has reduced incorporation into Z-disks, is less dynamic at Z-disks and tends to form aggregates outside of Z-disks [14], and were attributed to a loss of actin binding. The T247M variant also cause α-actinin-2 aggregation in iPSC-derived cardiomyocytes [123]. We propose that these aggregates reflect a high-affinity interaction of the T247M mutant with actin filaments outside of the Z-disk structure. Based on the nearly identical impact of the T247M and M228T variants on the structure and function of the ABD, reported here, we expect M228T will show cause similar aggregation and loss of Z-disk incorporation as T247M. Drug-like small molecules have been identified that partially ameliorate high-affinity actin binding of a L253P mutant β-

III-spectrin ABD [93]. Drug screening for α-actinin-2 may also identify actin-binding modulators useful in treatment in cardiomyopathy.

CHAPTER FOUR

CELLULAR CONSEQUENCES OF SCA5 MUTATIONS IN DROSOPHILA MELANOGASTER

4.0 Introduction

Spinocerebellar ataxia type 5 (SCA5) is a rare neurodegenerative disease caused by autosomal dominant mutations within the *SPTBN2* gene encoding β-III-spectrin. Beta-III-spectrin is enriched in cerebellar Purkinje neurons [65], localizing to the cell body and dendrites [65,66]. SCA5 pathogenesis targets Purkinje neurons of the cerebellar cortex [69]. In vivo studies of mouse and cultured neurons showed that β-III-spectrin is required for spine morphology, dendritic arborization, and synaptic signaling [66–68,73,85]. Similarly, the *Drosophila melanogaster* homolog, β-spectrin, is required for the stabilization of complex dendritic arbors extended by class IV dendritic arborization (da) sensory neuron population [91]. Beta-spectrin contains an N-terminal actin-binding domain (ABD) comprised of tandem calponin homology domains (CH1 and CH2) followed by 17 spectrin repeat domains (SRD) and a C-terminal pleckstrin homology (PH) domain. SCA5 mutations cluster in the ABD and along the SRDs, supporting the functional significance of these regions to the normal biology of β-III-spectrin. Beta-spectrin forms an anti-parallel heterotetramer with α-spectrin to crosslink actin filaments, forming a spectrin-actin cytoskeletal network underlying the plasma membrane.

Since the initial mapping of three SCA5 mutations to the *SPTBN2* gene in 2006, numerous additional mutations have been identified [58,69,78–81,84,88–90]. The L253P missense mutation was the first ABD-localized mutation identified and is associated with

adult-onset symptoms including atrophy of the cerebellar cortex, progressive upper and lower limb ataxia, unclear speech and patterns of abnormal eye movements [76,77,113]. A subset of more recently identified ABD-localized mutations also are associated with adult-symptoms [84,89]. However, other ABD-localized mutations were found in infants and children [78–81]. Many of these early onset SCA5 cases are additionally associated with motor and cognitive delays [78–81]. It is not clear why some ABD-localized mutations are associated with severe infantile-onset symptoms versus relatively mild adult-onset symptoms.

Prior studies showed that many ABD-localized mutations impact β-III-spectrin actin binding. The originally characterized L253P mutation was found to cause ~1000-fold increase in actin binding affinity (Avery 2016). L253P localizes to the interface of CH1 and CH2 ABD subdomains. The large increase in actin binding affinity results from the effect of L253P to destabilize the CH1-CH2 interface (Avery 2016). This promotes opening of the interface, which is required to expose CH1 residues that directly bind actin, and to prevent steric clash between CH2 and actin [19]. Recently we characterized nine additional SCA5 ABD-localized missense mutations. Like L253P, all of these mutations localize at the CH1-CH2 interface. Further these mutations are all destabilizing, although much less so than L253P [111]. Consistent with these observations, we found that all nine mutations increased actin binding affinity [57,111]. Of the mutations, L253P increases actin-binding affinity the most. Further, we suggested that higher actin binding affinity is associated with earlier onset of symptoms. However, L253P is a major outlier in this correlation, as L253P causes the highest actin-binding affinity yet is associated with adult-onset disease. These studies established that many

ABD-localized mutations increase actin binding. However, it still remains unclear why some mutations are associated with different severity of SCA5 disease.

We previously used the Drosophila system to explore the impact of the L253P mutation on neuron function and dendritic arborization. In these studies, fly-lines were generated that contain a wild-type fly β-spectrin transgene or a fly β-spectrin transgene containing the human L253P mutation (L246P in Drosophila). Expression of the transgenes using a pan-neuronal driver showed that the L246P mutant was highly neurotoxic, causing lethality before flies reach the adult life stage [91]. In class IV da neurons, the L246P mutant strongly reduced dendritic arborization. This loss of arborization was also associated within an accumulation of the mutant in the soma and proximal dendrites, with little mutant spectrin localizing to distal dendrites. However, it is not known how other ABD-localized SCA5 mutations impact neuron function or dendritic arborization. Perhaps ABD-localized mutations associated with severe, infantile-onset symptoms will show more pronounced or distinct phenotypes compared to adult-onset SCA5 associated mutations such as L253P (L246P)? Alternatively, if the fly neuron phenotypes reflect differences in actin-binding affinities, then the L253P (L246P) may be the most neurotoxic and disruptive to arborization. Here, using newly generated transgenic fly lines, we studied the neuronal impact of several additional ABD-localized SCA5 mutations in Drosophila.

4.1 Materials and Methods

4.1.1 Drosophila stocks

All fly stocks were maintained in Bloomington Formulation cornmeal and soy based standard food. All experiments were performed at 22°C. The following stocks were

obtained from Bloomington Drosophila Stock Center: *477-Gal4/Cyo, ppk-CD4-tdTom (10a)/Tm6,Tb, ppk-CD4-tdGFP(1b),* and *elav-Gal4*. A fly line containing a recombinant X chromosome containing the recessive lethal loss-of-function $\beta spec^{em21}$ allele and pan-neuronal *elav-Gal4* driver was previously described [91]. The *attP154* fly stock was kindly provided by Norbert Perrimon, Harvard Medical School, Boston [125]. The *UAS-*$\beta spec^{WT}$, *UAS-*$\beta spec^{L246P}$, *UAS-*$\beta spec^{WT\text{-}GFP}$, and *UAS-*$\beta spec^{L246P\text{-}GFP}$ fly lines were previously generated and reported by our group [91,92].

4.1.2 Generation of UAS-βspec transgenic fly lines

Using the previously generated pUASTattB-β-spectrin wild-type construct as a template, a 3kb N-terminal fragment was PCR amplified using the following primers 5'-AGCGGAGACTCTAGCGAG-3' and 5'-AAATCTAGAACCGGTCAGATCCATCTCCAGACTGTCGG-3' [91]. The resulting PCR product was digested with *Kpn*I and *Xba*I restriction enzymes and ligated (T4 DNA ligase, Thermoscientific) into pcDNA3.1 using the same restriction sites. Mutations were introduced into the generated pcDNA3.1-fly-βspec-3kb intermediate construct through site directed PCR mutagenesis (PfuUltra High-Fidelity DNA Polymerase, Agilent) using the primers outlined in Table 4.1. Mutant DNAs were digested with *EcoR*I and *Age*I restriction enzymes were ligated (T4 DNA ligase, Thermoscientific) into the previously generated pUASTattB-β-spectrin wild-type [91] plasmid using the same restriction enzymes. The resulting constructs; pUASTattB-β-spec-T55I, pUASTattB-β-spec-F153C, pUASTattB-β-spec-T264I, pUASTattB-β-spec-Y265H, and pUASTattB-β-spec-H271R, were sequence verified and inserted into the attP154 landing site using the PhiC31 integrase mediated transgenesis at BestGene, Inc.

Table 4.1: Mutagenic primers used for introduction of mutations into the Drosophila β-spectrin coding sequence.

Mutation	Sense Primer	Antisense Primer
T55I	GAGAGTGTGCAAAAGAAGAT ATTCACCAAGTGGGTCAATT	AATTGACCCACTTGGTGAATA TCTTCTTTTGCACACTCTC
F153C	TGGACCATCATCCTGCGCTGC CAGATCCAGGACATCACCA	TGGTGATGTCCTGGATCTGGC AGCGCAGGATGATGGTCCA
T264I	CCGGACGAGAAGTCCATCATC ATCTACGTGGTCACCTACTAT C	GATAGTAGGTGACCACGTAGA TGATGATGGACTTCTCGTCCGG
Y265H	GACGAGAAGTCCATCATCACC CACGTGGTCACCTACTATCAC	GTGATAGTAGGTGACCACGTG GGTGATGATGGACTTCTCGTC
H271R	CTACGTGGTCACCTACTATCG CTACTTTAGCAAACTCAAGC	GCTTGAGTTTGCTAAAGTAGC GATAGTAGGTGACCACGTAG

4.1.3 Generation of SCA5 mutant UAS-βspec^{GFP} transgenic fly lines

The previously generated pUASTattB-β-spectrin-mEGFP wild-type construct was used as a template for generation of SCA5 ABD GFP-tagged fly β-spec mutants [92]. The newly generated pUASTattB-β-spec-T55I, pUASTattB-β-spec-F153C, pUASTattB-β-spec-Y265H, and pUASTattB-β-spec-H271R were digested with *Mre*I and *Xba*I restriction enzymes and ligated (T4 DNA ligase, Thermoscientific) into the previously generated pUASTattB-β-spectrin-mEGFP wild-type construct using the same restriction enzymes. The final sequence verified constructs; pUASTattB-β-spec-T55I-mEGFP, pUASTattB-β-spec-F153C-mEGFP, pUASTattB-β-spec-Y265H-mEGFP, and pUASTattB-β-spec-H271R-mEGFP were inserted into the attP154 landing site at BestGene, Inc.

4.1.4 Rescue experiments

Crosses of female flies harboring a recombinant X chromosome *βspec^{em21}, elav-Gal4*, over the balancer *FM6* and male flies homozygous for *UAS-βspec* transgenes with

and without GFP tags or *attP154* landing site, on the third chromosome were performed at 22°C incubation. All adult progenies were scored within 24 hours of emerging.

4.1.5 Western Blot

Crosses of female flies harboring *βspec*^{em21}, *elav-Gal4*/*FM6* and male flies homozygous for *UAS-βspec-GFP* transgenes or *attP154* landing site were performed at 22 °C incubation. Adult female progeny containing both *βspec*^{em21}, *elav-Gal4* and *UAS-βspec-GFP* transgenes were collected and stored at -80 °C within 24 hours of emerging. Fly heads were separated from bodies with vigorous shaking of 15 mL conical tubes, frozen in liquid nitrogen, containing the pooled females for each genotype. Heads were collected from bodies using mesh sieves No. 25 to retain bodies and No. 40 to retain heads. Heads were collected for each genotype and proteins extracted as previously described [92]. SDS-PAGE was performed on the soluble and insoluble samples using 4-20% gradient TGX gels (Bio-Rad). Using Immobilon-FL membranes (Millipore), proteins were transferred from the gels. Membranes were blocked with 1% casein (Hammersten; Alfa Aesar) in 1X PBS-L (9 g NaCl, 2 g Na2HPO4, 0.83 g NaH2PO4·H2O, dissolved in 1 L H2O) for 1 hour at room temperature with shaking. Membranes were probed overnight at 4 °C with either α-actin JLA20 (mouse) (Developmental Studies Hybridoma Bank) of α-GFP (rabbit) (Millipore), both diluted 1:2000 in 1X PBS-L with 1% casein and 0.1% Tween 20 with gentle rocking. Following incubation, primary antibodies were removed, and membranes were washed with 1X PBS and 0.1% Tween 20. Membranes were probed with either α-mouse IRDye 800CW (LI-COR Biosciences) or α-rabbit IRDye 680RD (LI-COR Biosciences) secondary antibodies diluted 1:5000 in 1X PBS-L with 1% Casein, 0.1% Tween 20, and 0.01% SDS for 1 hour

with gentle rocking, protected from light. Membranes were washed of secondary antibodies with 1X PBS-L and 0.1% Tween 20. Membranes were imaged on the 680 nm and 800 nm channels of a Sapphire scanner (Azure). Quantitation of protein band fluorescence intensities was performed in ImageStudio lite (LI-COR Biosciences). Identical boxes were placed around each band and background was subtracted using median pixel intensity to the left and right bounds of each box.

4.1.6 Dendritic Arbor Analysis

UAS-βspec transgenic male flies were crossed with female flies carrying *477Gal4; ppk-Cd4-tdGFP/TM6* transgene at 22 °C incubation. Crosses were able to mate for 24 to 48 hours prior to egg laying on grape juice plates. Flies were allowed to lay eggs on grape juice plates containing yeast paste for four-hour time spans. Grape juice plates containing eggs were incubated at 22 °C for 120 hours, yielding third-instar larvae. Female larvae were imaged using HC PL APO 20x/0.80 NA dry objective on a Leica DMi8 inverted microscope with an attached X-Light V2 spinning-disc (CrestOptics), LDI laser unit (89 North), and photometrics Prime 95B CMOS camera. Z-stack images of class IV da neurons at a slice depth of 0.5 µm were obtained in quadrants from abdominal segments A3 and A4 (one to four neurons per larva). Images were processed in ImageJ software to obtain maximum intensity projections [91,126]. Quadrants of arbors were reconstructed in Adobe Photoshop 21.0.1. ImageJ software was used to quantify total branch length, branch points and Sholl analysis, as previously described [91,126]. Statistical analysis was performed on total branch length and number of branch points in Prism 10.3.1 (Graphpad) using two-tailed unpaired *t* tests with Welch's correction (n =

22 for $\beta spec^{WT}$, n = 16 for $\beta spec^{L246P}$ and $\beta spec^{F153C}$, n = 15 for $\beta spec^{T55I}$, $\beta spec^{T264I}$, $\beta spec^{Y265H}$, and $\beta spec^{H271R}$).

4.1.7 Subcellular localization

UAS-βspec-GFP transgenic male flies were crossed with female flies carrying *477Gal4; ppk-Cd4-tdTom/TM6* transgene at 22 °C incubation on standard Bloomington Formulation soy and cornmeal food. Female third instar larvae were imaged using HC PL APO 63x/1.40-0.60 OIL oil-immersion objective on a Leica DMi8 inverted microscope with an attached X-Light V2 spinning-disc (CrestOptics), LDI laser unit (89 North), and photometrics Prime 95B CMOS camera. Z-stack images of class IV da neurons at a slice depth of 0.25 µm were obtained in abdominal segments A3 and A4 (1 to 4 neurons per larva). Images were taken of cell bodies and primary dendrites. Analysis was performed in the imaging software, Metamorph (Molecular Devices) as previously described [91]. GFP fluorescence was measured in place of mEos3.2 and a six-pixel-wide line scan was used in place of a three-pixel-wide line scan. Statistical analysis was performed in Prism 10.3.1 (Graphpad) using two-tailed, unpaired *t* tests with Welch's correction (n = 13 for $\beta spec^{WT\text{-}GFP}$, n= 5 for $\beta spec^{L246P\text{-}GFP}$, n = 16 for $\beta spec^{T55I\text{-}GFP}$, n = 10 for $\beta spec^{F153C\text{-}GFP}$, and n = 15 for $\beta spec^{Y265H\text{-}GFP}$ and $\beta spec^{H271R\text{-}GFP}$).

4.2 Results

4.2.1 Genetic Rescue Experiments

We used the Drosophila system to explore the cellular impact of five additional SCA5, ABD-localized missense mutations: T62I, F160C, T271I, Y272H and H278R. Previously we showed that all of these mutations cause increased actin-binding affinity in vitro, although none increase actin binding as much as L253P (~75 nM Kd). We recently

reported the following Kd values: T62I (2.4 μM), H278R (6.7 μM), F160C (submicromolar), T271I (submicromolar), Y272H (15 μM), compared to 55 μM for wild-type [111]. Most of these mutations are associated with infantile-onset SCA5 (T62I, F160C, T271I) or adolescent-onset (H278R). Y272H, which caused the smallest increase in actin binding, and was identified in as a compound mutation (with W2065*) in an infantile-onset patient. An adult parent carrying Y272H by itself (Y272H/+) was not symptomatic. To test the impact of these ABD-localized SCA5 mutations on neuron function and dendritic arborization, new fly-lines were generated containing transgenes with the upstream activation sequence (UAS) fused to the Drosophila β-spectrin cDNA. All of these mutations occur amino acids conserved in fly β-spectrin. The equivalent mutations in Drosophila β-spectrin are as follows: Human T62I (T55I in Drosophila), F160C (F153C), T271I (T264I), Y272H (Y265H), and H278R (H271R), see Table 4.2.

Table 4.2: Conservation of residues between human β-III-spectrin and Drosophila β-spectrin allowed homologous residues to be mutated.

Mutation in human β-III-spectrin	Mutation in fly β-spectrin
T62I	T55I
F160C	F153C
T271I	T264I
Y272H	Y265H
H278R	H271R
L253P	L246P

In addition, for all mutations except T271I, a complementary set of transgenic fly lines were generated in which the GFP coding sequence was fused in-frame to the 3' of the β-spectrin cDNA. All transgenes were inserted into the *attP154* genomic locus for equal expression at the level of transcription [125]. To test if the *βspec* transgenes are functional, genetic rescue experiments were performed using a recessive lethal loss-of-

function allele (*βspec*^{em21}). The *βspec*^{em21} allele contains a nonsense mutation in the endogenous *βspec* gene, resulting in a β-spectrin protein truncated in the thirteenth spectrin repeat domain [92]. *βspec*^{em21} is lethal in males (*βspec*^{em21}/*Y*) and homozygous (*βspec*^{em21}/*βspec*^{em21}) females. However, heterozygous females (*βspec*^{em21}/+) are healthy. In these rescue experiments, we used a fly line containing a recombinant X chromosome containing the *βspec*^{em21} allele and the pan-neuronal driver, *elav-Gal4*, balanced over *FM6* (*βspec*^{em21}, *elav-Gal4/FM6*). *FM6* is an X chromosome that contains the native wild-type *βspec* gene and multiple DNA rearrangements to prevent recombination. Female *βspec*^{em21}, *elav-Gal4/FM6* flies were crossed to male flies homozygous for *βspec* transgenes. To determine rescue, we scored the number of adult male progeny that contained *βspec*^{em21} together different *βspec* transgenes (*βspec*^{em21}/*Y; βspec*/+). The wild-type β-spectrin transgene (*βspec*^{WT}) without GFP fusion rescued adult lethality in 32% of male progeny harboring *βspec*^{em21}, Table 4.3.

Table 4.3: Rescue of *βspec*^{em21} lethality by UAS-βspec transgenes at 22°C. Females carrying the *βspec*^{em21}, *elav-Gal4* recombinant chromosome balanced over the *FM6* were crossed to males homozygous for *UAS-βspec* transgenes on the 3rd chromosome inserted at the *attP154* landing site.

Transgene	Progeny class: total number of adults			
	em21, elav-Gal4/Y; transgene/+	*FM6/Y*; transgene/+	*em21, elav-Gal4/+*; transgene/+	*FM6/+*; transgene/+
attp154	0	144	118	112
UAS-βspec^{WT}	72	224	265	257
UAS-βspec^{L246P}	0	156	0	221
UAS-βspec^{T55I}	35	155	165	158
UAS-βspec^{F153C}	35	141	185	162
UAS-βspec^{T264I}	31	251	266	298
UAS-βspec^{Y265H}	44	87	93	83
UAS-βspec^{H271R}	55	109	107	125

Further, the wild-type β-spectrin transgene with GFP fusion (*βspec*$^{WT\text{-}GFP}$) rescued 57% of male progeny harboring the *βspec*^{em21} allele, Table 4.4.

Table 4.4. Rescue of *βspec*^{em21} lethality by *UAS-βspec-GFP* transgenes at 22°C. Females carrying the *βspec*^{em21}, *elav-Gal4* recombinant chromosome balanced over FM6 were crossed to males homozygous for *UAS-βspec-GFP* transgenes on the 3rd chromosome inserted at the *attP154* landing site.

Transgene	*em21, elav-Gal4/Y*; transgene/+	*FM6/Y*; transgene/+	*em21, elav-Gal4/+*; transgene/+	*FM6/+*; transgene/+
attp154	0	144	118	112
UAS-βspec$^{WT\text{-}GFP}$	107	185	203	210
UAS-βspec$^{L246P\text{-}GFP}$	0	118	0	159
UAS-βspec$^{T55I\text{-}GFP}$	31	198	206	235
UAS-βspec$^{F153C\text{-}GFP}$	58	116	137	134
UAS-βspec$^{Y265H\text{-}GFP}$	74	143	188	128
UAS-βspec$^{H271R\text{-}GFP}$	65	109	124	122

In agreement with our previous reporting, the *βspec*^{L246P} mutant transgene [91], with or without GFP, failed to rescue *βspec*^{em21} lethality. Further, the *βspec*^{L246P} transgene dominantly induced lethality in *βspec*^{em21}, *elav-Gal4/+* females. In contrast, the *βspec* transgenes carrying other mutations (T55I, F153C, T264I, Y265H, H271R) were capable of rescuing lethality in *βspec*^{em21} males. For the non-GFP tagged *βspec* transgenes, the lowest rescue percentages observed were for T264I (12%) and T55I (23%). Similarly, for GFP-tagged transgenes, T55I showed low rescue (a GFP transgene was not available for T264I). This indicates that the T55I, F153C, T264I, Y265H, H271R mutations do not eliminate β-spectrin function in neurons. However, the lower rescue percentages observed for T254I and T55I suggest these mutations partially reduce spectrin function. Further, none of the newly tested mutations induced lethality in females heterozygous for *βspec*^{em21}. This strongly suggests the newly tested mutations are far less toxic than L246P in Drosophila neurons.

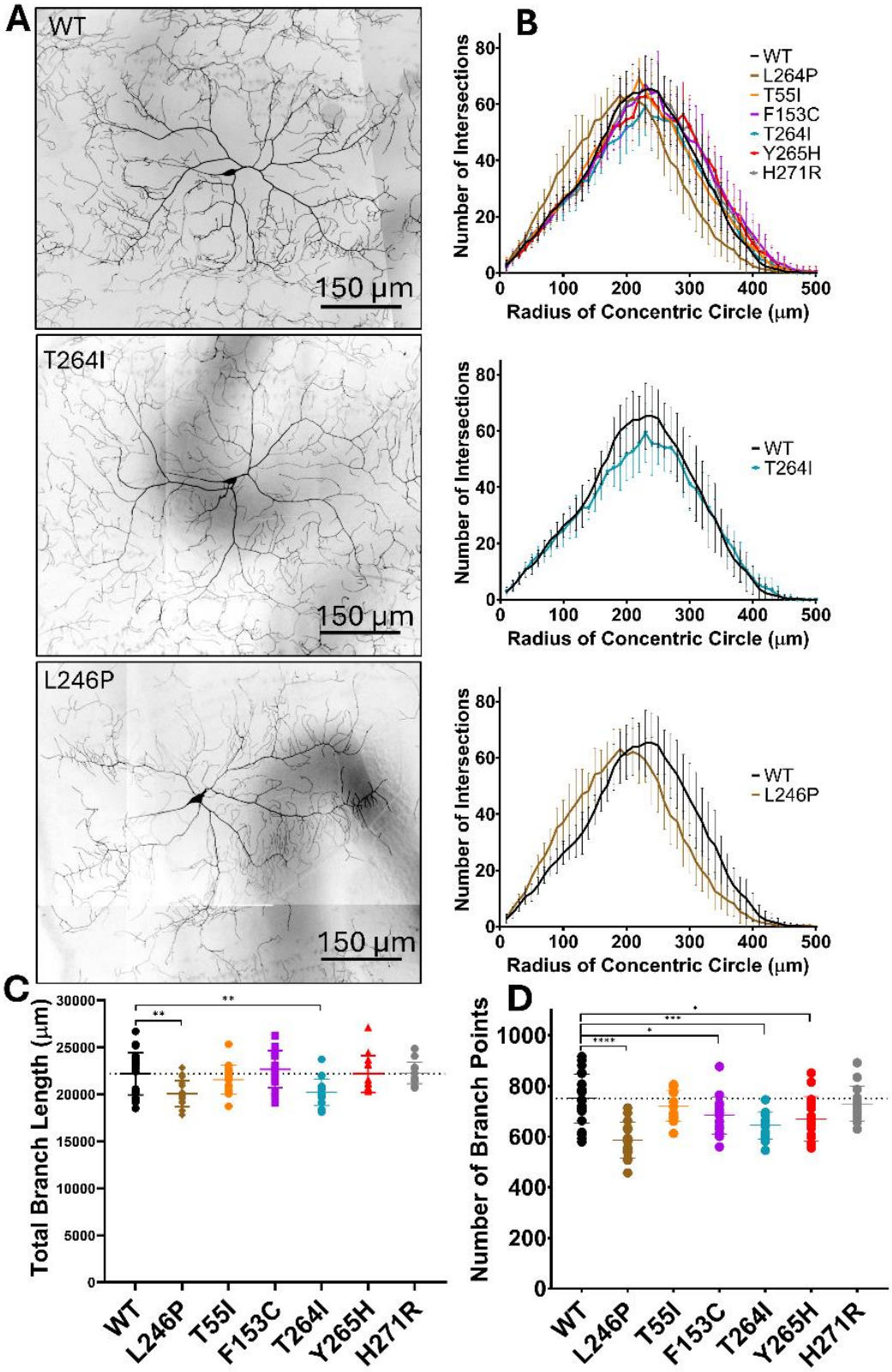
A
WT
150 μm
T264I
150 μm
L246P
150 μm
B
Number of Intersections
Radius of Concentric Circle (μm)
WT
L264P
T55I
F153C
T264I
Y265H
H271R
WT
T264I
WT
L246P
C
Total Branch Length (μm)
D
Number of Branch Points
WT
L246P
T55I
F153C
T264I
Y265H
H271R

Figure 4.1. Dendritic arborization defects induced by β-spectrin transgenes. A. Representative images of transgenic: wild-type β-spectrin (top), T264I β-spectrin (middle), and L246P β-spectrin (bottom) in Drosophila class IV da neurons. B. Sholl analysis of β-spectrin transgenes. Only L246P β-spectrin reduced dendritic outgrowth relative to the soma (top and bottom). T264I β-spectrin induced a thinning of dendrite density (middle). C. Total branch length was significantly reduced by mutations L246P (**P = 0.0012) and T264I (**P = 0.0023). For wild-type, n=22 neurons. For L246P and F153C, n=16 neurons. For T55I, T264I, Y265H and H271R, n=15 neurons. One to three neurons were imaged for each larva. Statistical significance determined by Unpaired t test with Welch's correction in GraphPad Prism 10.3.1. D. Branch point was significantly reduced by mutations L246P (****P < 0.0001), F153C (*P = 0.0185), T264I (***P = 0.0001), and Y265H (*P = 0.0116). For L246P and F153C, n=16 neurons. For T55I, T264I, Y265H and H271R, n=15 neurons. One to three neurons were imaged for each larva. Statistical significance determined by Unpaired t test with Welch's correction in GraphPad Prism 10.3.1.

4.2.2 Impacts of SCA5 Mutants on Dendritic Arborization

To test how the SCA5 mutations impact dendritic arborization, the wild-type and SCA5 mutant *βspec* transgenes were expressed in class IV dendritic arbor (da) sensory neurons using the *477-Gal4* driver. Consistent with our previous reporting, $\beta spec^{L246P}$ caused a pronounced a reduction in arborization compared to control neurons expressing $\beta spec^{WT}$ (Figure 4.1). Specifically, Sholl analysis shows that the L246P mutation shifts the position of most dendrites towards the cell body. Further, L246P causes a ~10% decrease in total dendritic branch length, and a ~25% reduction in number of branch points, consistent with our prior characterization of this mutation [91,92]. Notably, the larger effect of the mutation on number of branch points compared to total dendritic branch length (25% vs 10% reduction) suggests that number of branch points is a more sensitive measure of SCA5-induced arbor defects. Of the newly tested SCA5 mutations, T264I also caused both a statistically significant decrease in number of branch points (14%) and total branch length (9%). F153C caused a 9% decrease in number of branch

points and Y265H showed an 11% decrease in branch points. Number of branch points trended down for H271R, but did not reach statistical significance. Further, none of the newly tested SCA5 mutations shifted the position of most dendritic branch points, as observed for L246P. In sum, many of the newly tested SCA5 mutations caused defects in arborization, but these defects were smaller than those caused by L246P.

4.2.3 Subcellular Localization of β-spectrin in Neurons

To evaluate the subcellular localization of wild-type and SCA5 mutant β-spectrin, live imaging of β-spectrin-GFP proteins in class IV da neurons was performed in Drosophila larvae. In agreement with our prior findings [91], the wild-type β-spectrin protein is observed in the soma and throughout the dendritic arbor, (Figure 4.2). In contrast, the L246P mutant accumulated in the soma and proximal dendrites but was absent from distal dendrites, as we previously reported [91]. We further assessed the localization of the T55I, F153C, Y265H and H271R mutants (a GFP-tagged version of T264I was not available). Of the available GFP-tagged SCA5 mutants, T55I showed a small but statistically significant accumulation in the cell body. In contrast, F153C showed a small but statistically significant decrease in cell body localization, relative to the wild-type protein. None of the GFP-tagged mutant β-spectrin proteins showed a statistically significant difference in localization to distal dendrites, although T55I and H271R trended upward. Altogether, these data indicate that of the newly tested SCA5 mutations, only T55I and F153C, were associated with small changes in the amount β-spectrin present in the soma. This contrasts with the large changes in subcellular localization caused by L246P.

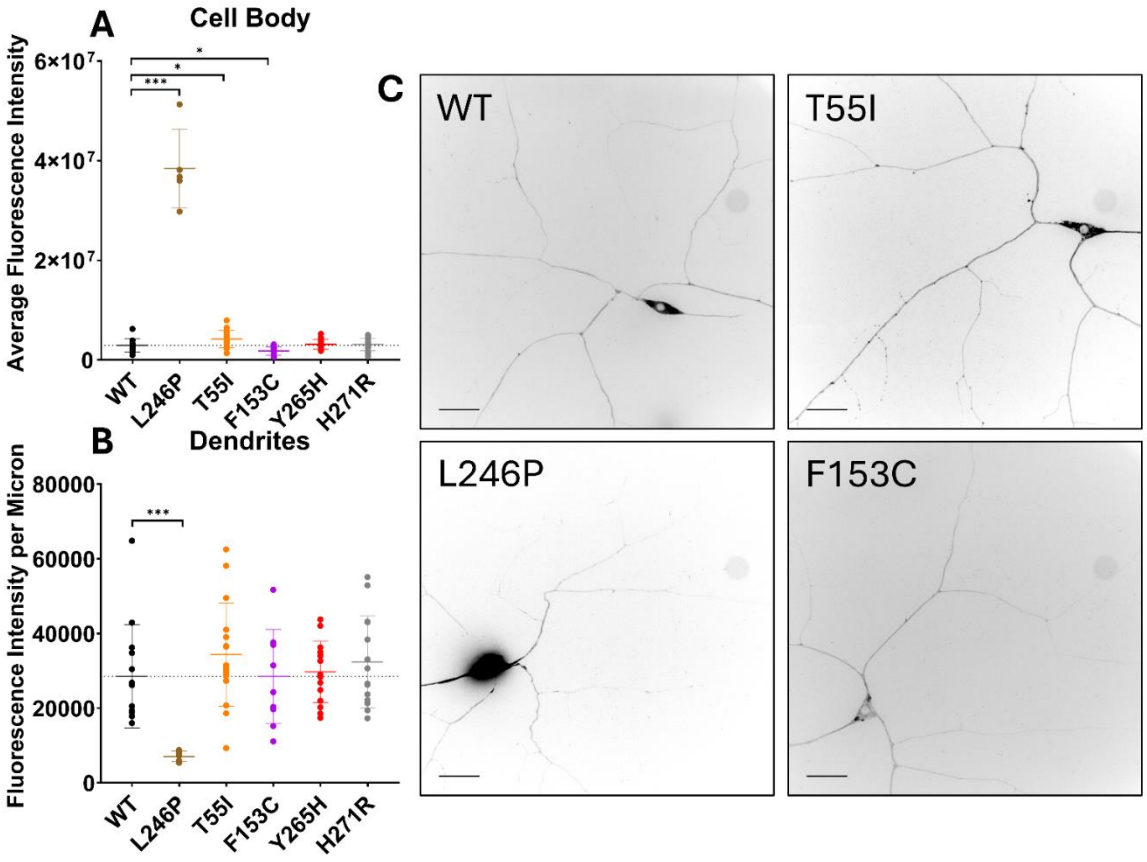

Figure 4.2. Subcellular localization of GFP tagged β-spectrin in cell bodies and dendrites of class IV da neurons. A. β-spectrin-GFP signals were quantified in the cell bodies of transgenic larvae. For wild-type, n=13 neurons from one to three neurons per larva. For L246P, n=5 neurons from one to three neurons per larva. ***P = 0.0005. For T55I, n=16 neurons from one to three neurons per larva. *P = 0.0275. For F153C, n=10 neurons from one to three neurons per larva. *P = 0.0225. For Y265H and H271R, n=15 neurons from one to three neurons per larva. Statistical significance determined by Unpaired t test with Welch's correction in GraphPad Prism 10.3.1. B. β-spectrin-GFP signals were quantified in primary dendrites of 50 µm in length beginning 100 µm from the cell body. For wild-type, n=13 neurons from one to three neurons per larva. For L246P, n=5 neurons from one to three neurons per larva. ***P = 0.0001. For T55I, n=16 neurons from one to three neurons per larva. For F153C n=10 neurons from one to three neurons per larva. For Y265H n=15 neurons from one to three neurons per larva. For H271R n=14 neurons from one to three neurons per larva. Statistical significance determined by Unpaired t test with Welch's correction in GraphPad Prism 10.3.1. C. Confocal images of class IV da neurons expressing β-spectrin-GFP transgenes. WT (top left), T55I (top right) and F153C (bottom right) β-spectrin-GFP localize throughout the cell body and primary dendrites. L246P β-spectrin-GFP (bottom left) localizes primarily to the cell body and proximal primary dendrites but is absent from distal dendrites. (Scale bar, 25 µm). Error bars are representative of SD in all graphs.

4.2.4 SCA5 Mutations Cause Increased β-spectrin Protein Levels

To determine the impact of the SCA5 mutations on β-spectrin protein levels, the wild-type and mutant *βspec*^{GFP} transgenes were expressed with the pan-neuronal *elav-Gal4* driver and head extracts were prepared from adult flies. Soluble and insoluble fractions were probed by western blot using GFP antibody, or for loading control, actin

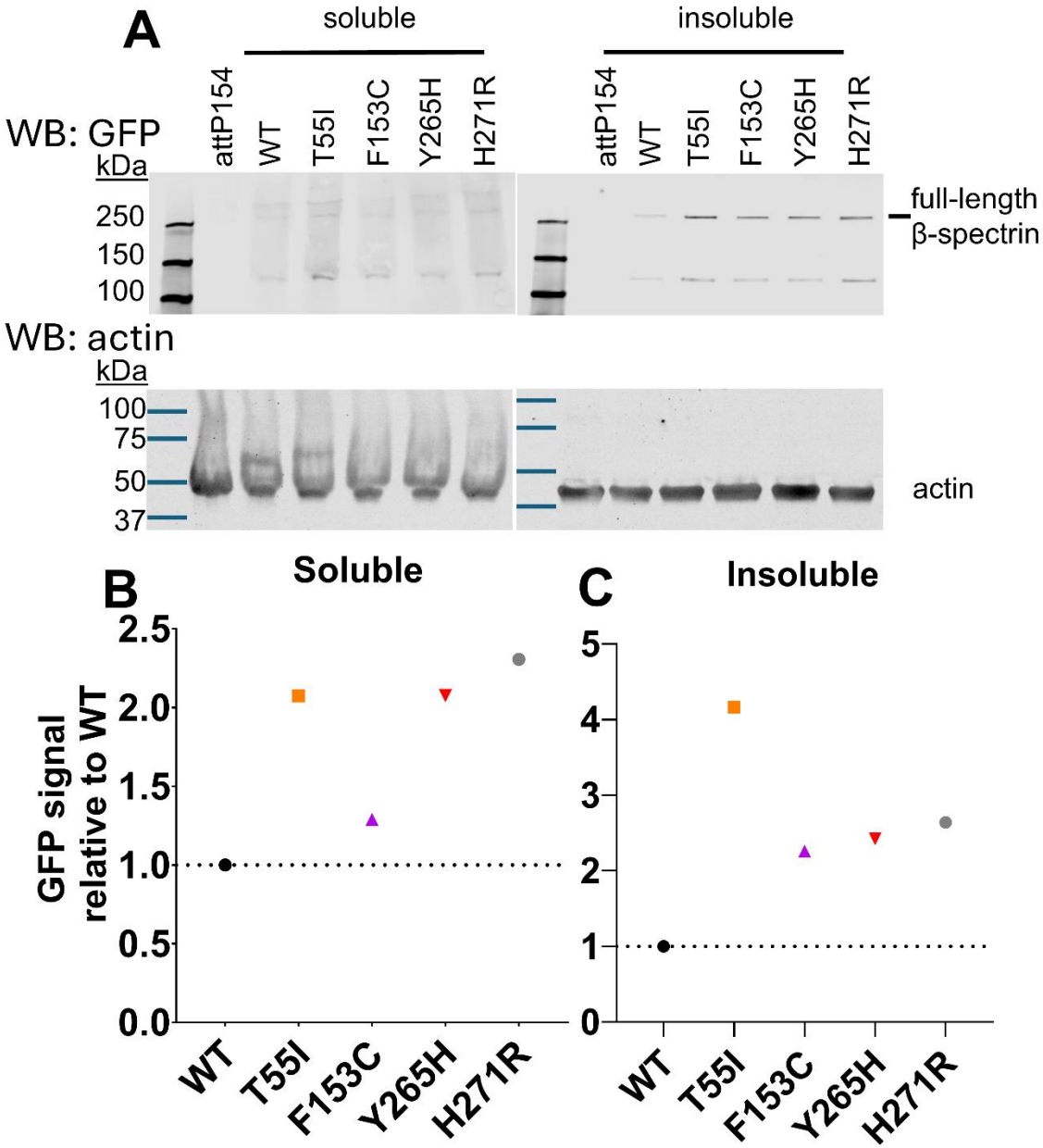

Figure 4.3. ABD mutations impact β-spectrin protein levels. A. Western blot of prepared head extracts from adult female Drosophila pan-neuronally expressing *UAS-βspec*^{GFP} transgenes driven by *elav-Gal4*. Head extracts from adult female Drosophila containing the *attP154* landing site were used as a control. GFP tagged β-spectrin proteins were visualized through probing with a GFP antibody. Actin was probed as a loading control. GFP and actin western blot images were cropped to the regions showing GFP and actin proteins.

antibody (Figure 4.3). The GFP-tagged β-spectrin proteins were present in both the soluble and insoluble fractions, but protein bands were most well resolved in the insoluble fractions. Here the β-spectrin proteins run just over 250 kDa, consistent with the predicted 293 kDa size of the full-length, GFP-tagged protein. An additional lower running band is present, ~125 kDa, consistent with a known major proteolytical fragment [92]. Quantitation shows that all the mutants accumulate in the insoluble fraction, which is enriched in F-actin associated with membrane material. The accumulation of the mutants in the insoluble fraction is similar to our prior finding that the L246P mutant accumulates in the soma [91]. However, L246P caused a ~20-fold increase in amount of β-spectrin in the insoluble fraction, relative to wild-type. In contrast, the newly characterized SCA5 mutants accumulate in the insoluble fraction by ~2-4-fold relative to wild-type. Previously, we found that the L246P mutant also was ~5-fold more abundant than wild-type in the soluble fractions. Similarly, most of the newly tested SCA5 mutants show slight increased abundance (~2-fold) in the soluble fraction. In sum, all the newly tested SCA5 mutation cause clear accumulation of β-spectrin protein in the insoluble fraction, as observed previously for L246P. This accumulation in the insoluble fraction is consistent with the effect of the mutations to increase actin-binding affinity, as the insoluble fraction is enriched with F-actin.

4.3 Discussion

Many SCA5 missense mutations are known to localize to the β-III-spectrin ABD. Interestingly, some of these mutations are associated with severe infantile-onset SCA5, while others are associated with milder adult-onset SCA5. In total, our group has tested ten of the mutations for an impact on actin binding in vitro [57,111]. All ten mutations were found to increase β-III-spectrin actin binding, supporting a shared molecular consequence. However, the actin-binding affinities varied greatly across the mutations. We suggested a positive correlation between increased actin-binding affinity and earlier onset of symptoms [111]. However, L253P, which causes the largest increase in affinity is a major outlier, as it is associated with adult onset SCA5. Previously we showed that L253P (L246P in Drosophila) causes pronounced dendritic arbor defects in flies. Here we tested how five additional ABD-localized mutations (T62I, F160C, T271I, Y272H and H278R) impact neuron function and dendritic arborization using the fly system.

In the Drosophila studies presented here, we anticipated two possible outcomes: 1) ABD-localized mutations associated with severe, infantile-onset symptoms will show more pronounced neuronal phenotypes compared to adult-onset SCA5 mutations, such as L253P. Or 2), the severity of neuron phenotypes will mirror differences in actin-binding affinities. In the second possibility, the L253P would be expected to cause the most severe phenotypes because it causes the largest increase in actin binding affinity. Our Drosophila data on the newly tested mutations is most consistent with the second possibility. The L253P mutation rendered fly β-spectrin not functional in genetic rescue assays. Further the L253P mutant was highly neurotoxic, inducing lethality in otherwise healthy flies. The L253P mutation also caused a strong reduction in dendritic arborization

and accumulation of the mutant protein in the soma, and the insoluble fraction of head extracts. In contrast, the five newly tested mutations (T62I, F160C, T271I, Y272H and H278R) caused much milder or no neuronal phenotype. Specifically, all of the five newly tested mutation were capable of rescuing $\beta spec^{em21}$ lethality to some extent. T271I, which causes an increase actin-binding affinity second to only L253P, had the lowest rescue efficiency. Further, none of the newly tested mutations in fly β-spectrin dominantly induced lethality when expressed with a pan-neuronal driver. This strongly supports that the five newly tested SCA5 mutations are far less neurotoxic in the fly system, compared to L253P. In arborization studies, most of the mutations caused mild dendritic defects. Of the five newly tested mutations, arbor defects were most pronounced for T271I and T62I. Of the five newly tested mutations, these two are associated with high affinity actin binding. We did not observe striking changes in the neuronal subcellular localization of the newly tested mutants. However, all of the mutations caused β-spectrin to accumulate in the insoluble fraction of fly head extracts, similar to L253P. However, this accumulation in the insoluble fractions was much lower than that observed previously for L253P. Because the insoluble fraction is enriched in F-actin (associated with membrane material), the accumulation of the mutants in the insoluble fraction is consistent with increased actin binding. In sum, the impact of the ABD-localized SCA5 mutations on neuron structure and function in Drosophila appears to correlate with how severely the mutations alter actin binding.

Why are many SCA5 mutations that cause high-affinity actin binding, like T62I, F160C and T271I, associated infantile/early onset SCA5, while the L253P, which causes the largest increase in actin-binding affinity, is associated with adult-onset SCA5? One

clue may stem from our Drosophila studies on the effect of these mutations on the neuronal subcellular localization of the mutant spectrins. The L253P mutation traps the mutant spectrin in the soma, presumably due to a reduced mobile pool, as the mutant is attached to F-actin. In contrast, the other mutants that bind actin with lower affinity (relative to L253P) are more mobile and can better penetrate the dendritic arbor. In the SCA5 target neuron, cerebellar Purkinje cells, wild-type β-III-spectrin localizes throughout the dendritic arbor. It is plausible that a mutant spectrin that binds actin with high affinity and can enter dendrites, will interfere with the dendritic functions of spectrin in ways that are distinct (and more severe), than a mutant that binds actin with high affinity, but cannot enter dendrites.

CHAPTER FIVE

DISCUSSION

The evolutionarily linked, spectrin superfamily of cytoskeletal proteins are found in many molecular organizational roles at the cell membrane. The work presented in this dissertation explored impacts on the structure and function of disease associated mutations within the actin binding domain (ABD) of two actin-crosslinking proteins: α-actinin-2 and β-III-spectrin. We sought to understand the significance of disease associated mutations localizing to the ABDs of both proteins. Clustering of the disease associated mutations in both proteins to the ABD supports the functional significance of this region. We predicted that mutations localizing to the ABD would impact actin-binding affinity and that the aberrant actin-binding affinity contributes to disease pathogenesis.

Our characterization of the ABD-localized mutations builds upon previous works to characterize the L253P missense mutation in β-III-spectrin. In previous studies, *in vitro* binding assays showed that the L253P mutation results in a 1000-fold increase in the actin-binding affinity for the β-III-spectrin ABD [57]. The L253 residue resides in a hydrophobic pocket at the CH1-CH2 interface [57]. Biophysical analysis indicated the introduction of the L253P mutation results in an opening of the CH1-CH2 interface, allowing a distinct actin-binding surface of CH1 to bind actin without the steric interference of CH2 [19]. Significantly, this mechanism is supported by observations in other spectrin superfamily proteins [22,23]. In the closed conformation of the β-III-spectrin ABD, residues of CH1 and CH2 localizing to the interface are predicted to form

an interaction network that is likely important in bridging the two subdomains of the ABD [57,111]. We wondered if other ABD localized mutations clustering to the interface of CH1 and CH2 or the actin-binding surface of CH1 lead to altered actin-binding affinity. Additionally, we wanted to understand structural changes to ABD proteins upon introduction of disease related mutations.

These studies revealed a common molecular consequence of ABD mutations that localize to the CH1-CH2 interface. *In vitro* binding assays showed that like the L253P mutation in β-III-spectrin, nine additional mutations (V58M, K61E, T62I, K65E, F160C, D255G, T271I, Y272H, and H278R) in β-III-spectrin localizing to the interface cause increased actin-binding affinity. Though several mutations induced submicromolar actin-binding affinity (K61E, K65E, F160C, and T271I), none of the mutations increased actin-binding affinity as much as L253P. Other mutations induced more modest increases in actin-binding affinity (V58M (10.2 μM), T62I (2.4 μM), D255G (7.3 μM), Y272H (15.3 μM) and H278R (6.7 μM)). Two mutations in α-actinin-2 (T247M and M228T) also localize to the CH1-CH2 interface and resulted in increased actin-binding affinity. In contrast, the A119T mutation within α-actinin-2 localizes to an actin-binding surface of CH1, and as predicted, reduced actin-binding affinity α-actinin-2 ABD protein. Notably, L253 and M228, and T271 and T247, are equivalent residues in β-III-spectrin and α-actinin-2, respectively, and mutation of these residues resulted in high-affinity actin binding with submicromolar dissociation constants. Additional *in vitro* circular dichroism studies assessing the folded-state of wild-type and mutant β-III-spectrin and α-actinin-2 revealed that none of the mutations significantly reduced the highly alpha-helical fold of the ABDs.

Further *in vitro* biophysical studies showed that the mutations induce destabilization of the ABD proteins. Previous characterization of the L253P mutant ABD showed a cooperative unfolding pattern characterized by a two-state single transition melt curve with a 15°C decrease in melting temperature compared to the wild-type ABD protein [57]. Thermal denaturation of the nine additional β-III-spectrin ABD mutants also revealed statistically significant decreases in thermal stability, maintaining a cooperative unfolding pattern. Interestingly, like the *in vitro* actin-binding assays, none of the mutations reduced melting temperature as drastic as the L253P mutation. Analysis of the α-actinin-2 ABD proteins likewise revealed thermal destabilization. However, the melt curves for the α-actinin-2 ABD also showed a loss of cooperative unfolding, characterized by multiple intermediate unfolding events. Thus the mutations in the α-actinin-2 ABD appears to causes ABD substructures (CH1 vs CH2, or subregions within) to unfold separately from each other. To our knowledge this type of unfolding has not been reported for other spectrin superfamily proteins, including our studies of β-III-spectrin. Thus, we think the unique unfolding patterns observed for the mutant α-actinin-2 ABDs suggest that the α-actinin-2 substructures are more weakly associated with each other.

Drosophila melanogaster expresses β-spectrin and α-actinin proteins that are highly similar to human β-III-spectrin and α-actinin-2, respectively. Thus, Drosophila provides a tractable system to gain insights into the function of human β-III-spectrin and α-actinin-2 and how human disease mutations impact the function of these proteins. Using Drosophila, we previously showed a human SCA5 L253P mutation in fly β-spectrin causes defects in neuron structure and function. Expression of the L253P β-

spectrin in class IV dendritic arborization sensory neurons induced pronounced defects in dendritic arborization. Specifically, the mutant decreased number of branch points, total branch length and arbor radius, determined through Sholl analysis. Rescue experiments found that the L253P mutation not only failed to rescue lethality caused by a nonsense mutation in the native *βspec* gene, but also induced lethality in flies containing the wild-type *βspec* gene. Further, western blot analyses showed an accumulation of L253P mutant protein in neuronal tissue. Based on this earlier work, we performed similar studies for several β-spectrin ABD localized mutations (T62I, F160C, T271I, Y272H and H278R). For these mutations, we observed milder disruptions to dendritic arborization and far less neurotoxicity. These milder disruption to spectrin function in vivo are consistent with the milder impact these mutations had on actin binding, compared to L253P. Drosophila studies could likewise be performed for the human α-actinin-2 mutations, to determine how fly α-actinin protein function in muscle tissue is impacted by introduction of the human cardiomyopathy-associated variants. We anticipate that the mutations would disrupt incorporation of the α-actinin protein into muscle sarcomere Z-disk, resulting in defects in muscle contractions.

Notably, the spectrin superfamily of proteins contains several disease associated proteins, including, β-II, III, and IV-spectrin, α-actinin-1, -2, and -4; and dystrophin [8,57–64]. This indicates the importance of the undisturbed function of these proteins in a healthy cellular environment. While α-actinin and β-spectrin are closely related proteins, the process of evolution and cellular specialization has facilitated acquisition of diverse roles, new structural elements and distinct tissue expression patterns. Thus, the mutations in two evolutionarily linked proteins, such as β-III-spectrin and α-actinin-2, result in

drastically different diseases. However, our studies indicate that some β-III-spectrin and α-actinin-2 mutations/variants have similar molecular consequences. Our group has recently made progress in identifying a small molecule that modulates β-III-spectrin binding to actin, supporting SCA5 therapeutic development [93,127]. Additional drug screening may be useful in identifying small molecule therapeutics aiming to selectively target aberrant actin binding caused by mutations in the α-actinin-2 ABD.

REFERENCES

[1] T.D. Pollard, Actin and Actin-Binding Proteins, Cold Spring Harb Perspect Biol 8 (2016) a018226. https://doi.org/10.1101/cshperspect.a018226.

[2] M. Glotzer, Cytokinesis in Metazoa and Fungi, Cold Spring Harb Perspect Biol 9 (2017) a022343. https://doi.org/10.1101/CSHPERSPECT.A022343.

[3] H.L. Sweeney, D.W. Hammers, Muscle Contraction, Cold Spring Harb Perspect Biol 10 (2018) a023200. https://doi.org/10.1101/CSHPERSPECT.A023200.

[4] M.A. Titus, Myosin-Driven Intracellular Transport, Cold Spring Harb Perspect Biol 10 (2018) a021972. https://doi.org/10.1101/CSHPERSPECT.A021972.

[5] T. Svitkina, The Actin Cytoskeleton and Actin-Based Motility, Cold Spring Harb Perspect Biol 10 (2018) a018267. https://doi.org/10.1101/CSHPERSPECT.A018267.

[6] H. Lee Sweeney, E.L.F. Holzbaur, Motor Proteins, Cold Spring Harb Perspect Biol 10 (2018) a021931. https://doi.org/10.1101/CSHPERSPECT.A021931.

[7] A. Schmidt, M.N. Hall, SIGNALING TO THE ACTIN CYTOSKELETON, 1998. www.annualreviews.org.

[8] R.K.H. Liem, Cytoskeletal integrators: The spectrin superfamily, Cold Spring Harb Perspect Biol 8 (2016). https://doi.org/10.1101/cshperspect.a018259.

[9] M.J.F. Broderick, S.J. Winder, SPECTRIN, a-ACTININ, AND DYSTROPHIN, (2005). https://doi.org/10.1016/S0065-3233(04)70007-8.

[10] G. Franzot, B. Sjöblom, M. Gautel, K.D. Carugo, The crystal structure of the actin binding domain from alpha-actinin in its closed conformation: structural insight into phospholipid regulation of alpha-actinin, J Mol Biol 348 (2005) 151–165. https://doi.org/10.1016/J.JMB.2005.01.002.

[11] N.H. Keep, S.J. Winder, C.A. Moores, S. Walke, F.L.M. Norwood, J. Kendrick-Jones, Crystal structure of the actin-binding region of utrophin reveals a head-to-tail dimer, Structure 7 (1999) 1539–1546. https://doi.org/10.1016/S0969-2126(00)88344-6.

[12] F.L.M. Norwood, A.J. Sutherland-Smith, N.H. Keep, J. Kendrick-Jones, The structure of the N-terminal actin-binding domain of human dystrophin and how mutations in this domain may cause Duchenne or Becker muscular dystrophy, Structure 8 (2000) 481–491. https://doi.org/10.1016/S0969-2126(00)00132-5.

[13] E. Borrego-Diaz, F. Kerff, S.H. Lee, F. Ferron, Y. Li, R. Dominguez, Crystal structure of the actin-binding domain of α-actinin 1: Evaluating two competing actin-binding models, J Struct Biol 155 (2006) 230–238. https://doi.org/10.1016/J.JSB.2006.01.013.

[14] N.J. Haywood, M. Wolny, B. Rogers, C.H. Trinh, Y. Shuping, T.A. Edwards, M. Peckham, Hypertrophic cardiomyopathy mutations in the calponin-homology domain of ACTN2 affect actin binding and cardiomyocyte Z-disc incorporation, Biochemical Journal 473 (2016) 2485–2493. https://doi.org/10.1042/BCJ20160421.

[15] T.D. Pollard, A Guide to Simple and Informative Binding Assays, Mol Biol Cell 21 (2010) 4061–4067. https://doi.org/10.1091/mbc.e10-08-0683.

[16] A.R. Harris, B. Belardi, P. Jreij, K. Wei, H. Shams, A. Bausch, D.A. Fletcher, Steric regulation of tandem calponin homology domain actin-binding affinity., Mol Biol Cell 30 (2019) 3112–3122. https://doi.org/10.1091/mbc.E19-06-0317.
[17] S. Bañuelos, M. Saraste, K.D. Carugo, Structural comparisons of calponin homology domains: implications for actin binding, Structure 6 (1998) 1419–1431. https://doi.org/10.1016/S0969-2126(98)00141-5.
[18] V.E. Galkin, A. Orlova, A. Salmazo, K. Djinovic-Carugo, E.H. Egelman, Opening of tandem calponin homology domains regulates their affinity for F-actin, Nat Struct Mol Biol 17 (2010) 614–616. https://doi.org/10.1038/nsmb.1789.
[19] A.W. Avery, M.E. Fealey, F. Wang, A. Orlova, A.R. Thompson, D.D. Thomas, T.S. Hays, E.H. Egelman, Structural basis for high-affinity actin binding revealed by a β-III-spectrin SCA5 missense mutation, Nat Commun 8 (2017) 1–7. https://doi.org/10.1038/s41467-017-01367-w.
[20] B. Sjöblom, A. Salmazo, K. Djinović-Carugo, α-Actinin structure and regulation, Cellular and Molecular Life Sciences 65 (2008) 2688–2701. https://doi.org/10.1007/s00018-008-8080-8.
[21] E.D.A. Ribeiro, N. Pinotsis, A. Ghisleni, A. Salmazo, P. V. Konarev, J. Kostan, B. Sjöblom, C. Schreiner, A.A. Polyansky, E.A. Gkougkoulia, M.R. Holt, F.L. Aachmann, B. Žagrović, E. Bordignon, K.F. Pirker, D.I. Svergun, M. Gautel, K. Djinović-Carugo, The structure and regulation of human muscle α-Actinin, Cell 159 (2014) 1447–1460. https://doi.org/10.1016/j.cell.2014.10.056.
[22] A. Kumari, S. Kesarwani, M.G. Javoor, K.R. Vinothkumar, M. Sirajuddin, Structural insights into actin filament recognition by commonly used cellular actin markers, EMBO J 39 (2020). https://doi.org/10.15252/EMBJ.2019104006.
[23] D. V. Iwamoto, A. Huehn, B. Simon, C. Huet-Calderwood, M. Baldassarre, C. V. Sindelar, D.A. Calderwood, Structural basis of the filamin A actin-binding domain interaction with F-actin, Nat Struct Mol Biol 25 (2018) 918–927. https://doi.org/10.1038/s41594-018-0128-3.
[24] K. Djinovic-Carugo, M. Gautel, J. Ylänne, P. Young, The spectrin repeat: a structural platform for cytoskeletal protein assemblies, FEBS Lett 513 (2002) 119–123. https://doi.org/10.1016/S0014-5793(01)03304-X.
[25] V. Bennett, J. Davis, W.E. Fowler, Brain spectrin, a membrane-associated protein related in structure and function to erythrocyte spectrin, Nature 299 (1982) 126–131. https://doi.org/10.1038/299126A0.
[26] T.J. Byers, D. Branton, Visualization of the protein associations in the erythrocyte membrane skeleton, Proc Natl Acad Sci U S A 82 (1985) 6153–6157. https://doi.org/10.1073/PNAS.82.18.6153.
[27] S.C. Liu, L.H. Derick, J. Palek, Visualization of the hexagonal lattice in the erythrocyte membrane skeleton, Journal of Cell Biology 104 (1987) 527–536. https://doi.org/10.1083/JCB.104.3.527.
[28] K. Xu, G. Zhong, X. Zhuang, Actin, spectrin, and associated proteins form a periodic cytoskeletal structure in axons, Science (1979) 339 (2013) 452–456. https://doi.org/10.1126/SCIENCE.1232251.

[29] S. Vassilopoulos, S. Gibaud, A. Jimenez, G. Caillol, C. Leterrier, Ultrastructure of the axonal periodic scaffold reveals a braid-like organization of actin rings, Nat Commun 10 (2019). https://doi.org/10.1038/S41467-019-13835-6.
[30] G. Travé, A. Pastore, M. Hyvönen, M. Saraste, The C-Terminal Domain of α-Spectrin is Structurally Related to Calmodulin, Eur J Biochem 227 (1995) 35–42. https://doi.org/10.1111/j.1432-1033.1995.tb20357.x.
[31] A.H. Beggs, T.J. Byers, J.H.M. Knoll, F.M. Boyce, G.A.P. Bruns, L.M. Kunkel, Cloning and characterization of two human skeletal muscle α-actinin genes located on chromosomes 1 and 11, Journal of Biological Chemistry (1992). https://doi.org/10.1016/s0021-9258(19)50420-3.
[32] J. Tang, D.W. Taylor, K.A. Taylor, The three-dimensional structure of alpha-actinin obtained by cryoelectron microscopy suggests a model for Ca(2+)-dependent actin binding, J Mol Biol 310 (2001) 845–858. https://doi.org/10.1006/JMBI.2001.4789.
[33] S. Lundberg, J. Björk, L. Löfvenberg, L. Backman, Cloning, Expression and Characterization of Two Putative Calcium-binding Sites in Human Non-Erythroid α-Spectrin, Eur J Biochem 230 (1995) 658–665. https://doi.org/10.1111/j.1432-1033.1995.0658h.x.
[34] T.J. Byers, A. Husain-Chishti, R.R. Dubreuil, D. Branton, L.S. Goldstein, Sequence similarity of the amino-terminal domain of Drosophila beta spectrin to alpha actinin and dystrophin., J Cell Biol 109 (1989) 1633–1641. https://doi.org/10.1083/jcb.109.4.1633.
[35] R.R. Dubreuil, T.J. Byers, A.L. Sillman, D. Bar-Zvi, L.S. Goldstein, D. Branton, The complete sequence of Drosophila alpha-spectrin: conservation of structural domains between alpha-spectrins and alpha-actinin., J Cell Biol 109 (1989) 2197–2205. https://doi.org/10.1083/jcb.109.5.2197.
[36] H. Youssoufian, M. McAfee, D.J. Kwiatkowski, Cloning and chromosomal localization of the human cytoskeletal alpha-actinin gene reveals linkage to the beta-spectrin gene., Am J Hum Genet 47 (1990) 62–72. http://www.ncbi.nlm.nih.gov/pubmed/2349951.
[37] D. Santoni, F. Castiglione, P. Paci, Identifying Correlations between Chromosomal Proximity of Genes and Distance of Their Products in Protein-Protein Interaction Networks of Yeast, PLoS One 8 (2013) e57707. https://doi.org/10.1371/journal.pone.0057707.
[38] J. Pascual, J. Castresana, M. Saraste, Evolution of the spectrin repeat, BioEssays 19 (1997) 811–817. https://doi.org/10.1002/bies.950190911.
[39] R.R. Dubreuil, Structure and evolution of the actin crosslinking proteins, BioEssays 13 (1991) 219–226. https://doi.org/10.1002/bies.950130504.
[40] G.H. Thomas, E.C. Newbern, C.C. Korte, M.A. Bales, S. V. Muse, A.G. Clark, D.P. Kiehart, Intragenic duplication and divergence in the spectrin superfamily of proteins, Mol Biol Evol 14 (1997) 1285–1295. https://doi.org/10.1093/oxfordjournals.molbev.a025738.
[41] J.C. Winkelmann, J.G. Chang, W.T. Tse, A.L. Scarpa, V.T. Marchesi, B.G. Forget, Full-length sequence of the cDNA for human erythroid β-spectrin, Journal of

Biological Chemistry 265 (1990) 11827–11832. https://doi.org/10.1016/s0021-9258(19)38473-x.
[42] V.T. Marchesi, E. Steers, Selective solubilization of a protein component of the red cell membrane, Science (1979) 159 (1968) 203–204. https://doi.org/10.1126/SCIENCE.159.3811.203.
[43] V. Bennett, A.J. Baines, Spectrin and ankyrin-based pathways: Metazoan inventions for integrating cells into tissues, Physiol Rev 81 (2001) 1353–1392. https://doi.org/10.1152/PHYSREV.2001.81.3.1353.
[44] V. Bennett, D.M. Gilligan, The spectrin-based membrane skeleton and micron-scale organization of the plasma membrane, Annu Rev Cell Biol 9 (1993) 27–66. https://doi.org/10.1146/ANNUREV.CB.09.110193.000331.
[45] R. Zhou, B. Han, C. Xia, X. Zhuang, Membrane-associated periodic skeleton is a signaling platform for RTK transactivation in neurons, Science 365 (2019) 929–934. https://doi.org/10.1126/SCIENCE.AAW5937.
[46] M. Hammarlund, E.M. Jorgensen, M.J. Bastiani, Axons break in animals lacking β-spectrin, Journal of Cell Biology 176 (2007) 269–275. https://doi.org/10.1083/JCB.200611117.
[47] S. Dubey, N. Bhembre, S. Bodas, S. Veer, A. Ghose, A. Callan-Jones, P. Pullarkat, P. Sens, The axonal actin-spectrin lattice acts as a tension buffering shock absorber, Elife 9 (2020). https://doi.org/10.7554/ELIFE.51772.
[48] M. Krieg, J. Stühmer, J.G. Cueva, R. Fetter, K. Spilker, D. Cremers, K. Shen, A.R. Dunn, M.B. Goodman, Genetic defects in β-spectrin and tau sensitize C. elegans axons to movement-induced damage via torque-tension coupling, Elife 6 (2017). https://doi.org/10.7554/ELIFE.20172.
[49] P.R. Stabach, J.S. Morrow, Identification and Characterization of βV Spectrin, a Mammalian Ortholog of Drosophila βHSpectrin, Journal of Biological Chemistry 275 (2000) 21385–21395. https://doi.org/10.1074/jbc.C000159200.
[50] A. Viel, α-Actinin and spectrin structures: an unfolding family story, FEBS Lett 460 (1999) 391–394. https://doi.org/10.1016/S0014-5793(99)01372-1.
[51] M.A. Mills, N. Yang, R. Weinberger, D.L. Vander Woude, A.H. Beggs, S. Easteal, K.N. North, Differential expression of the actin-binding proteins, alpha-actinin-2 and -3, in different species: implications for the evolution of functional redundancy, Hum Mol Genet 10 (2001) 1335–1346. https://doi.org/10.1093/HMG/10.13.1335.
[52] A. Blanchard, V. Ohanian, D. Critchley, The structure and function of α-actinin, J Muscle Res Cell Motil 10 (1989) 280–289. https://doi.org/10.1007/BF01758424.
[53] A. Virel, L. Backman, Molecular evolution and structure of α-actinin, Mol Biol Evol 21 (2004) 1024–1031. https://doi.org/10.1093/molbev/msh094.
[54] J. Xu, D. Wirtz, T.D. Pollard, Dynamic cross-linking by α-actinin determines the mechanical properties of actin filament networks, Journal of Biological Chemistry 273 (1998) 9570–9576. https://doi.org/10.1074/jbc.273.16.9570.
[55] J. Ylänne, K. Scheffzek, P. Young, M. Saraste, Crystal structure of the α-actinin rod reveals an extensive torsional twist, Structure 9 (2001) 597–604. https://doi.org/10.1016/S0969-2126(01)00619-0.

[56] V. Gupta, M. Discenza, J.R. Guyon, L.M. Kunkel, A.H. Beggs, α-Actinin-2 deficiency results in sarcomeric defects in zebrafish that cannot be rescued by α-actinin-3 revealing functional differences between sarcomeric isoforms, The FASEB Journal 26 (2012) 1892–1908. https://doi.org/10.1096/fj.11-194548.
[57] A.W. Avery, J. Crain, D.D. Thomas, T.S. Hays, A human β-III-spectrin spinocerebellar ataxia type 5 mutation causes high-affinity F-actin binding., Sci Rep 6 (2016) 21375. https://doi.org/10.1038/srep21375.
[58] L.-Z. Liu, M. Ren, M. Li, Y.-T. Ren, B. Sun, X.-S. Sun, S.-Y. Chen, S.-Y. Li, X.-S. Huang, A Novel Missense Mutation in the Spectrin Beta Nonerythrocytic 2 Gene Likely Associated with Spinocerebellar Ataxia Type 5, Chin Med J (Engl) 129 (2016) 2516–2517. https://doi.org/10.4103/0366-6999.191834.
[59] J.M. Kaplan, S.H. Kim, K.N. North, H. Rennke, L.A. Correia, H.Q. Tong, B.J. Mathis, J.C. Rodríguez-Pérez, P.G. Allen, A.H. Beggs, M.R. Pollak, Mutations in ACTN4, encoding alpha-actinin-4, cause familial focal segmental glomerulosclerosis., Nat Genet 24 (2000) 251–6. https://doi.org/10.1038/73456.
[60] A. Weins, P. Kenlan, S. Herbert, T.C. Le, I. Villegas, B.S. Kaplan, G.B. Appel, M.R. Pollak, Mutational and Biological Analysis of alpha-actinin-4 in focal segmental glomerulosclerosis., J Am Soc Nephrol 16 (2005) 3694–701. https://doi.org/10.1681/ASN.2005070706.
[61] A.C.H. Murphy, A.J. Lindsay, M.W. McCaffrey, K. Djinović-Carugo, P.W. Young, Congenital macrothrombocytopenia-linked mutations in the actin-binding domain of α-actinin-1 enhance F-actin association, FEBS Lett 590 (2016) 685–695. https://doi.org/10.1002/1873-3468.12101.
[62] D.M. Henderson, A. Lee, J.M. Ervasti, Disease-causing missense mutations in actin binding domain 1 of dystrophin induce thermodynamic instability and protein aggregation, Proceedings of the National Academy of Sciences 107 (2010) 9632–9637. https://doi.org/10.1073/pnas.1001517107.
[63] M.A. Cousin, B.A. Creighton, K.A. Breau, R.C. Spillmann, E. Torti, S. Dontu, S. Tripathi, D. Ajit, R.J. Edwards, S. Afriyie, J.C. Bay, K.M. Harper, A.A. Beltran, L.J. Munoz, L. Falcon Rodriguez, M.C. Stankewich, R.E. Person, Y. Si, E.A. Normand, A. Blevins, A.S. May, L. Bier, V. Aggarwal, G.M.S. Mancini, M.A. van Slegtenhorst, K. Cremer, J. Becker, H. Engels, S. Aretz, J.J. MacKenzie, E. Brilstra, K.L.I. van Gassen, R.H. van Jaarsveld, R. Oegema, G.M. Parsons, P. Mark, I. Helbig, S.E. McKeown, R. Stratton, B. Cogne, B. Isidor, P. Cacheiro, D. Smedley, H. V. Firth, T. Bierhals, K. Kloth, D. Weiss, C. Fairley, J.T. Shieh, A. Kritzer, P. Jayakar, E. Kurtz-Nelson, R.A. Bernier, T. Wang, E.E. Eichler, I.M.B.H. van de Laar, A. McConkie-Rosell, M.T. McDonald, J. Kemppainen, B.C. Lanpher, L.E. Schultz-Rogers, L.B. Gunderson, P.N. Pichurin, G. Yoon, M. Zech, R. Jech, J. Winkelmann, A.S. Beltran, M.T. Zimmermann, B. Temple, S.S. Moy, E.W. Klee, Q.K.G. Tan, D.N. Lorenzo, Pathogenic SPTBN1 variants cause an autosomal dominant neurodevelopmental syndrome, Nat Genet 53 (2021) 1006–1021. https://doi.org/10.1038/s41588-021-00886-z.
[64] E. Knierim, E. Gill, F. Seifert, S. Morales-Gonzalez, S.D. Unudurthi, T.J. Hund, W. Stenzel, M. Schuelke, A recessive mutation in beta-IV-spectrin (SPTBN4)

associates with congenital myopathy, neuropathy, and central deafness, Hum Genet 136 (2017) 903–910. https://doi.org/10.1007/S00439-017-1814-7.
[65] O. Ohara, R. Ohara, H. Yamakawa, D. Nakajima, M. Nakayama, Characterization of a new β-spectrin gene which is predominantly expressed in brain, Molecular Brain Research 57 (1998) 181–192. https://doi.org/10.1016/S0169-328X(98)00068-0.
[66] Y. Gao, E.M. Perkins, Y.L. Clarkson, S. Tobia, A.R. Lyndon, M. Jackson, J.D. Rothstein, β-III Spectrin Is Critical for Development of Purkinje Cell Dendritic Tree and Spine Morphogenesis, The Journal of Neuroscience 31 (2011) 16581–16590. https://doi.org/10.1523/JNEUROSCI.3332-11.2011.
[67] N. Efimova, F. Korobova, M.C. Stankewich, A.H. Moberly, D.B. Stolz, J. Wang, A. Kashina, M. Ma, T. Svitkina, βIII Spectrin Is Necessary for Formation of the Constricted Neck of Dendritic Spines and Regulation of Synaptic Activity in Neurons, The Journal of Neuroscience 37 (2017) 6442–6459. https://doi.org/10.1523/JNEUROSCI.3520-16.2017.
[68] M.C. Stankewich, B. Gwynn, T. Ardito, L. Ji, J. Kim, R.F. Robledo, S.E. Lux, L.L. Peters, J.S. Morrow, Targeted deletion of βIII spectrin impairs synaptogenesis and generates ataxic and seizure phenotypes, Proc Natl Acad Sci U S A 107 (2010) 6022–6027. https://doi.org/10.1073/pnas.1001522107.
[69] Y. Ikeda, K.A. Dick, M.R. Weatherspoon, D. Gincel, K.R. Armbrust, J.C. Dalton, G. Stevanin, A. Dürr, C. Zühlke, K. Bürk, H.B. Clark, A. Brice, J.D. Rothstein, L.J. Schut, J.W. Day, L.P.W. Ranum, Spectrin mutations cause spinocerebellar ataxia type 5, Nat Genet 38 (2006) 184–190. https://doi.org/10.1038/ng1728.
[70] K.R. Armbrust, X. Wang, T.J. Hathorn, S.W. Cramer, G. Chen, T. Zu, T. Kangas, A.N. Zink, G. Öz, T.J. Ebner, L.P.W. Ranum, Mutant β-III Spectrin Causes mGluR1α Mislocalization and Functional Deficits in a Mouse Model of Spinocerebellar Ataxia Type 5, The Journal of Neuroscience 34 (2014) 9891. https://doi.org/10.1523/JNEUROSCI.0876-14.2014.
[71] M. Jackson, W. Song, M.Y. Liu, L. Jin, M. Dykes-Hoberg, C.L.G. Lin, W.J. Bowers, H.J. Federoff, P.C. Sternweis, J.D. Rothstein, Modulation of the neuronal glutamate transporter EAAT4 by two interacting proteins, Nature 410 (2001) 89–93. https://doi.org/10.1038/35065091.
[72] Y.L. Clarkson, E.M. Perkins, C.J. Cairncross, A.R. Lyndon, P.A. Skehel, M. Jackson, β-III spectrin underpins ankyrin R function in Purkinje cell dendritic trees: protein complex critical for sodium channel activity is impaired by SCA5-associated mutations, Hum Mol Genet 23 (2014) 3875–3882. https://doi.org/10.1093/hmg/ddu103.
[73] E.M. Perkins, Y.L. Clarkson, N. Sabatier, D.M. Longhurst, C.P. Millward, J. Jack, J. Toraiwa, M. Watanabe, J.D. Rothstein, A.R. Lyndon, D.J.A. Wyllie, M.B. Dutia, M. Jackson, Loss of β-III Spectrin Leads to Purkinje Cell Dysfunction Recapitulating the Behavior and Neuropathology of Spinocerebellar Ataxia Type 5 in Humans, The Journal of Neuroscience 30 (2010) 4857–4867. https://doi.org/10.1523/JNEUROSCI.6065-09.2010.
[74] S. Lise, Y. Clarkson, E. Perkins, A. Kwasniewska, E. Sadighi Akha, R. Parolin Schnekenberg, D. Suminaite, J. Hope, I. Baker, L. Gregory, A. Green, C. Allan, S.

Lamble, S. Jayawant, G. Quaghebeur, M.Z. Cader, S. Hughes, R.J.E. Armstrong, A. Kanapin, A. Rimmer, G. Lunter, I. Mathieson, J.B. Cazier, D. Buck, J.C. Taylor, D. Bentley, G. McVean, P. Donnelly, S.J.L. Knight, M. Jackson, J. Ragoussis, A.H. Németh, Recessive Mutations in SPTBN2 Implicate β-III Spectrin in Both Cognitive and Motor Development, PLoS Genet 8 (2012). https://doi.org/10.1371/journal.pgen.1003074.

[75] K. Bürk, C. Zühlke, I.R. König, A. Ziegler, E. Schwinger, C. Globas, J. Dichgans, Y. Hellenbroich, Spinocerebellar ataxia type 5, Neurology 62 (2004) 327–329. https://doi.org/10.1212/01.WNL.0000103293.63340.C1.

[76] L.P.W. Ranum, L.J. Schut, J.K. Lundgren, H.T. Orr, D.M. Livingston, Spinocerebellar ataxia type 5 in a family descended from the grandparents of President Lincoln maps to chromosome 11, Nat Genet 8 (1994) 280–284. https://doi.org/10.1038/ng1194-280.

[77] G. Stevanin, A. Herman, A. Brice, A. Dürr, Clinical and MRI findings in spinocerebellar ataxia type 5, Neurology 53 (1999) 1355–1355. https://doi.org/10.1212/WNL.53.6.1355.

[78] P. Sancho, A. Andrés-Bordería, N. Gorría-Redondo, K. Llano, D. Martínez-Rubio, M.E. Yoldi-Petri, L. Blumkin, P. Rodríguez de la Fuente, F. Gil-Ortiz, L. Fernández-Murga, A. Sánchez-Monteagudo, V. Lupo, B. Pérez-Dueñas, C. Espinós, S. Aguilera-Albesa, Expanding the β-III Spectrin-Associated Phenotypes toward Non-Progressive Congenital Ataxias with Neurodegeneration, Int J Mol Sci 22 (2021) 2505. https://doi.org/10.3390/ijms22052505.

[79] G. Rea, S. Tirupathi, J. Williams, P. Clouston, P.J. Morrison, Infantile Onset of Spinocerebellar Ataxia Type 5 (SCA-5) in a 6 Month Old with Ataxic Cerebral Palsy, The Cerebellum 19 (2020) 161–163. https://doi.org/10.1007/s12311-019-01085-7.

[80] F. Nicita, M. Nardella, E. Bellacchio, P. Alfieri, G. Terrone, G. Piccini, F. Graziola, C. Pignata, A. Capuano, E. Bertini, G. Zanni, Heterozygous missense variants of SPTBN2 are a frequent cause of congenital cerebellar ataxia, Clin Genet 96 (2019) 169–175. https://doi.org/10.1111/cge.13562.

[81] S. Nuovo, A. Micalizzi, S. D'Arrigo, M. Ginevrino, T. Biagini, T. Mazza, E.M. Valente, Between SCA5 and SCAR14: Delineation of the SPTBN2 p.R480W-associated phenotype, European Journal of Human Genetics 26 (2018) 928–929. https://doi.org/10.1038/s41431-018-0158-7.

[82] E. Yıldız Bölükbaşı, M. Afzal, S. Mumtaz, N. Ahmad, S. Malik, A. Tolun, Progressive SCAR14 with unclear speech, developmental delay, tremor, and behavioral problems caused by a homozygous deletion of the SPTBN2 pleckstrin homology domain, Am J Med Genet A 173 (2017) 2494–2499. https://doi.org/10.1002/ajmg.a.38332.

[83] D.N. Lorenzo, R.J. Edwards, A.L. Slavutsky, Spectrins: molecular organizers and targets of neurological disorders, Nat Rev Neurosci 24 (2023) 195–212. https://doi.org/10.1038/s41583-022-00674-6.

[84] M. Sun, A.K. Johnson, V. Nelakuditi, L. Guidugli, D. Fischer, K. Arndt, L. Ma, E. Sandford, V. Shakkottai, K. Boycott, J.W. Chardon, Z. Li, D. del Gaudio, M. Burmeister, C.M. Gomez, D.J. Waggoner, S. Das, Targeted exome analysis

identifies the genetic basis of disease in over 50% of patients with a wide range of ataxia-related phenotypes, Genetics in Medicine 21 (2019) 195–206. https://doi.org/10.1038/s41436-018-0007-7.
[85] K. Fujishima, J. Kurisu, M. Yamada, M. Kengaku, βIII spectrin controls the planarity of Purkinje cell dendrites by modulating perpendicular axon-dendrite interactions, Development 147 (2020). https://doi.org/10.1242/dev.194530.
[86] B. Han, R. Zhou, C. Xia, X. Zhuang, Structural organization of the actin-spectrin–based membrane skeleton in dendrites and soma of neurons, Proceedings of the National Academy of Sciences 114 (2017). https://doi.org/10.1073/pnas.1705043114.
[87] Y.L. Clarkson, T. Gillespie, E.M. Perkins, A.R. Lyndon, M. Jackson, β-III spectrin mutation L253P associated with spinocerebellar ataxia type 5 interferes with binding to Arp1 and protein trafficking from the Golgi, Hum Mol Genet 19 (2010) 3634–3641. https://doi.org/10.1093/hmg/ddq279.
[88] R. Romaniello, A. Citterio, E. Panzeri, F. Arrigoni, M. De Rinaldis, A. Trabacca, M.T. Bassi, Novel SPTBN2 gene mutation and first intragenic deletion in early onset spinocerebellar ataxia type 5, Ann Clin Transl Neurol 8 (2021) 956–963. https://doi.org/10.1002/acn3.51345.
[89] X. Bian, S. Wang, S. Jin, S. Xu, H. Zhang, D. Wang, W. Shang, P. Wang, Two novel missense variants in SPTBN2 likely associated with spinocerebellar ataxia type 5, Neurological Sciences 42 (2021) 5195–5203. https://doi.org/10.1007/s10072-021-05204-3.
[90] L.E.L.M. Vissers, K.J.M. van Nimwegen, J.H. Schieving, E.-J. Kamsteeg, T. Kleefstra, H.G. Yntema, R. Pfundt, G.J. van der Wilt, L. Krabbenborg, H.G. Brunner, S. van der Burg, J. Grutters, J.A. Veltman, M.A.A.P. Willemsen, A clinical utility study of exome sequencing versus conventional genetic testing in pediatric neurology, Genetics in Medicine 19 (2017) 1055–1063. https://doi.org/10.1038/gim.2017.1.
[91] A.W. Avery, D.D. Thomas, T.S. Hays, β-III-spectrin spinocerebellar ataxia type 5 mutation reveals a dominant cytoskeletal mechanism that underlies dendritic arborization, Proceedings of the National Academy of Sciences 114 (2017) E9376–E9385. https://doi.org/10.1073/pnas.1707108114.
[92] S.A. Denha, A.E. Atang, T.S. Hays, A.W. Avery, β-III-spectrin N-terminus is required for high-affinity actin binding and SCA5 neurotoxicity, Sci Rep 12 (2022) 1–11. https://doi.org/10.1038/s41598-022-05762-2.
[93] P. Guhathakurta, R.T. Rebbeck, S.A. Denha, A.R. Keller, A.L. Carter, A.E. Atang, B. Svensson, D.D. Thomas, T.S. Hays, A.W. Avery, Early-phase drug discovery of β-III-spectrin actin-binding modulators for treatment of spinocerebellar ataxia type 5, Journal of Biological Chemistry 299 (2023) 102956. https://doi.org/10.1016/j.jbc.2023.102956.
[94] S. Lange, N. Pinotsis, I. Agarkova, E. Ehler, The M-band: The underestimated part of the sarcomere, Biochimica et Biophysica Acta (BBA) - Molecular Cell Research 1867 (2020) 118440. https://doi.org/10.1016/J.BBAMCR.2019.02.003.
[95] K. Wadmore, A.J. Azad, K. Gehmlich, O. Karpicheva, A.J.S.A. Azad@bham, A.J.A. Uk, The Role of Z-disc Proteins in Myopathy and Cardiomyopathy,

International Journal of Molecular Sciences 2021, Vol. 22, Page 3058 22 (2021) 3058. https://doi.org/10.3390/IJMS22063058.
[96] A. Azad, G. Poloni, N. Sontayananon, H. Jiang, K. Gehmlich, The giant titin: how to evaluate its role in cardiomyopathies, J Muscle Res Cell Motil 40 (2019) 159–167. https://doi.org/10.1007/S10974-019-09518-W/FIGURES/2.
[97] S. Broadway-Stringer, H. Jiang, K. Wadmore, C. Hooper, G. Douglas, V. Steeples, A.J. Azad, E. Singer, J.S. Reyat, F. Galatik, E. Ehler, P. Bennett, J.I. Kalisch-Smith, D.B. Sparrow, B. Davies, K. Djinovic-Carugo, M. Gautel, H. Watkins, K. Gehmlich, Insights into the Role of a Cardiomyopathy-Causing Genetic Variant in ACTN2, Cells 12 (2023). https://doi.org/10.3390/cells12050721.
[98] P.K. Luther, The vertebrate muscle Z-disc: Sarcomere anchor for structure and signalling, J Muscle Res Cell Motil 30 (2009) 171–185. https://doi.org/10.1007/S10974-009-9189-6/FIGURES/10.
[99] D. Frank, C. Kuhn, H.A. Katus, N. Frey, The sarcomeric Z-disc: a nodal point in signalling and disease, J Mol Med 84 (2006) 446–468. https://doi.org/10.1007/s00109-005-0033-1.
[100] M. Prondzynski, M.D. Lemoine, A.T. Zech, A. Horváth, V. Di Mauro, J.T. Koivumäki, N. Kresin, J. Busch, T. Krause, E. Krämer, S. Schlossarek, M. Spohn, F.W. Friedrich, J. Münch, S.D. Laufer, C. Redwood, A.E. Volk, A. Hansen, G. Mearini, D. Catalucci, C. Meyer, T. Christ, M. Patten, T. Eschenhagen, L. Carrier, Disease modeling of a mutation in α-actinin 2 guides clinical therapy in hypertrophic cardiomyopathy, EMBO Mol Med 11 (2019). https://doi.org/10.15252/emmm.201911115.
[101] C. Chiu, R.D. Bagnall, J. Ingles, L. Yeates, M. Kennerson, J.A. Donald, M. Jormakka, J.M. Lind, C. Semsarian, Mutations in Alpha-Actinin-2 Cause Hypertrophic Cardiomyopathy, J Am Coll Cardiol 55 (2010) 1127–1135. https://doi.org/10.1016/j.jacc.2009.11.016.
[102] F. Girolami, M. Iascone, B. Tomberli, S. Bardi, M. Benelli, G. Marseglia, C. Pescucci, L. Pezzoli, M.E. Sana, C. Basso, N. Marziliano, P.A. Merlini, A. Fornaro, F. Cecchi, F. Torricelli, I. Olivotto, Novel α-actinin 2 variant associated with familial hypertrophic cardiomyopathy and juvenile atrial arrhythmias: A massively parallel sequencing study, Circ Cardiovasc Genet (2014). https://doi.org/10.1161/CIRCGENETICS.113.000486.
[103] R.D. Bagnall, L.K. Molloy, J.M. Kalman, C. Semsarian, Exome sequencing identifies a mutation in the ACTN2 gene in a family with idiopathic ventricular fibrillation, left ventricular noncompaction, and sudden death, BMC Med Genet 15 (2014) 99. https://doi.org/10.1186/s12881-014-0099-0.
[104] J.L. Theis, J.M. Bos, V.B. Bartleson, M.L. Will, J. Binder, M. Vatta, J.A. Towbin, B.J. Gersh, S.R. Ommen, M.J. Ackerman, Echocardiographic-determined septal morphology in Z-disc hypertrophic cardiomyopathy, Biochem Biophys Res Commun 351 (2006) 896–902. https://doi.org/10.1016/j.bbrc.2006.10.119.
[105] B. Mohapatra, S. Jimenez, J.H. Lin, K.R. Bowles, K.J. Coveler, J.G. Marx, M.A. Chrisco, R.T. Murphy, P.R. Lurie, R.J. Schwartz, P.M. Elliott, M. Vatta, W. McKenna, J.A. Towbin, N.E. Bowles, Mutations in the muscle LIM protein and α-

actinin-2 genes in dilated cardiomyopathy and endocardial fibroelastosis, Mol Genet Metab 80 (2003) 207–215. https://doi.org/10.1016/S1096-7192(03)00142-2.
[106] L.-L. Fan, H. Huang, J.-Y. Jin, J.-J. Li, Y.-Q. Chen, R. Xiang, Whole-Exome Sequencing Identifies a Novel Mutation (p.L320R) of Alpha-Actinin 2 in a Chinese Family with Dilated Cardiomyopathy and Ventricular Tachycardia, Cytogenet Genome Res 157 (2019) 148–152. https://doi.org/10.1159/000496077.
[107] J.A. Towbin, Inherited Cardiomyopathies, Circulation Journal 78 (2014) 2347–2356. https://doi.org/10.1253/circj.CJ-14-0893.
[108] Z.D. Goff, H. Calkins, Sudden death related cardiomyopathies - Hypertrophic cardiomyopathy, Prog Cardiovasc Dis 62 (2019) 212–216. https://doi.org/10.1016/j.pcad.2019.04.001.
[109] C.W. Tsao, A.W. Aday, Z.I. Almarzooq, C.A.M. Anderson, P. Arora, C.L. Avery, C.M. Baker-Smith, A.Z. Beaton, A.K. Boehme, A.E. Buxton, Y. Commodore-Mensah, M.S.V. Elkind, K.R. Evenson, C. Eze-Nliam, S. Fugar, G. Generoso, D.G. Heard, S. Hiremath, J.E. Ho, R. Kalani, D.S. Kazi, D. Ko, D.A. Levine, J. Liu, J. Ma, J.W. Magnani, E.D. Michos, M.E. Mussolino, S.D. Navaneethan, N.I. Parikh, R. Poudel, M. Rezk-Hanna, G.A. Roth, N.S. Shah, M.-P. St-Onge, E.L. Thacker, S.S. Virani, J.H. Voeks, N.-Y. Wang, N.D. Wong, S.S. Wong, K. Yaffe, S.S. Martin, Heart Disease and Stroke Statistics—2023 Update: A Report From the American Heart Association, Circulation 147 (2023). https://doi.org/10.1161/CIR.0000000000001123.
[110] M.J. Landrum, J.M. Lee, M. Benson, G.R. Brown, C. Chao, S. Chitipiralla, B. Gu, J. Hart, D. Hoffman, W. Jang, K. Karapetyan, K. Katz, C. Liu, Z. Maddipatla, A. Malheiro, K. McDaniel, M. Ovetsky, G. Riley, G. Zhou, J.B. Holmes, B.L. Kattman, D.R. Maglott, ClinVar: improving access to variant interpretations and supporting evidence, Nucleic Acids Res 46 (2018) D1062–D1067. https://doi.org/10.1093/nar/gkx1153.
[111] A.E. Atang, A.R. Keller, S.A. Denha, A.W. Avery, Increased Actin Binding Is a Shared Molecular Consequence of Numerous SCA5 Mutations in β-III-Spectrin, Cells 12 (2023) 2100. https://doi.org/10.3390/cells12162100.
[112] S.R. Stevens, M.E. van der Heijden, Y. Ogawa, T. Lin, R. V. Sillitoe, M.N. Rasband, Ankyrin-R Links Kv3.3 to the Spectrin Cytoskeleton and Is Required for Purkinje Neuron Survival, The Journal of Neuroscience 42 (2022) 2–15. https://doi.org/10.1523/JNEUROSCI.1132-21.2021.
[113] K. Bürk, C. Zühlke, I.R. König, A. Ziegler, E. Schwinger, C. Globas, J. Dichgans, Y. Hellenbroich, Spinocerebellar ataxia type 5: clinical and molecular genetic features of a German kindred, Neurology 62 (2004) 327–329. https://doi.org/10.1212/01.WNL.0000103293.63340.C1.
[114] S. Legardinier, B. Legrand, C. Raguénès-Nicol, A. Bondon, S. Hardy, C. Tascon, E. Le Rumeur, J.-F. Hubert, A Two-amino Acid Mutation Encountered in Duchenne Muscular Dystrophy Decreases Stability of the Rod Domain 23 (R23) Spectrin-like Repeat of Dystrophin, Journal of Biological Chemistry 284 (2009) 8822–8832. https://doi.org/10.1074/jbc.M805846200.

[115] A. Roy, A. Kucukural, Y. Zhang, I-TASSER: a unified platform for automated protein structure and function prediction, Nature Protocols 2010 5:4 5 (2010) 725–738. https://doi.org/10.1038/nprot.2010.5.
[116] A.E. Atang, R.T. Rebbeck, D.D. Thomas, A.W. Avery, Cardiomyopathy-associated variants alter the structure and function of the α-actinin-2 actin-binding domain, Biochem Biophys Res Commun 670 (2023) 12–18. https://doi.org/10.1016/j.bbrc.2023.05.050.
[117] R.E. Hershberger, D.J. Hedges, A. Morales, Dilated cardiomyopathy: the complexity of a diverse genetic architecture, Nature Reviews Cardiology 2013 10:9 10 (2013) 531–547. https://doi.org/10.1038/nrcardio.2013.105.
[118] B.J. Maron, J.M. Gardin, J.M. Flack, S.S. Gidding, T.T. Kurosaki, D.E. Bild, Prevalence of Hypertrophic Cardiomyopathy in a General Population of Young Adults, Circulation 92 (1995) 785–789. https://doi.org/10.1161/01.CIR.92.4.785.
[119] E. Muchtar, L.A. Blauwet, M.A. Gertz, Restrictive Cardiomyopathy, Circ Res 121 (2017) 819–837. https://doi.org/10.1161/CIRCRESAHA.117.310982.
[120] A.R. Clark, G.M. Sawyer, S.P. Robertson, A.J. Sutherland-Smith, Skeletal dysplasias due to filamin A mutations result from a gain-of-function mechanism distinct from allelic neurological disorders†, Hum Mol Genet 18 (2009) 4791–4800. https://doi.org/10.1093/hmg/ddp442.
[121] G.M. Sawyer, A.R. Clark, S.P. Robertson, A.J. Sutherland-Smith, Disease-associated Substitutions in the Filamin B Actin Binding Domain Confer Enhanced Actin Binding Affinity in the Absence of Major Structural Disturbance: Insights from the Crystal Structures of Filamin B Actin Binding Domains, J Mol Biol 390 (2009) 1030–1047. https://doi.org/10.1016/j.jmb.2009.06.009.
[122] R.M. Duff, V. Tay, P. Hackman, G. Ravenscroft, C. McLean, P. Kennedy, A. Steinbach, W. Schöffler, P.F.M. van der Ven, D.O. Fürst, J. Song, K. Djinović-Carugo, S. Penttilä, O. Raheem, K. Reardon, A. Malandrini, S. Gambelli, M. Villanova, K.J. Nowak, D.R. Williams, J.E. Landers, R.H. Brown, B. Udd, N.G. Laing, Mutations in the N-terminal Actin-Binding Domain of Filamin C Cause a Distal Myopathy, The American Journal of Human Genetics 88 (2011) 729–740. https://doi.org/10.1016/j.ajhg.2011.04.021.
[123] A.T.L. Zech, M. Prondzynski, S.R. Singh, N. Pietsch, E. Orthey, E. Alizoti, J. Busch, A. Madsen, C.S. Behrens, M. Meyer-Jens, G. Mearini, M.D. Lemoine, E. Krämer, D. Mosqueira, S. Virdi, D. Indenbirken, M. Depke, M.G. Salazar, U. Völker, I. Braren, W.T. Pu, T. Eschenhagen, E. Hammer, S. Schlossarek, L. Carrier, ACTN2 Mutant Causes Proteopathy in Human iPSC-Derived Cardiomyocytes, Cells 11 (2022) 2745. https://doi.org/10.3390/cells11172745.
[124] A. Kumari, S. Kesarwani, M.G. Javoor, K.R. Vinothkumar, M. Sirajuddin, Structural insights into actin filament recognition by commonly used cellular actin markers, EMBO J 39 (2020). https://doi.org/10.15252/embj.2019104006.
[125] M. Markstein, C. Pitsouli, C. Villalta, S.E. Celniker, N. Perrimon, Exploiting position effects and the gypsy retrovirus insulator to engineer precisely expressed transgenes, Nat Genet 40 (2008) 476–483. https://doi.org/10.1038/NG.101.

[126] A.L. Neisch, A.W. Avery, J.B. Machamer, M. Li, T.S. Hays, Methods to identify and analyze gene products involved in neuronal intracellular transport using Drosophila, in: 2016: pp. 277–309. https://doi.org/10.1016/bs.mcb.2015.06.015.
[127] R.T. Rebbeck, A.K. Andrick, S.A. Denha, B. Svensson, P. Guhathakurta, D.D. Thomas, T.S. Hays, A.W. Avery, Novel drug discovery platform for spinocerebellar ataxia, using fluorescence technology targeting β-III-spectrin, Journal of Biological Chemistry 296 (2021) 100215. https://doi.org/10.1074/jbc.RA120.015417.

APPENDIX

cayuse Hazard Safety

Reference: IBC Protocol # IBC-00001103

Protocol Title: Structural and functional studies of the spectrin superfamily of cytoskeletal proteins

Principal Investigator: Avery, Adam

Approval Period: 09/21/2022 - 09/21/2025

Dear Professor Avery, Adam:

The Institutional Biosafety Committee (IBC), responsible for the review of research involving materials of human origin, recombinant DNA, and biohazardous, infectious or toxic materials, has reviewed the original proposal, noted the revisions provided by you upon committee's request (if applicable), and approved the project referenced above. This is your formal approval notice; please save it for your records.

The proposed activities are approved for a period of three years, starting 09/21/2022 and ending 09/21/2025, and assigned the approval # IBC-00001103. Please be aware that protocols expire at 12:01 AM on the expiration date. The highest BSL level approved for the protocol can be found on the Overview page of the protocol form.

Any unanticipated problems, changes in, or halting of the activities proposed in the project, as described, must be promptly reported to the IBC or the biosafety officer.

In addition, all faculty, staff, and students involved in the project must be trained and qualified to conduct the project in a responsible manner. Please note, in this regard, that you, the Principal Investigator, are fully responsible at all times for limiting or restricting access to laboratories and for assessing, in each circumstance, who may enter or work in a laboratory when biohazardous materials are in use.

Prior to initiating any work on this approved project, please contact me by email (luongo@oakland.edu) to schedule a startup Biosafety Audit. This audit will verify that all biosafety controls described in your application have been implemented.

Please let me know if you have any questions. Thank you.

Sincerely,

Domenic Luongo, CHMM
Director - Laboratory Safety and Compliance

(email ID #400090)